Diuranyl(VI) Complexes with Some Tri- and Tetradentate Ligands and Their Applications

A Thesis Submitted for the Degree of Doctor of Philosophy

By

SABARI GHOSH



School of Chemistry University of Hyderabad Hyderabad 500 046 India

December 2019

Dedicated to

My Parents

STATEMENT

I hereby declare that the matter embodied in this thesis entitled "Diuranyl(VI) Complexes with Some Tri- and Tetradentate Ligands and Their Applications" is the result of the investigation carried out by me in the School of Chemistry, University of Hyderabad, under the supervision of Prof. Samudranil Pal.

In keeping the general practice of reporting scientific observations, due acknowledgement has been made wherever the work described is based on findings of other's investigations. Any omission which might have occurred by oversight or error is regretted.

5th December, 2019

Sabari Ghosh

DECLARATION

I Sabari Ghosh hereby declare that this thesis entitled "Diuranyl(VI) Complexes

with Some Tri- and Tetradentate Ligands and Their Applications" submitted by

me under the supervision and guidance of Prof. Samudranil Pal, School of

Chemistry, University of Hyderabad is a bonafide research work which is also

free from plagiarism. I also declare that it has not been submitted previously in

part or full to this University or any other University or Institution for the award

of any degree or diploma. I hereby agree that my thesis can be deposited in

shodhganga/INFLIBNET.

Date: 5th December, 2019

Sabari Ghosh

Reg.No:14CHPH07

Signature of the supervisor:

Prof. Samudranil Pal

ii



CERTIFICATE

This is to certify that the thesis entitled "Diuranyl(VI) Complexes with Some Triand Tetradentate Ligands and Their Applications" submitted by Sabari Ghosh bearing registration number 14CHPH07 in partial fulfillment of the requirements for award of Doctor of Philosophy in the School of Chemistry is a bonafide work carried out by her under my supervision and guidance. This thesis is free from plagiarism and has not been submitted previously in part or in full to this or any other University or Institution for award of any degree or diploma. Further the student has six publications before submission of the thesis for adjudication and has produced evidences for the same in the form of reprints.

Parts of this thesis have been published in the following three publications:

- 1. S. Ghosh, S. K. Kurapati, A. Ghosh, A. K. Srivastava, S. Pal, *ChemistrySelect*, **2018**, *3*, 1–9. (Chapter 2)
- 2. S. Ghosh, A. K. Srivastava, S. Pal, New J. Chem., 2019, 43, 970–978. (Chapter 3)
- 3. S. Ghosh, A. K. Srivastava, R. Govu, U. Pal, S. Pal, *Inorg. Chem.*, **2019**, *58*, 14410–14419. (Chapter 4)

She has also made presentations in the following conferences:

- 1. Poster presentation in the Symposium on Modern Trends in Inorganic Chemistry, 2015.
- 2. Poster presentation in the 18th CRSI National Symposium in Chemistry, 2016.
- 3. Poster presentation at CHEMFEST-2016, 2017, 2018 Annual In-house Symposium of School of Chemistry, University of Hyderabad.
- 4. Poster presentation in the 24th International Union of Crystallography (IUCr), 2017
- 5. Poster presentation in the Symposium on Modern Trends in Inorganic Chemistry, 2017.

Further the student has passed the following courses towards fulfillment of coursework requirement for Ph. D.:

Course	Title	Credits	Pass/Fail
1. CY-801	Research Proposal	3	Pass
2. CY-802	Chemistry Pedagogy	3	Pass
3. CY-805	Instrumental Methods A	3	Pass
4. CY-806	Instrumental Methods B	3	Pass

Prof. Samudranil Pal (Thesis Supervisor)

Dean School of Chemistry

ACKNOWLEDGEMENTS

First and foremost, I would like to express deepest gratitude and heart felt respect to my research supervisor **Prof. Samudranil Pal** for his constant guidance, motivation and support throughout my research work that helped me to grow not only as a successful research scholar but also shaped me into a responsible person. It was my privilege to be a part of his research group and to do my doctoral study under his supervision.

I would like to thank the former and present Deans, School of Chemistry for providing all essential facilities to carry out my research work. I am extremely thankful individually to all the faculty members of the school particularly my doctoral committee members Prof. K. C. Kumara Swamy and Prof. Samar Kumar Das for their cooperation and fruitful suggestions regarding my research work.

I thank all non-teaching staff of the School of Chemistry for their help and cooperation to execute my research work. I am thankful to IGM library for providing an excellent collection of books and journals.

I sincerely thank University Grants Commission (UGC-BSR), New Delhi for a research fellowship (Letter No.F.25-1/2014-15(BSR)/5-129/20079BSR), dt.05.11.2015)). Financial support and instrumental facilities provided by the Department of Science and Technology, New Delhi through the FIST and the PURSE programs and by the University Grants Commission, New Delhi through the CAS and the UPE programs are gratefully acknowledged.

I am extremely thankful to my seniors in the lab: Dr. Sathish Kumar Kurapati, Dr. Narendra Babu, and post-doctoral fellows Dr. Rupesh Narayana Prabhu and Dr. Srinivas for their help and cooperation. I thank my present lab-mates: Ankit Kumar Srivastava, Kinche Shakunthala, Seema Nagarajan and post-doctoral fellow Dr. Sampath Gajula for their help and creating a cheerful atmosphere in the lab.

Apart from my lab-mates I would also like to extend my acknowledgment to a number of people from School of Chemistry. I am really thankful to my seniors Dr. Arpita Ghosh, Dr. Debparna Datta, Dr. Navendu Mondol, Dr. Kaushik Ghosh, Dr. Sugata Goswami, Dr. P. Srujana, Dr. Suman Ghosh. I would like to extend my special thanks to my friends Tasnim, Ankit and Sneha for their support. I would also like to thank Subhabrata, Sudipta, Divya, Anjana, Anil, Jagjeet, Junaid and all my other batchmates from School of Chemistry. I would also like to acknowledge Suchana, Moumita, Mou, Saradamoni, Sameeta, Shipra, Apurba, Saddam, Senthil, Chandni, Olivia, Somnath, Sumanta, Suman, Soutrik, Anupam

and all my other juniors. My special thanks to my beloved friends Suprita, Saheli and Jeena for being a constant source of support all throughout.

I owe everything to god and my parents for their love, support and care. My parents have offered me the highest degree of freedom in life. No words can describe their importance in my life. Wherever I am standing today or I will be in the future is only because of Maa and Baba. Thank You for everything.

Sabari Ghosh

CONTENTS

STATE	STATEMENT		
DECLA	DECLARATION		
CERTIF	CERTIFICATE		
ACKNO	OWLEDGEMENTS	iv	
SYNOP	PSIS	vi	
СНАРТ	TER 1 Introduction		
1.1.	Uranium Chemistry	1	
1.2.	Importance of trans-uranyl (UO ₂) ²⁺ Complexes	2	
1.3.	About the Present Investigation 7		
1.4.	References	8	
	TER 2 Diacetato-bridged Diuranyl(VI) Complexed ties and Extraction Studies	s : Structures,	
2.1.	Introduction	13	
2.2.	Experimental	14	
2.3.	Results and discussion	20	
2.4.	Conclusions	40	
2.5.	References	42	
СНАРТ	TER 3 Syntheses, Structural Insight and	Photocatalytic	
Applica	ations of Di-μ-hydroxo Diuranyl(VI) Complexes		
3.1.	Introduction	47	
3.2.	Experimental	48	
3.3.	Results and discussion	51	
3.4.	Conclusions	69	
3.5.	References	70	

CHAPTER 4	Electrocatalytic and Photocatalytic Hydrogen Evolution	
using a Diuranyl(VI) Complex from Neutral Aqueous Medium		

4.1.	Introduction	75
4.2.	Experimental	76
4.3.	Results and discussion	81
4.4.	Conclusions	101
4.5.	References	102
СНАРТ	TER 5 Catecholase Activity of Chiral Diuranyl(VI)	Complexes:
Experin	nental and Computational Study	
5.1.	Introduction	106
5.2.	Experimental	107
5.3.	Results and discussion 114	
5.4.	Conclusions 1	
5.5.	References	135
Append	lix	139
Plagiarism Report		151
List of Publications		

SYNOPSIS

This thesis entitled "Diuranyl(VI) Complexes with Some Tri- and Tetradentate Ligands and Their Applications" consists of five chapters. These are (1) Introduction, (2) Diacetato-bridged Diuranyl(VI) Complexes: Structures, Properties and Extraction Studies, (3) Syntheses, Structural Insight and Photocatalytic Applications of Di-μ-hydroxo Diuranyl(VI) Complexes, (4) Electrocatalytic and Photocatalytic Hydrogen Evolution Using a Diuranyl(VI) Complex from Neutral Aqueous Medium, (5) Catecholase Activity of Chiral Diuranyl(VI) Complexes: Experimental and Computational Study. Each of the chapters, except for introduction, contains the following sections: Introduction, Experimental Section, Results and Discussions, Conclusions and References.

Chapter 1

Introduction

In this chapter we have discussed the coordination chemistry of the uranyl (UO_2^{2+}) moiety and its applications in the field of extraction, photocatalysis and electrocatalysis.

Chapter 2

Diacetato-bridged Diuranyl(VI) Complexes: Structures, Properties and Extraction Studies

Reactions of equimolar amounts of $UO_2(OAc)_2 \cdot 2H_2O$ and N-(2- pyridyl)-N'-(5-R-salicylidene)hydrazines (HL^n ; n=1-3 for R=H, Me, and OMe, respectively) in methanol produced [$(UO_2)_2(\mu\text{-OAc})_2(L^n)_2$] (**1**-3 for n=1-3) in ~70% yields. Elemental analysis, various spectroscopic, and electrochemical measurements were used to characterize **1**-3. X-ray crystal structures revealed an 8- membered $U(OCO)_2U$ ring with a chair conformation and pentagonal-bipyramidal UN_2O_5 coordination spheres in each of **1**-3. The N,N,O-donor (L^n) and the two O-atoms of the two bridging $(OAc)^-$ form the pentagonal plane around the U-atom of trans-(UO_2)²⁺. Intermolecular H-bonding assisted self-assembly of the complexes lead to 1- and 2-dimensional supramolecular structures. Infrared (IR) and proton

nuclear magnetic resonance (^{1}H NMR) spectra of **1–3** are consistent with their molecular structures. The electronic spectra showed four strong absorption bands in the range 466–288 nm. The complexes undergo two irreversible reductions near –0.65 and –0.88 V (vs. Ag/AgCl). Time-dependent density functional theory (TD-DFT) calculations suggest that a ligand centered transition causes the highest energy absorption band, while, the remaining three are ligand-to-metal charge transfer (LMCT) bands and the two successive reductions are due to $U(VI)-U(VI) \rightarrow U(V)-U(VI) \rightarrow U(V)-U(V)$ processes. A maximum extraction of 98% of *trans*- $(UO_2)^{2+}$ from the aqueous layer was observed in two phase extraction studies.

Chart 1. Chemical structure diagrams of HL^n and $[(UO_2)_2(\mu\text{-OAc})_2(L^n)_2]$.

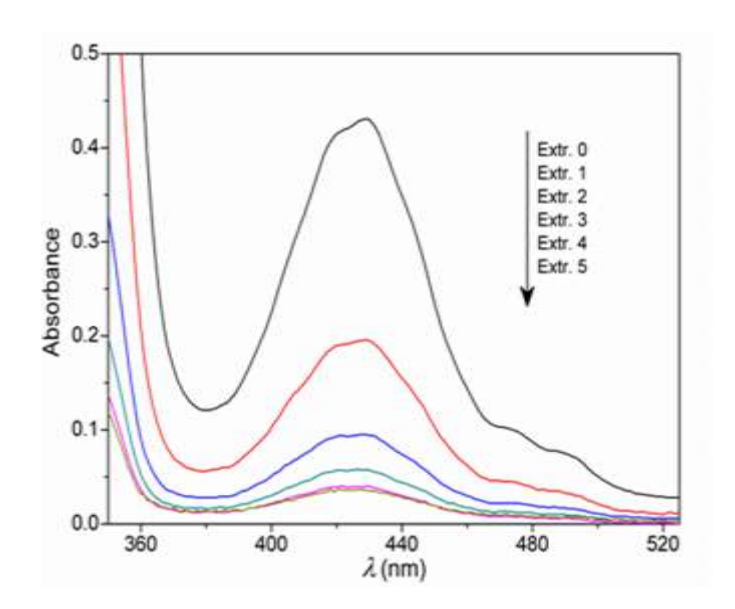


Figure 1: Electronic spectroscopic profiles of the aqueous phase (pH 6) containing UO₂(OAc)₂ recorded after sequential extractions of *trans*-uranyl(VI) dication using CHCl₃ solutions of HL².

Chapter 3

Syntheses, Structural Insight and Photocatalytic Applications of Di- μ -hydroxo Diuranyl(VI) Complexes

Two new dihyroxo-bridged diuranyl(VI) complexes of the molecular formula $[(UO_2)_2(\mu\text{-OH})_2(L^n)_2]$ (1 and 2) were synthesized in good yields (~64%) by reacting equimolar amounts of $[UO_2(OAc)_2]\cdot 2H_2O$ and 2-((2-(6-chloropyridazin-3-yl)hydrazono)methyl)-4-R-phenols (HLⁿ where n = 1 and 2 for R = H and OMe, respectively) in dimethylformamide. Both complexes were characterized by elemental analysis, various spectroscopic and cyclic voltammetric measurements. X-ray crystal structures of the two complexes crystallized as solvated species showed the rare $\{(UO_2)_2(\mu\text{-OH})_2\}^{2+}$ core where each metal center is in a distorted pentagonal-bipyramidal N_2O_5 coordination sphere assembled by the two axial oxo atoms, two equatorial bridging hydroxo-O atoms and the equatorial N,N,O-donor (Lⁿ)⁻. The solvated complexes assemble through intermolecular bifurcated N–H···(O,O) and simple O–H···O and N–H···O hydrogen bonding interactions and form supramolecular one-dimensional chain-

like and three-dimensional network structures in the crystal lattices. Infrared and proton NMR spectroscopic characteristics of the two complexes corroborate their molecular structures. Electronic spectra of $\bf 1$ and $\bf 2$ display three strong absorptions in the range 405–301 nm. A metal centered irreversible reduction having the E_{pc} near -1.06 V (vs. Ag/AgCl) has been observed in the cyclic voltammograms of $\bf 1$ and $\bf 2$. Both complexes are photocatalytically active in degradation of rhodamine B (RhB) and methylene blue (MB) under visible light irradiation. Photodegradation of RhB up to a maximum of 96% and that of MB up to a maximum of 85% was achieved in 150 and 180 min, respectively using $\bf 2$ as catalyst.

Chart 2. Chemical structure diagrams of 2-((2-(6-chloropyridazin-3-yl)hydrazono)methyl)-4-R-phenols (HLⁿ) and their corresponding complexes $[(UO_2)_2(\mu\text{-OH})_2(L^n)_2]$.

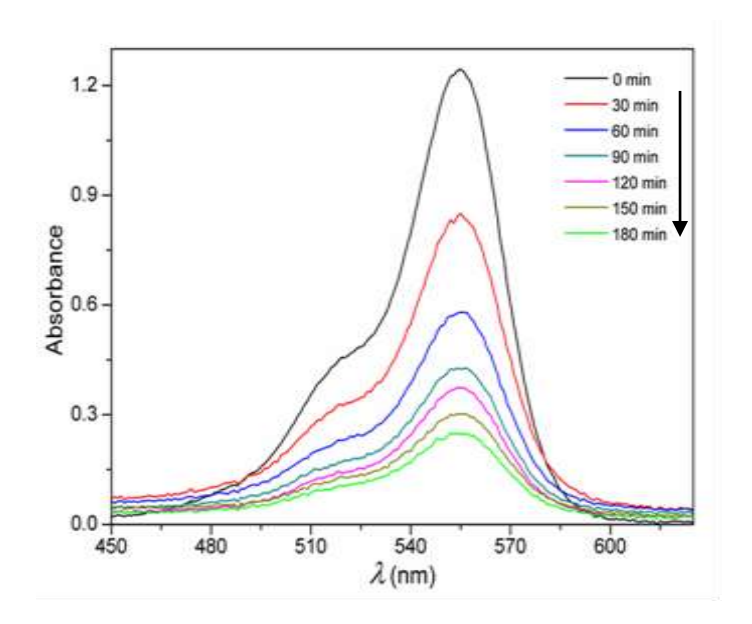


Figure 2: Degradation of Rhodamine B (RhB) under visible light irradiation in presence of $[(UO_2)_2(\mu\text{-OH})_2(L^1)_2]$ (1) as catalyst.

Chapter 4

Electrocatalytic and Photocatalytic Hydrogen Evolution using a Diuranyl(VI) Complex from Neutral Aqueous Medium

The reaction of equimolar amounts of $UO_2(OAc)_2 \cdot 2H_2O$, 2,6-diformyl-4-methylphenol and N-(hydroxyethyl)ethylenediamine in methanol affords a dinuclear *trans*-uranyl(VI) complex of the molecular formula $[(UO_2)_2(\mu-L)_2]$ (L^2 – 2-formyl-4-methyl-6-((2-(2-oxidoethylamino)ethylimino)methyl)phenolate) in 65% yield. Detailed structural elucidation of the complex was performed by using single crystal X-ray crystallographic and spectroscopic studies. In $[(UO_2)_2(\mu-L)_2]$, the metal centers are in edge-shared pentagonal bipyramidal N_2O_5 coordination spheres assembled by the two meridional ONNO-donor bridging L^2 and two pairs of mutually *trans*-oriented oxo groups. The complex is redox active and displays two successive metal centered one-electron reductions at $E_{pc} = -0.71$ and -1.03 V in *N,N*-dimethylformamide solution. The redox active complex was used as a heterogeneous catalyst for electrochemical hydrogen evolution from aqueous medium at pH 7 with a turnover frequency (TOF) of 384 h^{-1} and a Tafel slope of 274 mV dec $^{-1}$. The Faradaic efficiency of $[(UO_2)_2(\mu-L)_2]$

was found as 84%. Beyond electrocatalytic response, the $[(UO_2)_2(\mu-L)_2]$ -TiO₂-N719 composite also exhibited significant heterogeneous photocatalytic hydrogen evolution activity in neutral aqueous medium under visible light and provided a yield of 3439 μ mol g_{cat}^{-1} of H_2 in 4 h with a TOF of 172 h⁻¹ and apparent quantum yield (AQY) of 7.6%.

Scheme 3. Synthesis of $[(UO_2)_2(\mu-L)_2]$.

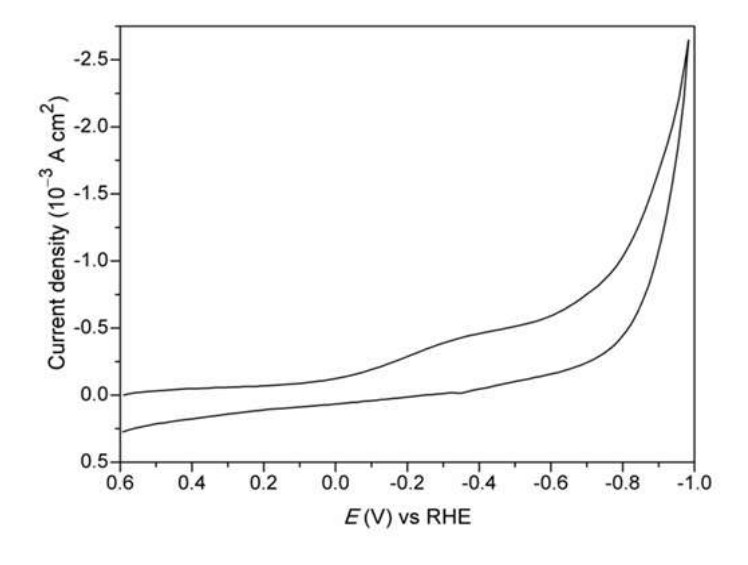


Figure 3: Cyclic voltammogram of $[(UO_2)_2(\mu-L)_2]$ at a scan rate of 100 mV s⁻¹ representing electrocatalytic hydrogen evolution.

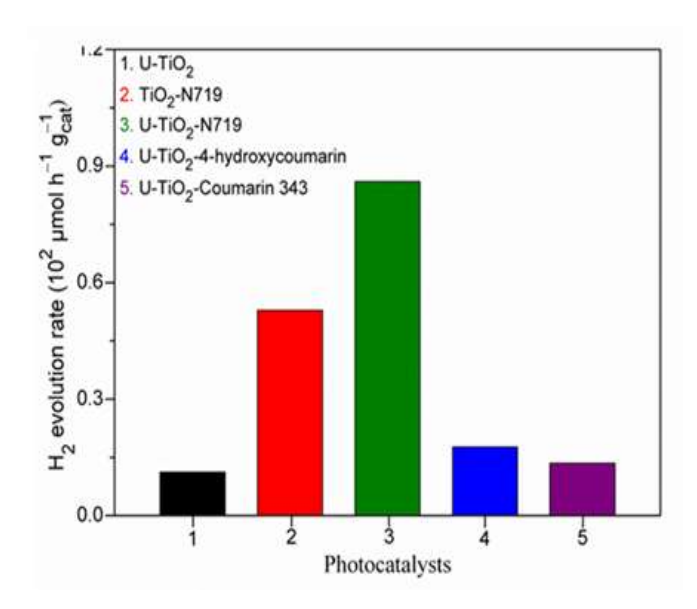


Figure 4: Bar graph representation of the photocatalytic hydrogen production activity.

Chapter 5

Catecholase Activity of Chiral Diuranyl(VI) Complexes: Experimental and Computational Study

Four chiral dinuclear uranyl(VI) complexes with the general molecular formulas $[(UO_2)_2(R/S-L^1)_2(H_2O)_2]\cdot 2CH_3CN$ (1·2CH₃CN and 2·2CH₃CN) and $[(UO_2)_2(R/S-L^1)_2(H_2O)_2]\cdot 2CH_3CN$ L^2 ₂(Me₂NCHO)₂] (3 and 4) (where, $(R/S-L^1)^{2-} = (R/S)-2-((1-\text{oxidopropan-}2-\text$ $(R/S-L^2)^{2-} = (R/S)-1-((1-oxidopropan-2$ ylimino)methyl)-phenolate and ylimino)methyl)naphthalen-2-olate) were synthesized in 70-75 % yields. The complexes were characterized by elemental analyses, mass spectrometric, magnetic susceptibility and solution electrical conductivity measurements. Single crystal X-ray diffraction studies confirmed the dinuclear structure and pentagonal-bipyramidal NO₆ coordination sphere around the metal atoms in 1–4. In each complex, the metal centers of the two trans-UO₂²⁺ units reside in a NO₄ pentagonal plane constituted by the two alkoxide end bridging ONO-coordinating $(L^{1/2})^{2-}$ and the two O-coordinating solvent (H₂O or Me₂NCHO) molecules. Spectroscopic (IR, UV–Vis and ¹H-NMR) features of the complexes corroborate well with their X-ray molecular structures. Complexes 3 and 4 exhibit good catecholase-like activity (oxidation of 3,5-di-tert-butylcatechol (3,5-DTBC) to 3,5-di-tert-butylquinone (3,5-DTBQ)) in Me₂NCHO solution with TOF as high as 3686 and 3774 h⁻¹. For both complexes, the catalytic reaction follows a radical pathway, as is confirmed by a sharp EPR signal at g = 1.99. A computational study of the reaction mechanism suggests a η^2 -syn type conformation of the adduct between the substrate and each of the two catalysts 3 and 4, which is favorable for an effective catalysis. On the other hand, an unfavorable η^1 -anti conformation of the substrate—catalyst adduct has been found for both 1 and 2. This conformation results in inactivity of both 1 and 2 towards the catecholase activity.

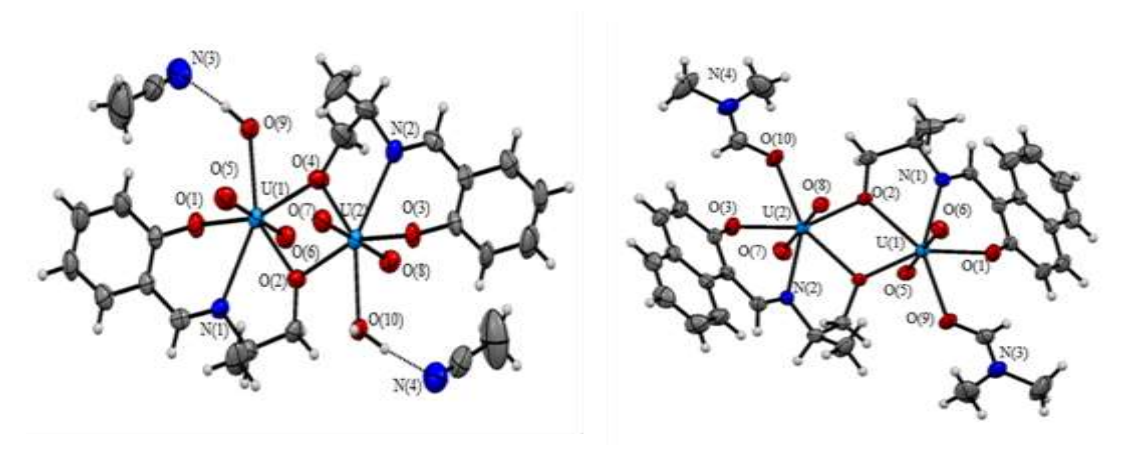


Figure 5: Molecular structures of $[(UO_2)_2(R-L^1)_2(H_2O)_2]\cdot 2CH_3CN$ (1·2CH₃CN) (left) and $[(UO_2)_2(R-L^2)_2(Me_2NCHO)_2]$ (3) (right).

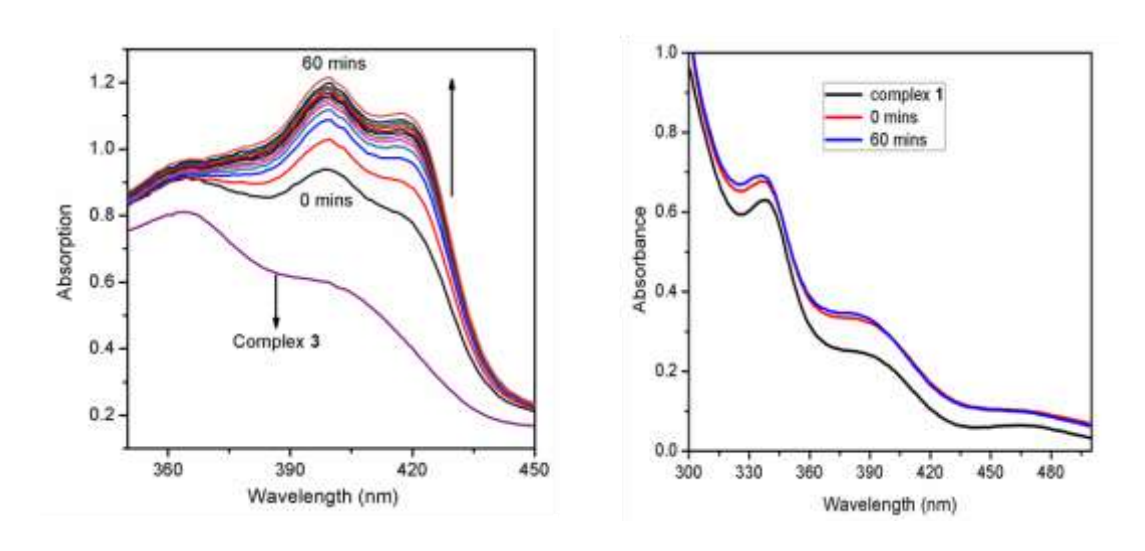


Figure 6: Complex **3** showing catecholase activity (left). Inactivity of complex **1** towards oxidation of 3,5-DTBC to 3,5-DTBQ (right).

Introduction

1.1. Uranium Chemistry:

Uranium is the heaviest element that occurs naturally in significant amount. The element essentially exists in the form of two isotopes, about 99.3% of the non-fissile U-238 and only about 0.7% of the fissile U-235. The element can exist in a variety of oxidation state starting from +2 to +6. Among all the oxidation states +6 is the most stable and mainly exists as uranyl ion (UO₂²⁺). This uranyl dication is the leading functional unit in uranium chemistry.

The strongly covalent U-O bonds in trans-(UO₂)²⁺ is the most dominant functional unit in uranium chemistry and is known for its remarkable thermal and chemical stability, which contributes various interesting physicochemical properties to it and its complexes. In comparison to the other well-known dioxometal ions² such as $(VO_2)^+$, $(MoO_2)^{2+}$ and $(WO_2)^{2+}$, the chemistry of trans-uranyl dication moiety is much less explored.³ However, in the recent years there is an active interest towards actinide chemistry⁴ and to study the role of uranium in both fundamental research as well as potential applications. The structure and geometry of trans-uranyl(VI) complexes are governed by the local geometry of the central metal atom. Since the axial planes around the metal is already occupied by the trans oriented oxo groups, the ligand orientation is restricted to only the equatorial plane only giving rise to a variety of coordination environments ranging from tetragonal six-coordination or octahedral to pentagonal seven-coordination or pentagonal-bipyramidal to hexagonal eightcoordination or hexagonal-bipyramidal. Schiff bases being one of the major chelating ligands have been known to form interesting coordination complexes with the linear uranyl (UO₂)²⁺ ion.⁵ In the recent years, uranium chemistry particularly the uranyl moiety has been largely exploited not only due to its fascinating coordination chemistry but also because of its application towards remediation of nuclear waste along with extraction of uranium from ground and sea water. In addition to its reactivity and coordination behavior, the trans-

(UO₂)²⁺ has also gained considerable attention for its optical, catalytic as well as ion exchange applications.⁶ Some of the important applications of the uranyl moiety has been discussed in detail below.

1.2. Importance of trans-uranyl (UO₂)²⁺ Complexes

1.2.1. Extraction of uranium from ground and sea water:

The oceans contain as large as 4.5 billion tons of uranium and hence can be a potential source for nuclear fuel. Presence of uranium in underground water is one of the major sources of human ingestion of uranium. Thus, it is both strategically as well as ecologically important to extract uranium(VI) from aqueous solutions. The uranium present in the ocean as uranyl dication (UO₂)²⁺, which is soluble in water and is also present in very low concentration dissolved in significantly large volume. Moreover, the uranyl present in the sea water is bound to various anions and has other metal ions present in much higher concentrations. Thus, extraction of uranium from sea as well as ground water is quite challenging along with being equally important from societal point of view. Various methods such as sorption, solvent extraction, coprecipitation and membrane filtration have been employed for extraction of uranium(VI) from aqueous solution. A variety of ligand systems such as organic crown ethers, calixarenes and modified calixarenes and Schiff bases have been used as efficient extractants (Figure 1) for actinide removal from aqueous layer.

Figure 1: Examples of ligand systems used as extractants for uranyl extraction.

1.2.2. Photocatalytic Activities:

Photocatalysis is used very effectively for elimination of organic pollutants from the environment. The most commercial phtocatalysts used till date is TiO₂ which is UV light driven and also suffers the problem of high band gap, thus restricting their practical applications. ¹⁴ Owing to the problem of photo-corrosion several visible light driven phtocatalysts such as CdS and CdSe has limited usage. ¹⁵ These factors led to the increasing demand of constructing band gap tunable, stable, visible light driven photocatalysts for degradation of organic dyes, the common organic pollutants.

Photocatalytic behavior of uranyl compounds have been exploited since early 1800s. 16 Absorptions of the uranyl-organic complexes in the UV and visible region is attributed to the charge transfer transitions within the uranyl moiety.¹⁷ These transitions clearly indicate that uranyl complexes are responsive to both UV as well as visible light. In the recent past uranyl organic frameworks (UOFs) have been exhibiting many interesting physical and chemical properties photocatalysis being one of them.¹⁸ The photoexcitation of UO₂²⁺ leads to *UO2²⁺. This excited uranyl species on one hand, relaxes back to its ground state by emitting visible light and on the other hand it is a very reactive species having a oxidation potential as high as 2.6 eV.¹⁹ Thus, a complex containing one or more uranyl moiety may be capable of exhibiting both photocatalytic as well as photoluminescent properties simultaneously. Comparing the conventional photocatalyst TiO₂ with uranyl ion (UO₂²⁺) it is found that the latter has a much higher efficiency than the former. The efficacy of uranyl catalysts over TiO₂ can be accredited to not only its strong absorption upon visible light irradiation but also because of its distinct photocatlytic mechanism involving electron transfer and hydrogen abstraction.

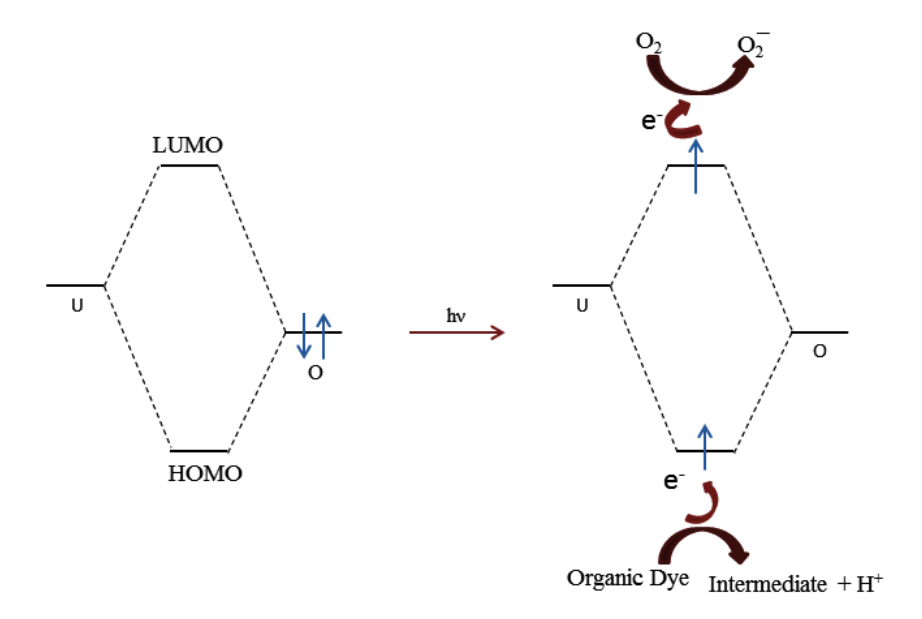


Figure 2: Mechanism of electron transfer during photocatalytic activities in uranyl complexes.

1.2.3. Electrocatalytic and photocatalytic hydrogen evolution:

Hydrogen is the next generation fuel. It is not only a clean and green source of energy but also has the highest energy density for any known fuel till date.²⁰ Current H₂ formation relies on steam reformation of fossil fuels emitting greenhouses gases.²¹ So, producing hydrogen is not the only concern, but the method of hydrogen production is equally important. Production of H₂ from water is the most desirable as the by–product is only oxygen. Till date Pt is known to be the state-of-art electrocatalyst and considered as the benchmark for deciding the electrocatalytic activity of other hydrogen evolution reaction (HER) catalysts.²² Other Pt group metals are also known to show excellent HER activity followed by transition metals iron (Fe), cobalt (Co), nickel (Ni), copper (Cu), molybdenum (Mo), and tungsten (W). Various nonmetals such as boron (B), carbon (C), phosphorous (P) and selenium (Se) are also used for constructing noble metal–free HER electrocatalysts.²³ However, the high cost and low abundance of the Pt group metals have urged the need of constructing electrocatalysts based on abundant non–noble based metals.

Hydrogen evolution via water splitting can take place in neutral, alkaline as well as in acidic medium according to the following equation.

Total reaction

$$H_2O \longrightarrow H_2 + 1/2 O_2$$

In acidic solution,

Cathode:
$$2H^+ + 2e^- \longrightarrow H_2$$

Anode: $H_2O \longrightarrow 2H^+ + 1/2 O_2 + 2e^-$

In neutral or alkaline solutions,

Cathode:
$$2H_2O + 2e^ \longrightarrow$$
 $H_2 + 2OH^-$
Anode: $2OH^ \longrightarrow$ $H_2O + 1/2 O_2 + 2e^-$

The thermodynamic potential required for water splitting is 1.23 V at 25 °C and 1 atm pressure. Thus, we must apply voltage greater than the thermodynamic voltage to achieve successful water splitting. This excess potential that is required is termed as the overpotential (η) .²³ Thus, lower the value of overpotential the more energy-efficient is the water splitting reaction. As a result, there is a tremendous effort to design efficient water splitting catalysts for hydrogen production with overpotential as low as possible from earth-abundant elements.

Use of renewable energy such as sunlight towards water splitting for generation of hydrogen has gained immense importance during the last decade. The first water splitting photocatalyst²⁴ designed by Fujishima and Honda in 1972 using anatase TiO₂ electrode as anode and platinum electrode as cathode used only 4% of the sunlight for hydrogen production. Thus, there is a continuous quest of preparing photocatalysts with better light harvesting capacity which can absorb light in the UV–Vis region which constitutes about 40% of the total sunlight.²⁵ Among all the semiconductors used for hydrogen production, TiO₂ has the best light harvesting capacity but suffers the problem of a large band gap (3.2 eV). To overcome this deficit, an approach towards designing hybrid systems containing various dyes and metal loaded with TiO₂ have been considered which not only decrease the band gap of TiO₂ but also possess better light harvesting ability.^{25,26}

Uranyl complexes, to the best of our knowledge, have not been used till date as a catalyst or a co-catalyst for photocatalytic water splitting.

Depleted uranium is the chief source of radioactive waste all over the world. Thus, utilization of depleted uranium is essential from environment point of view. In the recent decade, uranium has been exploited for activation of various small molecules such as CO₂, CO, N₂ and H₂O.²⁷ However, application of uranium towards electrochemical or photochemical hydrogen production via water reduction is in its infancy. Recently, Meyer and group reported electrolytic hydrogen evolution using low valent uranium²⁸ and it is the first report of uranium being used as an electrocatalyst for HER activity (Figure 3).

Figure 3: The first uranium catalyst used for electrocatalytic hydrogen production.

1.3. About the present work:

In the present study, the *trans*-uranyl(VI) coordination chemistry with four Schiff base ligand systems (Figure 4) has been extensively studied. Various dinuclear uranyl complexes containing diverse bridging units between the metal centers have been synthesized. Elemental analysis, mass spectrometry and detailed spectroscopic analysis using various techniques such as IR, UV-Vis, and NMR have been used for characterization of the prepared complexes. Redox properties have been investigated by cyclic and differential pulse voltammetry and coulometry. Structural elucidation of all the complexes has been done using X-ray crystallography. Along with the syntheses and characterization, the applications of the complexes in extraction, photocatalysis, hydrogen evolution and catechol to quinone oxidation have been demonstrated.

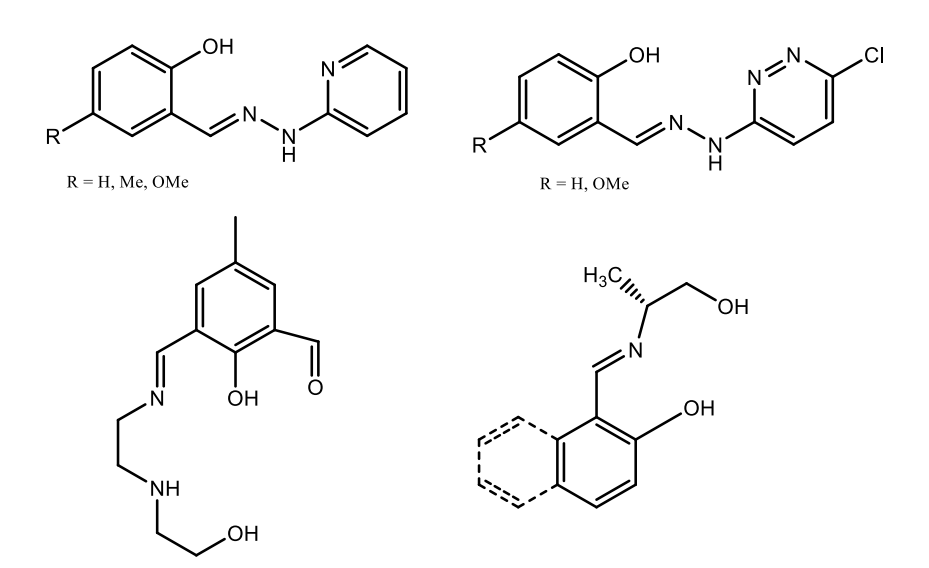


Figure 4: Ligand systems that have been investigated in the present study.

1.4. References

(a) P. L. Arnold, A.-F. Pécharman, E. Hollis, A. Yahia, L. Maron, S. Parsons, J. B. Love, *Nat. Chem.* 2010, 2, 1056. (b) J. L. Brown, G. Wu, T. W. Hayton, *J. Am. Chem. Soc.* 2010, 132, 7248. (c) J. J. Kiernicki, M. Zeller, S. C. Bart, *Angew. Chem.* 2017, 129, 1117 (d) R. G. Denning, *Struct. Bonding* 1992, 79, 215. (e) R. G. Denning, *J. Phys. Chem. A*, 2007, 111, 4125.

- (a) B. Mondal, M. G. B. Drew, T. Ghosh, *Inorg. Chim. Acta* 2010, 363, 2296. b) M. R. Maurya, *J. Chem. Sci.* 2011, 123, 215. (c) M. Sutradhar, A. J. L. Pombeiro, *Coord. Chem. Rev.* 2014, 265, 89. (d) R. D. Chakravarthy, D. K. Chand, *J. Chem. Sci.* 2011, 123, 187. (e) B. I. Ceylan, N. G. Deniz, S. Kahraman, B. Ulkuseven, *Spectrochim. Acta Part A* 2015, 141, 272. (f) A. A. Eagle, E. R. T. Tiekink, C. G. Young, *Inorg. Chem.* 1997, 36, 6315. (g) Y.-L. Wong, J.-F. Ma, F. Xue, T. C. W. Mak, D. K. P. Nag, *Organometallics* 1999, 18, 5075. (h) V. S. Sergienko, *Russ J. Inorg. Chem.* 2000, 45, S37. (i) Y.-L. Wong, L. H. Tong, J. R. Dilworth, D. K. P. Ng, H. K. Lee, *Dalton Trans.* 2010, 39, 4602. (j) V. Vrdoljak, J. Pisk, D. Agustin, P. Novak, J. P. Vukovic´, D. Matkovic´-Cˇ alogovic´, *New J. Chem.* 2014, 38, 6176.
- (a) M. R. Maurya, R. C. Maurya, Rev. Inorg. Chem. 1995, 15, 1. (b) J. L. Sessler, P. J. Melfi, G. D. Pantos, Coord. Chem. Rev. 2006, 250, 816. (c) P. A. Giesting, P. C. Burns, Crystallogr. Rev. 2006, 12, 205. (d) K.-X. Wang, J.-S. Chen, Acc. Chem. Res. 2011, 44, 531. e) R. J. Baker, Chem. Eur. J. 2012, 18, 16258. (f) K. Kiegiel, L. Steczek, G. Zakrzewska- Trznadel, J. Chem. 2013, 762819, doi: 10.1155/2013/762819. (g) A. G. Beirakhov, I. M. Orlova, Y. N. Mikhailov, Russ. J. Inorg. Chem. 2014, 59, 1679. (h) T. Loiseau, I. Mihalcea, N. Henry, C. Volkringer, Coord. Chem. Rev. 2014, 266–267, 69.
- (a) D. Wang, W.F. van Gunsteren, *Prog Chem.* 2011, 23, 1566. (b) A.R. Fox, S.C. Bart, K. Meyer, C.C. Cummins, *Nature* 2008, 455, 341. (c) T.E. Albrecht-Schmitt, *Springer* 2008, 127. (d) L.S. Natrajan, *Coordin. Chem.*

Rev. 2012, 256, 1583. (e) D. Wang, W.F. van Gunsteren, Z. Chai, Chem. Soc. Rev. 2012, 41, 5836.

- 5. (a) A. K. Sah, C. P. Rao, P. K. Saarenketo, E. K. Wegelius, E. Kolehmainen, K. Rissanen, Eur. J. Inorg. Chem. 2001, 2773. (b) S. Fortier, T. W. Hayton, Coord. Chem. Rev., 2010, 254, 197. (c) P. L. Arnold, A. J. Blake, C. Wilson, J. B. Love, *Inorg. Chem.* 2004, 43, 8206. (d) M. S. Bharara, K. Strawbridge, J. Z. Vilsek, T. H. Bray, A. E. V. Gorden, *Inorg*. Chem. 2007, 46, 8309. (e) S. Zhang, X. W. Shu, Y. Zhou, L. Huang, D. B. Hua, Chem. Eng. J. 2014, 253, 55. (f) M. S. Bharara, K. Heflin, S. Tonks, K. L. Strawbridge, A. E. V. Gorden, Dalton Trans. 2008, 2966. (g) H. C. Hardwick, D. S. Royal, M. Helliwell, S. J. A. Pope, L. Ashton, R. Goodacre, C. A. Sharrad, Dalton Trans. 2011, 40, 5939. (h) Z. Asadi, M. Asadi, A. Zeinali, M. Ranjkeshshorkaei, K. Fejfarova, V. Eigner, M. Dusek, A. Dehnokhalaji, J. Chem. Sci. 2014, 126, 1673. (i) Y. Wei, L. Mol.Shen, D. Hua, J. Zhang, L. Liq., 2015, DOI: 10.1016/j.molliq.2015.04.056. (k) Y. Zhang, D. J. Fanna, N. D. Shepherd, I. Karatchevtseva, K. Lu, L. Kong, J. R. Price, RSC Adv. 2016, 6, 75045. (l) M. Azam, G. Velmurugan, S. M. Wabaidur, A. Trzesowska-Kruszynska, R. Kruszynski, S. I. Al-Resayes, Z. A. Al-Othman, P. Venuvanalingam, Sci. Rep. **2016**, 6, 1, doi: 10.1038/srep32898. (m) H. B. T. Jeazet, K. Gloe, T. Doert, J. Mizera, O. N. Kataeva, S. Tsushima, G. Bernhard, J. J. Weigand, L. F. Lindoy, K. Gloe, *Polyhedron* 2016, 103, 198. (n) E. E. Hardy, K. M. Wyss, M. A. Eddy, A. E. V. Gorden, Chem. Commun. 2017, 53, 5718. o) J. R. Pankhurst, N. L. Bell, M. Zegke, L. N. Platts, C. A. Lamfsus, L. Maron, L. S. Natrajan, S. Sproules, P. L. Arnold, J. B. Love, *Chem. Sci.* **2017**, *8*, 108. (p) J. E. Niklas, B. H. Farnum, J. D. Gorden, A. E. V. Gorden, Organometallics 2017, 36, 4626.
- (a) A. C. Bean, S. M. Peper, T. E. Albrecht-Schmitt, *Chem. Mater.* 2001,
 13, 1266. (b) L. Salmon, P. Thuerry, E. Riviére, J.-J. Girerd, M. Ephritikhine, *Dalton Trans.* 2003, 2872. (c) L. Salmon, P. Thuerry, E. Riviére, J.-J. Girerd, M. Ephritikhine, *Chem. Commun.* 2003, 762. (d) W.

- D. Wang, A. Bakac, J. H. Espenson, *Inorg. Chem.* **1995**, *34*, 6034. J. L. Sessler, P. J. Melfi, G. Dan Pantos, *Coord. Chem.Rev.* **2006**, 250, 816.
- (a) J. Kim, C. Tsouris, R. T. Mayes, Y. Oyola, T. Saito, C. J. Janke, S. Dai,
 E. Schneider, D. Sachde, Sep. Sci. Technol. 2013, 48, 367. (b) Y. Lu, Nat.
 Chem. 2014, 6, 175.
- (a) A. C. Sather, O. B. Berryman, J. Rebek Jr, J. Am. Chem. Soc. 2010, 132, 13572.
 (b) B. E. Johnson, P. H. Santschi, C. Y. Chuang, S. Otosaka, R. S. Addleman, M. Douglas, R. D. Rutledge, W. Chouyyok, J. D. Davidson, G. E. Fryxell, Environ. Sci. Technol. 2012, 46, 11251.
- 9. J. Lapka, A. Paulenova, M. Y. Alyapyshev, V. Babain, R. Herbst, J. D. Law, *Radiochim. Acta* **2009**, *97*, 291.
- (a) R. Ganesh, K. G. Robinson, L. Chu, D. Kucsmas, G. D. Reed, *Water Res.* 1999, *33*, 3447.
 (b) A. Baeza, M. Fernandez, M. Herranz, F. Legarda, C. Miro, A. Salas, *Water, Air, Soil Pollut.* 2006, *173*, 57.
- 11. A. J. Semi ao, H. Rossiter, A. I. Sch afer, J. Membr. Sci. 2010, 348, 174.
- P. D. Beer, G. D. Brindley, D. O. Fox, A. Grieve, M. I. Ogden, F. Szeme,
 M. G. B. Drew, J. Chem. Soc., Dalton Trans. 2002, 3101.
- 13. J. L. Sessler, P. J. Melfi, G. D. Pantos, Coord. Chem. Rev. 2006, 250, 816.
- 14. S. Sakthivel, H. Kisch, Angew. Chem. Int. Ed. 2003, 115, 5057.
- (a) K. G. Kim, D. W. Hwang, J. S. Lee, *J. Am. Chem. Soc.* **2004**, *126*, 8912.
 (b) Z. Lei, W. You, M. Liu, G. Zhou, T. Takata, M. Hara, K. Domen, C. Li, *Chem. Commun.* **2003**, 2142.
- 16. H. D. Burrows, T. J. Kemp, *Chem. Soc. Rev.* **1974**, 139.
- 17. R. G. Denning, J. O. W. Norris, I. G. Short, T. R. Snellgrove, D. R. Woodwark, In Lanthanide and Actinide Chemistry and Spectroscopy; Edelstein, N. M., Ed.; ACS Symposium Series 131; American Chemical Society: Washington, DC, 1980; Chapter 15.
- (a) Z. T. Yu, Z. L. Liao, Y. S. Jiang, G. H. Li, J. S. Chen, *Chem. Eur. J.* 2005, 11, 2642. (b) Z. L. Liao, G. D. Li, M. H. Bi, J. S. Chen, *Inorg. Chem.* 2008, 47, 4844. (c) Z. T. Yu, Z. L.Liao, Y. S. Jiang, G. H. Li, G. D. Li, J. S. Chen, *Chem. Commun.* 2004, 1814. (d) H. Wang, Z. Chang, Y. Li, R. M. Wen, X. H. Bu, *Chem. Commun.* 2013, 49, 6659.

- 19. T. M. McCleskey, C. J. Burns, W. Tumas, *Inorg. Chem.* **1999**, *38*, 5924.
- (a) W. Lubitz, W. Tumas, *Chem. Rev.* 2007, 107, 3900. (b) S. Dutta, *J. Ind. Eng. Chem.* 2014, 20, 1148. (c) I. Staffell, D. Scamman, A. V. Abad, P. Balcombe, P. E. Dodds, P. Ekins, N. Shah, K. R. Ward, *Energy Environ. Sci.* 2019, 12, 463.
- 21. A. J. Esswein, D. G. Nocera, Chem. Rev. 2007, 107, 4022.
- 22. M. Zeng, Y. Li, J. Mater. Chem. A 2015, 3, 14942.
- 23. X. Zouc, Y. Zhang, Chem. Soc. Rev. 2015, 44, 5148.
- 24. A. Fujishima, K. Honda, Nature 1972, 238, 37.
- (a) A. A. Ismail, D. W. Bahnemann, *Sol. Energy Mater. Sol. Cells* 2014, 128, 85. (b) S. Rajaambal, K. Sivaranjani, C. S. Gopinath, *J. Chem. Sci.* 2015, 127, 33. (c) T. Jafari, E. Moharreri, A. S. Amin, R. Miao, W. Song, S. L. Suib, *Molecules* 2016, 21, 900. (d) K. Takanabe, *ACS Catal.* 2017, 7, 8006. (e) Z. Wang, C. Li, K. Domen, *Chem. Soc. Rev.* 2019, 48, 2109.
- (a) R. J. Abe, *Photochem. Photobiol. C* 2010, 11, 179. (b) X. B. Chen, S. H. Shen, L. J. Guo, S. S. Mao, *Chem. Rev.* 2010, 110, 6503. (c) Y. Qu, X. Duan, *Chem. Soc. Rev.* 2013, 42, 2568. (d) X. H. Zhang, T. Y. Peng, S. S. Song, *J. Mater. Chem. A* 2016, 4, 2365. (e) H. Junge, N. Rockstroh, S. Fischer, A. Brückner, R. Ludwig, S. Lochbrunner, O. Kühn, M. Beller, *Inorganics* 2017, 5, doi:10.3390/inorganics5010014.
- 27. (a) H. S. La Pierre, K. Meyer, Prog. *Inorg. Chem.* **2014**, *58*, 303. (b) A.-C. Schmidt, A. V. Nizovtsev, A. Scheurer, F. W. Heinemann, K. Meyer, *Chem. Commun.* **2012**, *48*, 8634.
- 28. D. P. Halter, F. W. Heinemann, J. Bachmann, K. Meyer, *Nature* **2016**, *530*, 317.

Diacetato-bridged Diuranyl(VI) Complexes: Structures, Properties and Extraction Studies §

Reactions of equimolar amounts of UO₂(OAc)₂·2H₂O and N-(2- pyridyl)-N'-(5-R-salicylidene)hydrazines (HLⁿ; n=1-3 for R=H, Me, and OMe, respectively) in methanol produced $[(UO_2)_2(\mu\text{-OAc})_2(L^n)_2]$ (1–3 for n=1–3) in ~70% yields. Elemental analysis, various spectroscopic, and electrochemical measurements were used to characterize 1–3. X–ray crystal structures revealed an 8– membered U(OCO)₂U ring with a chair conformation and pentagonal-bipyramidal UN₂O₅ coordination spheres in each of 1–3. The N,N,O-donor (Lⁿ)[–] and the two O-atoms of the two bridging (OAc) form the pentagonal plane around the U-atom of trans-(UO₂)²⁺. Intermolecular H-bonding assisted self-assembly of the complexes lead to 1- and 2-dimensional supramolecular structures. Infrared (IR) and proton nuclear magnetic resonance (¹H NMR) spectra of 1-3 are consistent with their molecular structures. The electronic spectra showed four strong absorption bands in the range 466-288 nm. The complexes undergo two irreversible reductions near -0.65 and -0.88 V (vs. Ag/AgCl). Time-dependent density functional theory (TD-DFT) calculations suggest that a ligand centered transition causes the highest energy absorption band, while, the remaining three are ligand-to-metal charge transfer (LMCT) bands and the two successive reductions are due to $U(VI)-U(VI) \rightarrow U(V)-U(VI) \rightarrow U(V)-U(V)$ processes. A maximum extraction of 98% of trans-(UO₂)²⁺ from the aqueous layer was observed in two phase extraction studies.

[§] This work has been published in *ChemistrySelect* **2018**, *3*, 1–9.

2.1. Introduction

The synthesis of stable environment friendly complexes of uranium and development of advanced techniques for uranium extraction from underground as well as seawater, in both micro as well as macro level, are crucial and challenging from not only the environmental point of view but also for use in energy production. In recent years, among the chelating organic ligands, Schiff-Bases have attracted considerable interest in exploring the coordination chemistry of the linear uranyl(VI) ion.² The primary reasons are as follows: Schiff bases are easy to design and synthesize; their steric and electronic characteristics can be tuned by changing substituents; they can provide very stable complexes and hence can act as an efficient sequestering agent for the extraction of the transuranyl(VI) dication. Hydrazine based Schiff bases and their complexes with various transition metal ions have been widely studied due to the variety in their coordination chemistry as well as their applications in the fields of biological, materials and pharmaceutical research.^{3,4} These ligands have turned out to be excellent in coordinating and stabilizing *cis*-dioxomolybdenum(VI) (*cis*-MoO₂²⁺) and a variety of oxo-vanadium(IV/V) units. The N,N,O-donor N-(2-pyridyl)-N'-(5-R-salicylidene)hydrazines (HLⁿ; where H represents the dissociable phenolic proton and n = 1-3 for R = H, Me, and OMe, respectively) (Chart 1) belong to this class of Schiff bases. These Schiff bases (HLⁿ) are known to exhibit amineimine and also imine-azo tautomerism processes involving the 2-pyridine-NHand the -NH-N=CH- fragments, respectively. 4e,f,5 In the present chapter, coordination chemistry of trans-(UO₂)²⁺ with HLⁿ has been investigated and in this process three new dinuclear diacetato bridged complexes having the general molecular formula $[(UO_2)_2(\mu\text{-OAc})_2(L^n)_2]$ (1–3 for n = 1–3) have been isolated (Chart 1). It may be noted that examples of discrete dinuclear complexes of {O₂U(*u*-OAc)₂UO₂}²⁺ core having pentagonal-bipyramidal metal centers, which are stable in both solid and solution states, are very rare. To the best of our knowledge, till date, only five X-ray structurally characterized complexes of this diacetato-bridged diuranyl(VI) core have been reported in literature.⁶ But the ligands around the pentagonal bipyramidal metal centers are either monodentate solvents/phosphine-oxide or monodenate/bidentate carboxylate ligands in all five complexes. We have also examined the dicationic *trans*-uranyl(VI) extraction abilities of HLⁿ from aqueous medium using both quantitative gravimetric filtration as well as sequential extraction methods. In the following account, we have described the synthetic details, physical properties and X–ray structures of complexes **1–3** and the extraction characteristics of HLⁿ.

Chart 1: Chemical structure diagrams of HL^n and $[(UO_2)_2(\mu\text{-OAc})_2(L^n)_2]$.

2.2. Experimental Section

2.2.1. Materials:

The Schiff bases N-(2-pyridyl)-N'-(5-R-salicylidene)-hydrazines (HL¹⁻³) were prepared from equimolar amounts of 2-hydrazinopyridine and the corresponding 5-R-salicylaldehydes (R = H, Me and OMe) using a reported procedure.⁷ All other chemicals and solvents used in this work were of analytical reagent grade available commercially and were used as received without further purification.

2.2.2. Physical Measurements:

Elemental (CHN) analyses were performed on a Thermo Finnigan Flash EA1112 series elemental analyser. A Shimadzu LCMS 2010 liquid chromatograph mass

spectrometer was used for the purity verification of HL¹⁻³. Magnetic susceptibilities were measured using a Sherwood Scientific balance. A Digisun DI-909 conductivity meter was used to measure the solution electrical conductivities. A Thermo Scientific Nicolet 380 or a Bruker Tensor-II FT-IR spectrophotometer was used to record the infrared spectra. Electronic spectra were collected using a Shimadzu UV-3600 UV-Vis-NIR spectrophotometer. The ¹H (400 MHz) NMR spectra were recorded on a Bruker NMR spectrometer. A CH Instruments model 620A electrochemical analyzer was used for cyclic and differential pulse voltammetric measurements. Coulometric experiments were performed with the help of a Zahner Zennium electrochemical workstation.

2.2.3. Synthesis of the Complexes $[(UO_2)_2(\mu\text{-}OAc)_2(L^{1-3})_2]$ (1-3):

All three complexes (1–3) were synthesized by employing the following general procedure. Solid UO₂(OAc)₂·2H₂O (425 mg, 1 mmol) was added to a hot methanol solution (25 mL) of the corresponding HLⁿ (1 mmol). The mixture was refluxed for 6 h. The resulting brown solution was filtered while hot to remove any precipitate appeared and then kept at room temperature for slow evaporation. After about 4 days, the volume of the reaction mixture reduced to approximately one-fifth of its original value and the complex was separated as a dark brown amorphous material with few crystalline particles. It was collected by filtration, washed with methanol and dried in vacuum.

[(UO₂)₂(μ -OAc)₂(L¹)₂] (1): Yield: 380 mg (70%). C₂₈H₂₆N₆O₁₀U₂ (1082.598): calcd. C 31.06, H 2.42, N 7.76; found C 31.17, H 2.36, N 7.65. Selected IR data: ν (cm⁻¹) = 3254 (N–H), 1621 (C=N), 1543 and 1426 (COO⁻), 883 (UO₂). UV–Vis data: λ_{max} (nm) (ε (10⁴ M⁻¹ cm⁻¹)) = 455^{sh} (1.51), 434 (1.71), 360 (2.40), 288 (2.39). ¹H NMR data: δ (ppm) (J (Hz)) = 10.01 (s, 1H, NH), 8.88 (s, 1H, H⁷), 7.96 (4) (dd \rightarrow t, 1H, H¹⁰), 7.54 (m, 3H, H^{9,11,12}), 7.22 (m, 2H, H^{3,4}), 7.04 (8) (d, 1H, H⁶), 6.74 (8) (dd \rightarrow t, 1H, H⁵), 2.33 (s, 3H, actate-CH₃). CV: E_{pc} (V) = -0.68, -1.03. DPV: E_{p} (V) = -0.60, -0.85.

[(UO_2)₂(μ -OAc)₂(L^2)₂] (2): Yield: 375 mg (68%). $C_{30}H_{30}N_6O_{10}U_2$ (1110.651): calcd. C 32.44, H 2.72, N 7.57; found C 32.51, H 2.78, N 7.65. Selected IR data:

 $v \text{ (cm}^{-1}) = 3234 \text{ (N-H)}, 1622 \text{ (C=N)}, 1545 \text{ and } 1427 \text{ (COO}^-), 885 \text{ (UO}_2). \text{ UV-Vis data: } \lambda_{\text{max}} \text{ (nm) } (\varepsilon (10^4 \text{ M}^{-1} \text{ cm}^{-1})) = 460^{\text{sh}} (0.94), 435 (1.14), 360 (1.83), 288 (2.04). {}^{1}\text{H NMR data: } \delta \text{ (ppm) } (J \text{ (Hz)}) = 10.02 \text{ (s, 1H, NH)}, 8.82 \text{ (s, 1H, H}^7), 7.95 \text{ (s, 1H, H}^{10}), 7.38 \text{ (4) (d, 1H, H}^{12}), 7.32 \text{ (s, 1H, H}^6), 7.23 \text{ (m, 1H, H}^{4,9,11}), 6.95 \text{ (5) (d, 1H, H}^3), 2.37 \text{ (s, 3H, CH}_3 \text{ at C}^5), 2.33 \text{ (s, 3H, acetate-CH}_3). CV: <math>E_{pc}$ (V) = -0.77, -1.10. DPV: E_{pc} (V) = -0.65, -0.87.

[(UO₂)₂(μ -OAc)₂(L³)₂] (3): Yield: 400 mg (70%). C₃₀H₃₀N₆O₁₂U₂ (1142.650): calcd. C 31.53, H 2.65, N 7.35; found C 31.42, H 2.58, N 7.45. Selected IR data: v (cm⁻¹) = 3308 (N–H), 1621 (C=N), 1528 and 1422 (COO⁻), 880 (UO₂). UV– Vis data: λ_{max} (nm) (ε (10⁴ M⁻¹ cm⁻¹)) = 460^{sh} (0.76), 436 (0.92), 360 (1.77), 297^{sh} (1.60). ¹H NMR data: δ (ppm) (J (Hz)) = 9.94 (s, 1H, NH), 8.83 (s, 1H, H⁷), 8.08 (m, 1H, H¹⁰), 7.91 (6) (d, 1H, H¹²), 7.63 (6) (dd \rightarrow t, 1H, H¹¹), 7.55 (4) (d, 1H, H⁹), 7.30 (6) (δ , 1H, H³), 7.22 (6) (d, 1H, H⁴), 6.94 (s, 1H, H⁶), 3.76 (s, 3H, –OCH₃ at C⁵), 2.32 (s, 3H, acetate-CH₃). CV: E_{pc} (V) = -0.69, -1.01. DPV: E_{p} (V) = -0.70, -0.93.

2.2.4. X-ray Crystallography:

Single crystals suitable for X-ray data collection for all three complexes were selected from the crystalline particles obtained during their syntheses. Both 1 and 3 crystallized without any solvent molecule, while single crystals of 2 were obtained as a solvated species, *i.e.* 2·4MeOH. Unit cell determination and intensity data collection for each of 1 and 2·4MeOH were performed on an Oxford Diffraction Xcalibur Gemini single crystal X-ray diffractometer using graphite monochromated Cu $K\alpha$ radiation (λ = 1.54184 Å) at 298 K. Data collection, reduction and absorption correction were performed employing the CrysAlisPro software.⁸ Determination of the unit cell parameters and intensity data collection for 3 were performed on a Bruker-Nonius SMART APEX CCD single crystal diffractometer using graphite monochromated Mo $K\alpha$ radiation (λ = 0.71073 Å) at 100 K. The SMART and the SAINT-Plus packages⁹ were used for data acquisition and data extraction, respectively. The SADABS program¹⁰ was used for absorption correction. In each of the three cases, some residual

absorption effect was treated with an additional correction using the XABS2 program. 11 The structures were solved by direct method and refined on F^2 using full-matrix least-squares procedures. In each structure, the non-hydrogen atoms were refined anisotropically. In the case of 1, the phenolate-O and the carbon atom to which it is attached were refined with restrained anisotropic thermal parameters. However, due to very low quality data several (nine) non-hydrogen atoms of 2:4MeOH were refined with restraints on their anisotropic thermal parameters. All hydrogen atoms were placed at idealized positions and refined as riding atoms with relative isotropic thermal parameters of their parent atoms. The SHELX-97 programs¹² accessible in the WinGX software suite¹³ were used for structure solution and refinement. The Mercury package¹⁴ was used to prepare the structural illustrations. Selected crystallographic data for 1, 2.4MeOH, and 3 are summarized in Table 1.Detailed X-ray crystallographic data for 1, 2·4MeOH and 3 have been deposited with the Cambridge Crystallographic Data Centre under the deposition numbers CCDC 1811353, 1811354, and 1811355 respectively.

Table 1: Selected crystal data and structure refinement summary for 1, 2·4MeOH, and 3.

Complex	1	2 ·4MeOH	3
Chemical formula	$C_{28}H_{26}N_6O_{10}U_2$	$C_{34}H_{46}N_6O_{14}U_2$	$C_{30}H_{30}N_6O_{12}U_2$
Formula weight	1082.61	1238.83	1142.66
Temperature [K]	298	298	100
λ [Å]	1.54184	1.54184	0.71073
Crystal system	Orthorhombic	Triclinic	Triclinic
Space group	Pbca	$P\bar{1}$	$P\bar{1}$
a [Å]	11.2313(4)	7.8666(6)	7.2580(3)
<i>b</i> [Å]	12.7888(7)	11.6952(9)	11.6813(6)
c [Å]	21.5714(9)	12.2524(9)	11.7663(8)
<i>α</i> [°]	90	103.803(7)	75.288(3)
$oldsymbol{eta}[^{\circ}]$	90	96.035(7)	74.594(3)
γ[°]	90	105.817(7)	79.050(3)
Volume [Å ³]	3098.4(2)	1035.62(14)	922.14(9)
Z	4	1	1
ρ [g cm ⁻³]	2.321	1.986	2.058
$\mu[\mathrm{mm}^{-1}]$	29.772	22.439	8.835
Reflections collected	8064	6844	8533
Reflections unique	2926	3880	3222
Reflections $[I \ge 2\sigma(I)]$	2335	3164	2861
Data/restr./param.	2926/1/209	3880/55/259	3222/0/228
$R1$, $wR2$ [$I \ge 2\sigma(I)$]	0.0666, 0.1817	0.0774, 0.1834	0.0328, 0.0816
<i>R</i> 1, <i>wR</i> 2 [all data]	0.0810, 0.1912	0.0926, 0.1962	0.0382, 0.0835
GoF on F^2	1.045	1.061	1.039
Max. / min. $\Delta \rho$ [e Å ⁻³]	2.527/-3.378	4.264/-3.927	2.624/-1.133

2.2.5. Extraction Studies:

Two different methods were employed for the extraction of *trans*-uranyl(VI) dication from aqueous medium using the Schiff base system HLⁿ.

Method 1: The Schiff base (HLⁿ) (0.4 mmol) was dissolved in 10 mL of an organic solvent (MeOH or CH₂Cl₂ or CHCl₃). A solution of UO₂(OAc)₂·2H₂O (0.2 mmol) was prepared in 10 mL of deionized water. The pH of this uranyl acetate solution was 4.8. Both solutions were mixed and vigorously stirred for a specific time (15, 30, 45 and 60 min). In each experiment, the quantitative estimation of the resultant complex that precipitated as a brown solid was performed gravimetrically using a pre-weighed G-4 sintered glass crucible.

Method 2: In this method, the sequential extraction of *trans*-(UO₂)²⁺ from the aqueous layer was performed using CHCl₃ solution of the Schiff base (HL²) as the organic layer. The pH of the aqueous phase was maintained at 6 by using HNO₃. A 8 mM CHCl₃ solution (5 mL) of HL² was added to a 4 mM aqueous solution of UO₂(OAc)₂·2H₂O and the mixture was stirred magnetically in a round bottom flask for 10 min. The aqueous phase was then separated and checked for *trans*-(UO₂)²⁺ concentrations by UV-Vis spectroscopy. To the same aqueous phase again a fresh 8 mM CHCl₃ solution (5 mL) of HL² was added and the extraction process was repeated several times until the absorbance of the characteristic *trans*-(UO₂)²⁺ absorption band at 429 nm in the aqueous phase¹⁵ becomes minimal and constant indicating the maximum extraction of uranium from the aqueous layer.

2.2.6. Theoretical Calculations:

The quantum chemical calculations for **1** and **3** were carried out using Gaussian09 (g09) suite of program. The structures of both complexes were optimized at the density functional theory level using B3LYP functional. The Stuttgart RSC 1997 effective core potential (ECP) was employed to describe the uranium atoms. The pseudo potential is used to represent the 60 core electrons in uranium, while a valence basis set is used for the remaining 32 electrons. To describe carbon, hydrogen, oxygen and nitrogen atoms 6-31G(d,p) basis set was

used. Harmonic vibrational frequency analysis of the fully optimized stationary points is carried out to ensure that each of the two structures is at minimum on the potential energy surface (PES). The optimized geometry of both complexes converges to the C_i symmetry point group. On the basis of the optimized ground state geometries, the electronic transitions in the DMF solution were also calculated by time-dependent DFT (TD-DFT) method using the same basis set and a polarized continuum model (PCM).

2.3. Results and Discussions

2.3.1. Synthesis and Characterization:

Complexes with the general molecular formula as $[(UO_2)_2(\mu\text{-OAc})_2(L^n)_2]$ (1–3) have been synthesized in good yields (65–70%) by treating the corresponding Schiff bases (HLⁿ, n = 1–3) with UO₂(OAc)₂·2H₂O in hot methanol under aerobic conditions. They have been isolated as brown solids. The elemental analysis data of 1–3 are in good agreement with their corresponding molecular formulas. Magnetic susceptibility measurements with powdered samples of the complexes at room temperature revealed their diamagnetic character. Thus the uranium center in each of 1–3 is in +6 oxidation state. All three complexes are insoluble in most of the common organic solvents except for dimethylformamide (DMF) and dimethylsulfoxide (DMSO). In these two solvents, they are highly soluble and provide yellow to yellow-brown solutions. The complexes behave as non-electrolytes in solution. The non-electrolytic nature of 1–3 is consistent with them being neutral species as indicated by their molecular formulas.

2.3.2. X-ray Molecular Structures:

The structures of **1** and **3** were determined in orthorhombic Pbca and triclinic $P\overline{1}$ space groups, respectively, while that of the solvated species **2**·4MeOH was solved in the triclinic space group $P\overline{1}$. The molecular structures of all three dinuclear complexes are very similar. The structures of the unsolvated complexes (**1** and **3**) are illustrated in Figure 1 and the structure of the solvated complex (**2**·4MeOH) is provided in Figure 2. The bond lengths and angles associated with

the uranium centers for all three complexes are listed in Table 2. In **2**·4MeOH, the methanol molecules exist as dimers via O–H···O interactions. Two such methanol dimers are attached to either side of **2** through two N–H···O interactions (Figure 2).

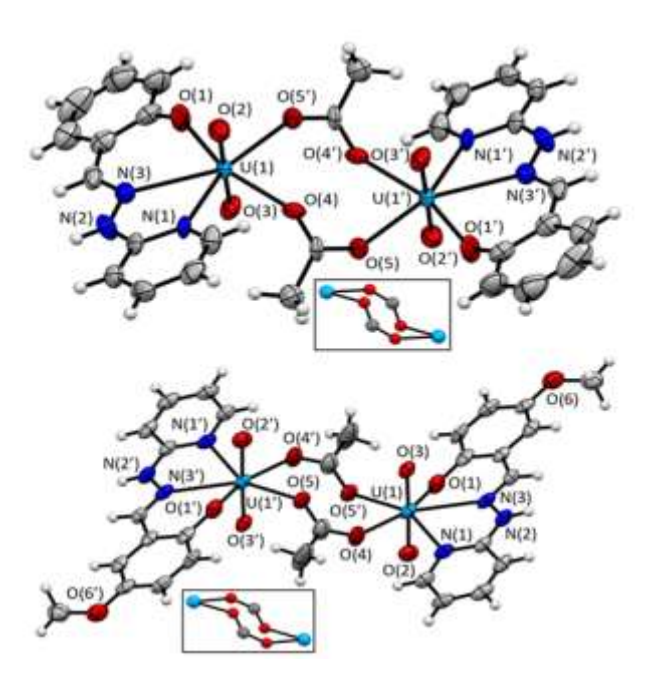


Figure 1: Molecular structures of $[(UO_2)_2(\mu\text{-OAc})_2(L^1)_2]$ (1) (top) and $[(UO_2)_2(\mu\text{-OAc})_2(L^3)_2]$ (3) (bottom). All the non-hydrogen atoms in each structure are represented by their 50% probability thermal ellipsoids. For clarity only the non-carbon atoms are labelled. Insets: the chair conformations of the $U_2C_2O_4$ rings.

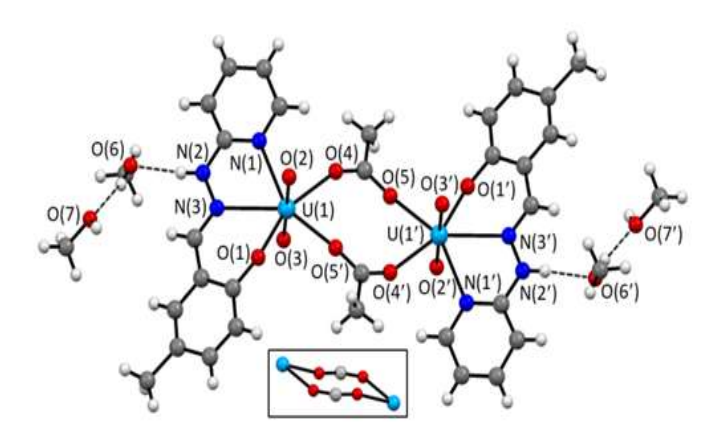


Figure 2: The structure of $[(UO_2)_2(\mu\text{-OAc})_2(L^2)_2]$ -4MeOH (2·4MeOH). For clarity only the non-carbon atoms are labelled. Inset: the chair conformation of the $U_2C_2O_4$ ring.

In each of 1–3, the two halves of the complex molecule, i.e. the two {(trans-UO₂)(OAc)(Lⁿ)} fragments, are related by an inversion center. As a result, the metal atoms of the two trans-(UO₂)²⁺ units are bridged by two acetate groups and a central $\{O_2U(\mu\text{-OAc})_2UO_2\}^{2+}$ core is formed in each molecule (Figures 1 and 2). In this central core of 1-3, the conformation of the centrosymmetric eightmembered U₂C₂O₄ ring can be best described as chair (Figures 1 and 2, insets). The dihedral angle between the UO₂ plane and the mean plane containing C₂O₄ (rms deviations: 0.12-0.45 Å) decreases in the order **1** $(43.3(5)^{\circ}) > 3 (33.8(3)^{\circ}) >$ 2 (14.9(6)°). These dihedral angles indicate that the flattening of both ends of the chair or in other words the planarity of the $U_2C_2O_4$ ring increases in the order 1 < 3 < 2. Interestingly, the metal···metal distance decreases with the increase of the planarity of the $U_2C_2O_4$ ring. The $U(1)\cdots U(1')$ distances are 5.7561(9), 5.5444(5), and 5.3547(9) Å in 1, 3, and 2, respectively. The uranium centers are in distorted pentagonal-bipyramidal N₂O₅ coordination sphere. The planar ligand (Lⁿ)⁻ acts as pyridine-N, azomethine-N, and phenolate-O donor and forms fused 5,6membered chelate rings at the metal center. The (Lⁿ)- and two O-atoms of the two bridging acetato groups form the equatorial pentagonal N₂O₃ plane (rms deviations: 0.23-0.28 Å) around the uranium atom of the trans- $(UO_2)^{2+}$ unit.

Table 2: Selected bond parameters (Å and °) for 1, 2·4MeOH and 3.

Complex	1	2 ·4MeOH	3
U(1)–O(1)			
, , , , , ,	2.178(13)	2.224(10)	2.217(5)
U(1)–O(2)	1.769(12)	1.790(13)	1.777(5)
U(1)–O(3)	1.795(12)	1.801(13)	1.774(4)
U(1)-O(4)	2.302(13)	2.356(12)	2.351(5)
$U(1)-O(5')^a$	2.371(12)	2.311(12)	2.338(4)
U(1)-N(1)	2.564(15)	2.582(13)	2.594(5)
U(1)-N(3)	2.650(14)	2.625(11)	2.609(5)
O(1)-U(1)-O(2)	89.5(6)	88.0(5)	87.0(2)
O(1)-U(1)-O(3)	90.9(6)	92.7(5)	94.6(2)
O(1)-U(1)-O(4)	159.2(5)	157.7(4)	158.10(18)
$O(1)-U(1)-O(5')^a$	79.8(5)	80.4(4)	80.68(17)
O(1)-U(1)-N(1)	125.1(5)	127.2(4)	127.96(18)
O(1)-U(1)-N(3)	67.4(5)	68.3(4)	69.53(16)
O(2)-U(1)-O(3)	178.6(6)	178.7(5)	178.2(2)
O(2)-U(1)-O(4)	95.1(5)	90.0(5)	89.3(2)
$O(2)-U(1)-O(5')^a$	85.1(6)	90.2(6)	89.09(19)
O(2)-U(1)-N(1)	81.3(5)	83.2(6)	84.18(19)
O(2)-U(1)-N(3)	100.1(5)	100.7(5)	101.59(19)
O(3)-U(1)-O(4)	84.0(5)	89.7(5)	88.9(2)
$O(3)-U(1)-O(5')^a$	93.7(5)	90.9(5)	90.34(19)
O(3)-U(1)-N(1)	99.5(5)	95.5(5)	95.47(18)
O(3)-U(1)-N(3)	81.3(5)	78.6(4)	79.80(18)
$O(4)-U(1)-O(5')^a$	80.5(5)	77.4(4)	77.68(17)
O(4)-U(1)-N(1)	75.6(4)	74.6(4)	72.96(18)
O(4)-U(1)-N(3)	131.1(4)	133.8(4)	132.31(17)
$O(5')^a - U(1) - N(1)$	151.2(5)	151.2(5)	149.91(19)
$O(5')^a - U(1) - N(3)$	146.6(5)	146.2(4)	147.54(17)
N(1)-U(1)-N(3)	61.4(4)	62.6(4)	62.42(18)

a Symmetry transformations used: -x, -y + 1, -z + 1 for 1; -x + 1, -y, -z + 1 for $2\cdot4$ MeOH and -x, -y+2, -z+1 for 3.

In all of 1–3, the O=U=O angles are very close to the ideal value of 180° and the U=O bond lengths are comparable to those found in *trans*-uranyl(VI) complexes.^{2,6} The remaining metal centered bond lengths and angles involving the coordinating atoms of $(L_n)^-$ and the bridging acetate groups (Table 2) are within the ranges reported for complexes of *trans*- $(UO_2)^{2+}$ containing pentagonal-bipyramidal uranium centers having similar coordinating atoms.^{2a-h,j-o,6}

2.3.3. Supramolecular Self-assembly:

All of **1**, **2**·4MeOH, and **3** contain classical (hydrazinic-NH or methanolic-OH) as well as non-classical (CH) hydrogen bond donor functionalities and also hydrogen bond acceptors such as oxo groups and phenolate-O atoms. Hence, each structure has been scrutinized for intermolecular hydrogen bonding interactions and if there is any such interaction then what type of supramolecular self-assembly pattern it leads to. Indeed there are three types of hydrogen bonds namely N–H···O, O–H···O, and C–H···O. The geometric parameters for these hydrogen bonding interactions are summarized in Table 3.

Table 3: Hydrogen bonding parameters for 1, 2.4MeOH and 3

Complex	D–H···A	D···A (Å)	<dha (°)<="" th=""></dha>
1	$N(2)$ – H ···O $(3)^a$	3.099(18)	165
2 ·4MeOH	N(2)-H···O(6)	2.798(16)	173
	O(6)–H···O(7)	2.612(9)	166
	O(7)– H ··· $O(1)$ ^b	2.763(18)	162
3	C(6)– H ··· $O(3)$ ^c	3.318(8)	135
	$C(12)$ -H···O $(3)^c$	3.403(8)	138

Symmetry transformations used: a –x + 1/2, y – 1/2, z. b –x, –y, –z. c –x, –y + 1, –z + 1.

In the case of $\mathbf{1}$, one of the two metal bound oxo groups is hydrogen bonded with the hydrazinic-NH of $(L^1)^-$. As the donor and the acceptor are approximately

orthogonal to each other, this intermolecular N–H···O interaction directs the self-assembly of **1** into a two-dimensional sheet-like structure (Figure 3).

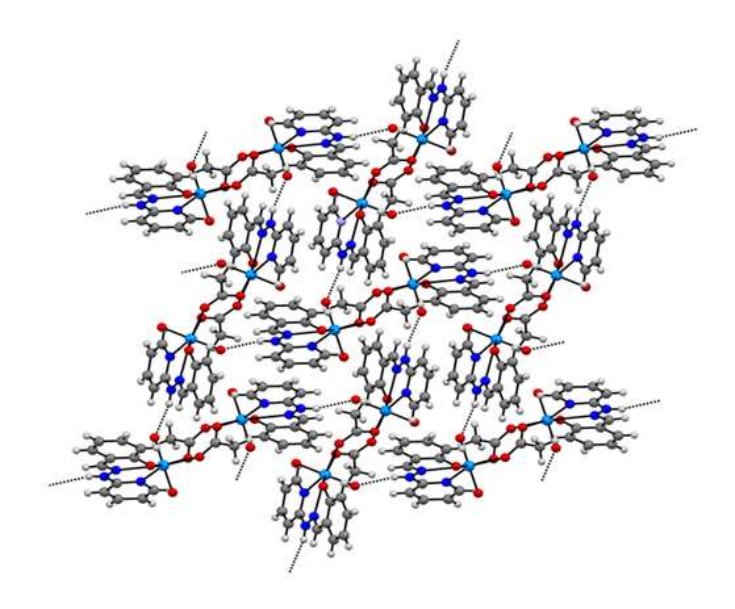


Figure 3: Intermolecular N–H···O interaction assisted two-dimensional sheet structure of $[(UO_2)_2(\mu\text{-OAc})_2(L^1)_2]$ (1).

The solvent molecules dictate the self-assembly and the supramolecular structure of $2\cdot4$ MeOH. Every pair of dinuclear molecules of 2 are bridged by two methanol dimers, which are O–H···O hydrogen bonded, through N–H···O and O–H···O hydrogen bonds involving the hydrazinic-NH group and the phenolate-O atom of each tridentate ligand (L^2)⁻ of 2 as donor and acceptor, respectively. These two intermolecular hydrogen bonding interactions lead to a one-dimensional chain-like -2-(MeOH)₂-2-(MeOH)₂- array in the crystal lattice (Figure 4).

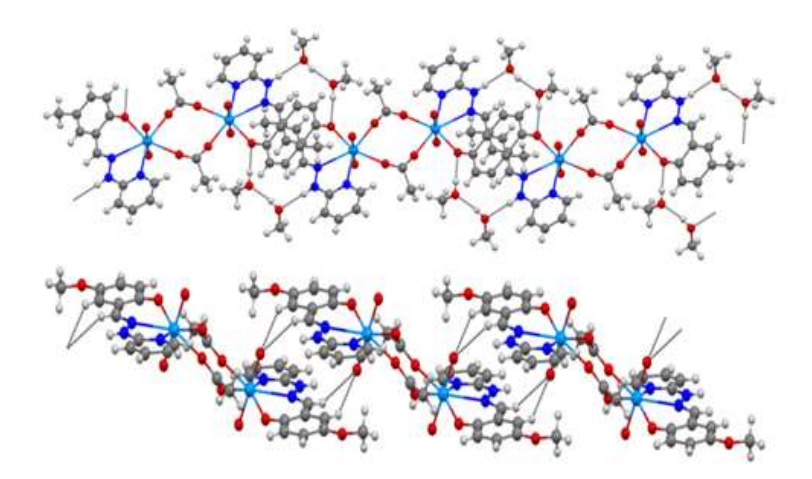


Figure 4: One-dimensional orderings of $[(UO_2)_2(\mu\text{-OAc})_2(L^2)_2]\cdot 4\text{MeOH}$ (2·4MeOH) via O–H···O and N–H···O hydrogen bonds (top) and $[(UO_2)_2(\mu\text{-OAc})_2(L^3)_2]$ (3) through intermolecular bifurcated C–H···O···H–C hydrogen bond (bottom).

2.3.4. Spectroscopic Characterization:

Infrared spectra of 1–3 were recorded using KBr discs in the range 4000–400 cm⁻¹. Each spectrum displays a large number of bands with various intensities. The spectra are shown in Figures 5, 6 and 7. Except for few selected bands, no attempt has been made to assign the remaining bands. None of the complexes displays any band assignable to the phenolic -OH group of the free Schiff base (HLⁿ). Thus the phenolic -OH is deprotonated and the Schiff base is monoanionic ((Lⁿ)⁻) in the complex. A weak and broad band observed in the range 3308-3234 cm⁻¹ is assigned to the hydrazinic -NH of (Lⁿ)^{-.4e,f,j} A sharp and strong band displayed at around 1621 cm⁻¹ by all three complexes is attributed to the metal coordinated azomethine (-HC=N-) group of their respective ligands.^{2,4e,f,j,5b} Two strong bands are observed in the ranges 1545–1528 and 1427–1422 cm⁻¹ in each spectrum. These two bands are assigned to the asymmetric and symmetric stretches, respectively of the carboxylate fragment of the bridging acetate group.¹¹ The typical strong band due to the asymmetric stretching vibration of the trans-uranyl(VI) moiety has been observed within 899–883 cm⁻¹.²

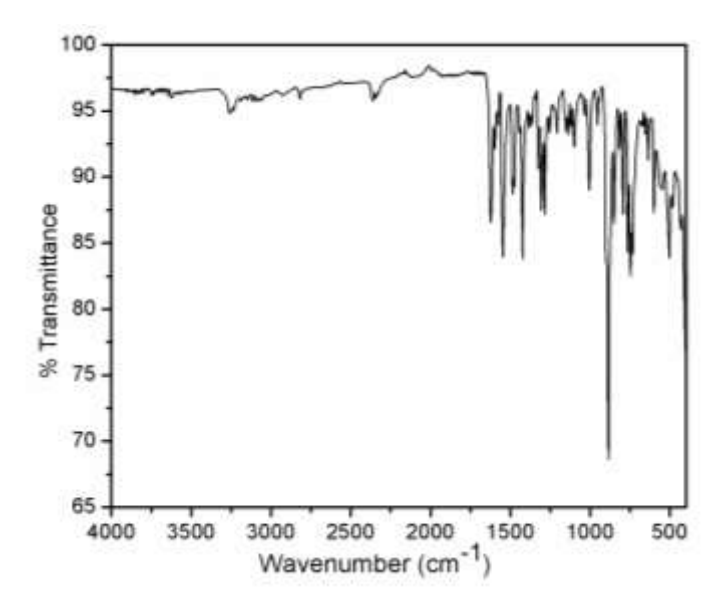


Figure 5: Infrared spectrum of $[(UO_2)_2(\mu\text{-OAc})_2(L^1)_2]$ (1) in KBr disk.

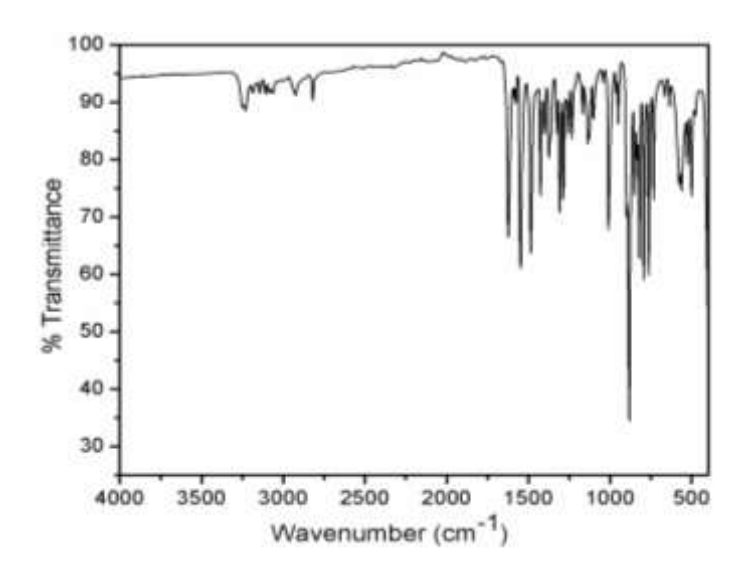


Figure 6: Infrared spectrum of $[(UO_2)_2(\mu\text{-OAc})_2(L^2)_2]$ (2) in KBr disk.

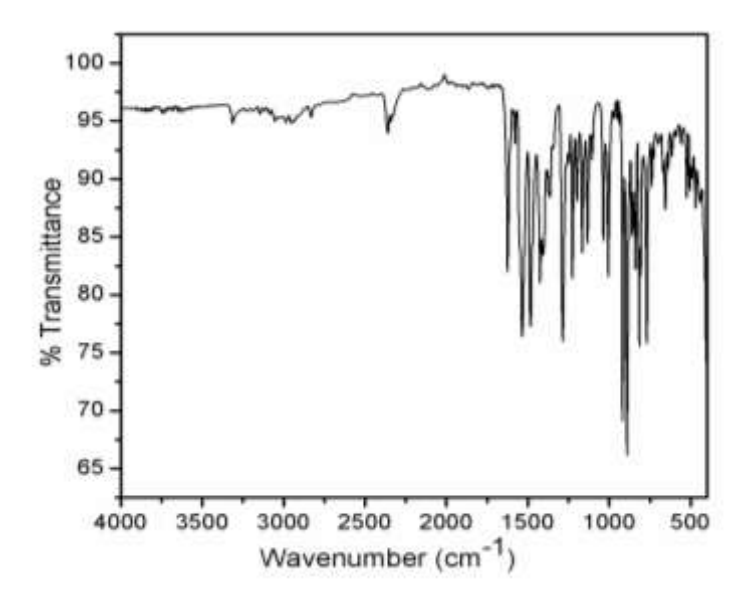


Figure 7: Infrared spectrum of $[(UO_2)_2(\mu\text{-OAc})_2(L^3)_2]$ (3) in KBr disk.

The electronic absorption spectra of 1-3 were recorded using their DMF solutions. The spectral profiles of all three complexes are very similar. The spectra of the complexes are displayed in Figure 8. A strong band at ~435 nm preceded by a shoulder at ~458 nm and two more strong bands at 360 and ~290 nm are observed in each spectrum. The free Schiff bases (HLⁿ) display a very strong band within 351-335 nm, a shoulder or band at ~312 nm and another strong absorption at ~240 nm.4j Comparison of the spectra of HLn with those of the complexes (1-3) indicates that the shoulder and the band at ~458 and ~435 nm, respectively are very likely to be due to ligand to metal charge transfer transitions.^{2,4j} To find out the origins of the remaining bands and for a better overall perception of the electronic spectra, TD-DFT calculations were carried out for 1 and 3 in DMF solution. Calculated band positions with the corresponding oscillator strengths and the percentages of contributing transitions along with the experimental band positions are summarized in Table 4. The calculated and experimental λ_{max} values complement each other very well. The compositions of the molecular orbitals involved in the contributing transitions (Table 5), indicate that the highest energy absorption (at ~290 nm) is due to a ligand centered transition, while the remaining three lower energy absorptions are due to ligand-to-metal charge transfer transitions.

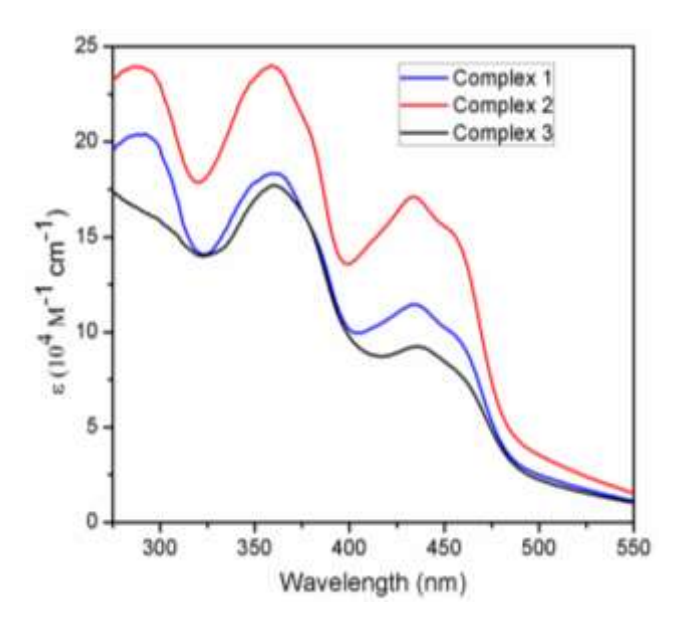


Figure 8: Electronic spectra of 1, 2 and 3.

The 1 H NMR spectra of all the complexes were recorded in DMSO-d₆ solutions using tetramethylsilane as the internal standard. The comparable spectral traces and the similar chemical shift values are consistent with similar type of coordination modes of the ligands $(L^{1-3})^-$ in 1–3. The spectra also indicate that both halves of each of the three dinuclear complexes are equivalent. The chemical shift values with the tentative assignments are provided in the experimental section under the respective complexes. As expected, due to the deprotonation upon metal coordination the spectra of 1–3 are devoid of the phenol proton resonance observed for the free Schiff bases (HL $^{1-3}$) at $\delta \sim 10.88$ ppm. The hydrazinic–NH proton of HL n resonates as a singlet at $\delta \sim 10.24$ ppm, while the corresponding singlet of (L n) $^-$ in the complexes shifts slightly upfield to $\delta \sim 9.99$ ppm. The singlet due to the resonance of the azomethine proton of (L n) $^-$ in the complexes appeared at $\delta \sim 8.84$ ppm.

Chapter 2

Table 4: Calculated absorptions of $[(UO_2)_2(\mu\text{-OAc})_2(L^1)_2]$ (1) and $[(UO_2)_2(\mu\text{-OAc})_2(L^3)_2]$ (3)

Comp	State	Calcd λ_{max} [nm]	Oscillator strength	<i>E</i> [eV]	Major contribution [%]	Exptl λ_{max} [nm]
1	DMF	319	0.0527	3.89	$HOMO-2 \rightarrow LUMO+8 (28\%)$ $HOMO-3 \rightarrow LUMO+9 (27\%)$	287
		377	0.0281	3.29	HOMO-4 \rightarrow LUMO (43%) HOMO-5 \rightarrow LUMO+1 (46%)	359
		419	0.0016	2.96	HOMO-4 \rightarrow LUMO (50%) HOMO-5 \rightarrow LUMO+1 (46%)	433
		462	0.0058	2.68	HOMO-6 → LUMO (37%) HOMO-7 → LUMO+1 (36%)	460
3	DMF	298	0.0014	4.16	$HOMO-2 \rightarrow LUMO+8 (45\%)$ $HOMO-3 \rightarrow LUMO+9 (46\%)$	270
		371	0.0024	3.34	HOMO-4 \rightarrow LUMO+2 (45%) HOMO-5 \rightarrow LUMO+3 (44%)	360
		417	0.0219	2.97	HOMO-4 \rightarrow LUMO (45%) HOMO-5 \rightarrow LUMO+1 (42%)	436
		477	0.0013	2.60	HOMO-6 \rightarrow LUMO (40%) HOMO-7 \rightarrow LUMO+1 (43%)	460

Table 5: Compositions of molecular orbitals for 1 and 3.

MOs	$[(UO_2)_2(\mu\text{-OAc})_2(L^1)_2]$ (1)		$[(UO_2)_2(\mu\text{-OAc})_2(L^3)_2]$ (3)	
	Metal [%]	Ligands [%]	Metal [%]	Ligands [%]
НОМО-7	16	84	14	86
НОМО-6	4	96	10	90
НОМО-5	6	94	20	80
HOMO-4	18	82	16	84
НОМО-3	4	96	8	92
НОМО-2	4	96	8	92
HOMO-1	10	90	16	84
НОМО	10	90	16	84
LUMO	92	8	92	8
LUMO+1	92	8	92	8
LUMO+2	98	2	98	2
LUMO+3	96	4	98	2
LUMO+4	90	10	90	10
LUMO+5	90	10	90	10
LUMO+6	94	6	94	6
LUMO+7	92	8	92	8
LUMO+8	8	92	8	92
LUMO+9	8	92	8	92

The observed downfield shift is consistent with the N-coordination of the azomethine and hence the deshielding of the azomethine proton. The three-proton singlet observed at $\delta \sim 2.33$ ppm is assigned to the bridging acetate methyl group in 1–3. The protons of the methyl substituent at C^5 of $(L^2)^-$ in 2 resonate as a singlet at $\delta \sim 2.37$ ppm, whereas the protons of the methoxy substituent at C^5 of $(L^3)^-$ in 3 are observed as singlet at $\delta \sim 3.78$ ppm. The chemical shifts and splitting patterns of the remaining aromatic protons of the tridentate ligands in 1–3 are unexceptional (Figures 9–11).

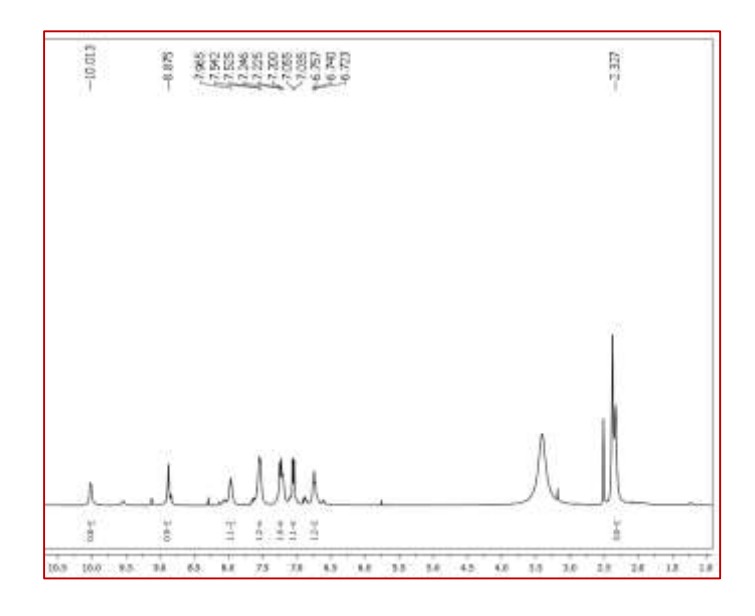


Figure 9: ${}^{1}\text{H-NMR}$ spectra of $1[(UO_2)_2(\mu\text{-OAc})_2(L^1)_2]$ (1) in DMSO-d₆.

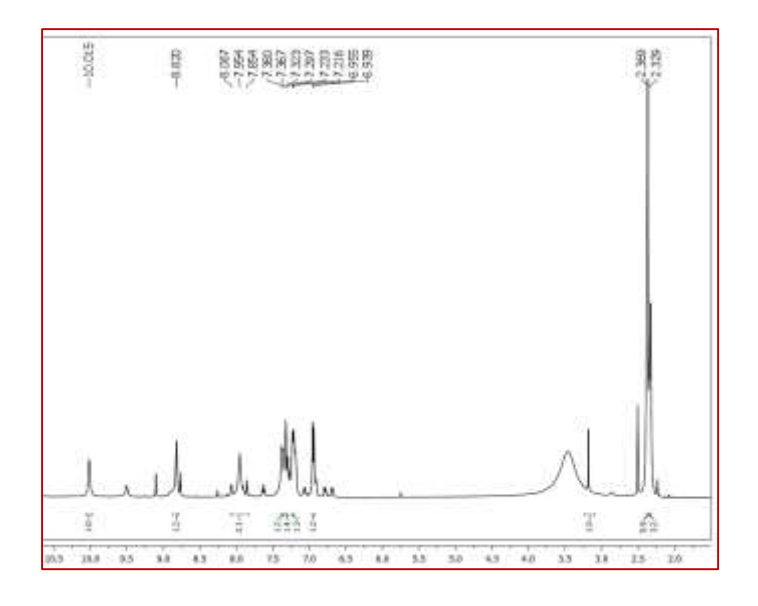


Figure 10: ${}^{1}\text{H-NMR}$ spectra of $1[(UO_{2})_{2}(\mu\text{-OAc})_{2}(L^{2})_{2}]$ (2) in DMSO-d₆.

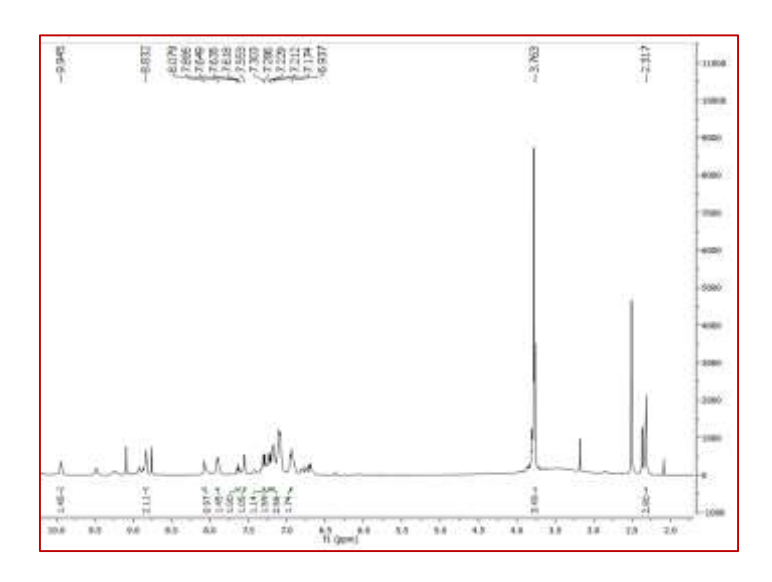


Figure 11: ${}^{1}\text{H-NMR}$ spectra of $1[(UO_{2})_{2}(\mu\text{-OAc})_{2}(L^{3})_{2}]$ (3) in DMSO-d₆.

2.3.5. Redox Behavior:

Cyclic and differential pulse voltammetric measurements with the Schiff bases (HL¹⁻³) and their complexes (1-3) were performed using their corresponding $\sim 10^{-3}$ M DMF solutions containing tetra-*n*-butylammonium perchlorate (TBAP) as the supporting electrolyte with a Pt-disk working electrode, a Pt-wire auxiliary electrode and an Ag/AgCl reference electrode under nitrogen atmosphere at 298 K. Under identical experimental conditions the ferrocenium/ferrocene (Fc⁺/Fc) couple was observed at $E_{1/2} = 0.61$ V with a peak-to-peak separation (ΔE_p) of 110 mV. Cyclic voltammograms of all the complexes are very similar and display two broad overlapping cathodic peaks and essentially no or very weak anodic peak on reverse scan. The cathodic peak potentials (E_{pc}) are about -0.7 and -1.0 V. The differential pulse voltammograms of 1-3 display two well-resolved peaks at potentials around -0.65 and -0.88 V. The voltammogram of a representative complex is shown in Figure 12 (left). Considering that the present complexes are diacetate bridged dinuclear species and complexes of trans-(UO₂)²⁺ with Schiff bases are known to display U(VI) to U(V) reduction response at comparable potential range, 2g-j,q,r the reductions observed for 1-3 can be assigned as $U(VI)-U(VI) \rightarrow U(V)-U(VI)$ and $U(V)-U(VI) \rightarrow U(V)-U(V)$ processes. However, the free Schiff bases (HLⁿ) are also redox active and display a single

Chapter 2

reduction response having large peak-to-peak separation ($E_{\rm pc}$ and $E_{\rm pa}$ values are around -1.02 and -0.04 V, respectively) and cathodic peak current (i_{pc}) to anodic peak current (i_{pa}) ratio. The i_{pc} values of the Schiff bases are higher than those of the corresponding complexes. As expected the differential pulse voltammograms of HL¹⁻³ show a single peak within -0.80 to -0.84 V. The voltammogram of HL¹ is illustrated in Figure 12 (right). Generally the reduction of metal coordinated ligand is expected to be easier and hence to be observed at higher potential than its reduction in the free state. Therefore, for 1-3 the first reduction can be assigned as a ligand centered process, while the second reduction can be due to a metal centered $UO_2^{2+} \rightarrow UO_2^+$ process. A similar situation of ligand reduction followed by metal reduction has been reported for a pentagonal-bipyramidal mononuclear complex of trans-(UO₂)²⁺ containing a redox-active tetradentate N₄donor Schiff base as primary ligand and a monodentate chloride as an ancillary ligand.^{2q} Thus for the present complexes there are two possibilities, *i.e.* both reductions are metal centered or the first reduction is ligand centered and the second reduction is metal centered. To decide between the above two possibilities the characteristics of the unoccupied molecular orbitals shown by the TD-DFT calculations have been examined. The compositions of LUMO to LUMO+7 (Table 5) indicate that at the present level of theory they are all metal centered in both 1 and 3. The locations of the LUMOs in the two complexes are illustrated in Figure 13. Thus the two closely spaced reductions are assigned to the successive reductions of the two metal centers in each of 1–3.

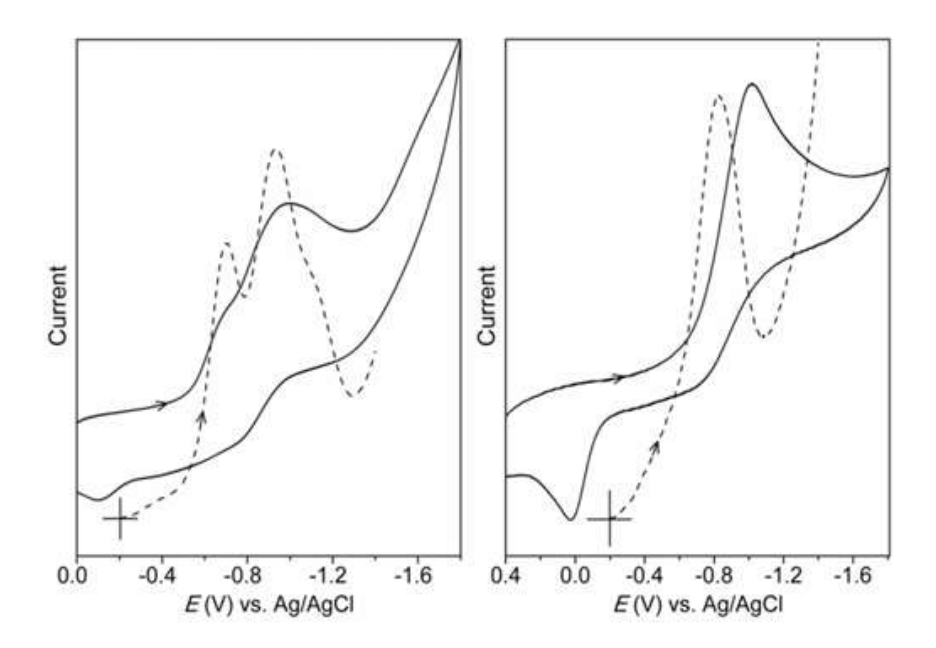


Figure 12: Cyclic and differential pulse voltammograms of $[(UO_2)_2(\mu-OAc)_2(L^3)_2]$ (3) (left) and HL^1 (right) in DMF.

To gain further insight, constant potential (at -1.3 V) coulometric reductions of 1-3 and one of the three Schiff bases (HL¹⁾ were performed using a Pt wire-gauze working electrode. The overall n-values (the ratio of Q_{obsvd} to Q_{calcd} for 1 e⁻ transfer) for the two successive reductions of the three complexes have been found to be in the range 1.8-2.1. In contrast, the n-value for the single reduction displayed by HL¹ is 3.1. The difference in the n-values of the complexes and the Schiff base, together with the TD-DFT results indicate that the coordinated ligands are not involved in any of the two reductions observed for the complexes. Hence, the two successive electron transfer responses of the complexes are indeed due to two metal centered single electron transfers, *i.e.* stepwise $U(VI)-U(VI) \rightarrow U(V)-U(VI) \rightarrow U(V)-U(V)$ reductions.

2.3.6. Extraction Studies:

Extraction abilities of HLⁿ for the *trans*-uranyl(VI) dication from aqueous medium have been investigated. Two methods were employed for the extraction process. These two methods are: gravimetric separation and sequential extraction using CHCl₃ as the organic layer.

In the gravimetric separation, a solution of the respective Schiff base (HLⁿ) in an organic solvent (MeOH or CH₂Cl₂ or CHCl₃) was mixed with an aqueous solution of UO₂(OAc)₂·2H₂O and stirred for a specific duration (15, 30, 45, and 60 min).

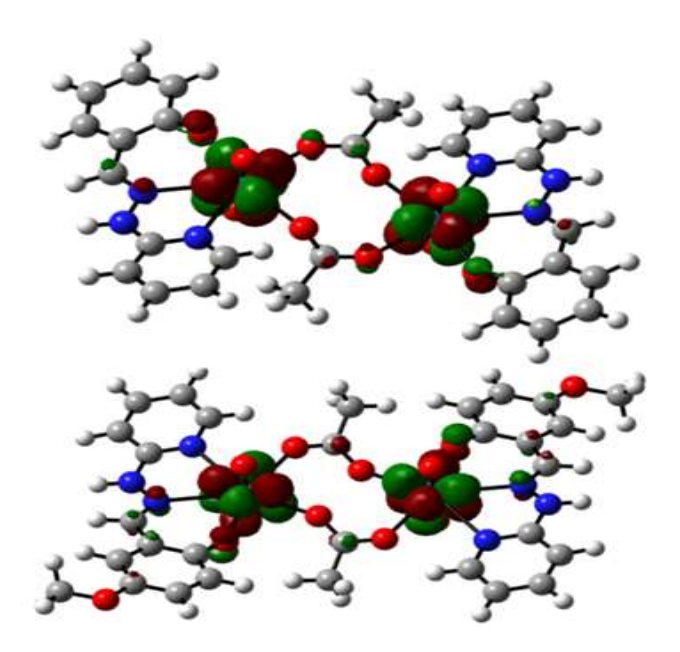


Figure 13: LUMOs of $[(UO_2)_2(\mu\text{-OAc})_2(L^1)_2]$ (1) (top) and $[(UO_2)_2(\mu\text{-OAc})_2(L^3)_2]$ (3) (bottom).

The amount of the complex precipitated after each extraction was quantitatively measured to determine the extent of extraction. The infrared spectra of the precipitates confirm their identities as $[(UO_2)_2(\mu\text{-OAc})_2(L^n)_2]$ (1–3). The results are summarized in Table 6. In general, the two-phase solvent systems $H_2O-CH_2Cl_2$ and $H_2O-CHCl_3$ show better results of extraction as compared to the H_2O-CH_3OH mixture. The maximum extraction of 98% of *trans*- $(UO_2)^{2+}$ was achieved in 60 min. using HL^2 as the ligand and $H_2O-CHCl_3$ as the reaction medium. A comparative study showing the extents of extraction of *trans*- $(UO_2)^{2+}$ using different solvent mixtures and HL^2 as the extractant is graphically represented in Figure 14. Considering that in the gravimetric separation method the best extraction was achieved with the use of HL^2 , only this Schiff base was employed in the sequential extraction method. Here a $CHCl_3$ solution of HL^2 was

used as the organic layer for the extraction of trans- $(UO_2)^{2+}$ from an aqueous solution having pH 6.

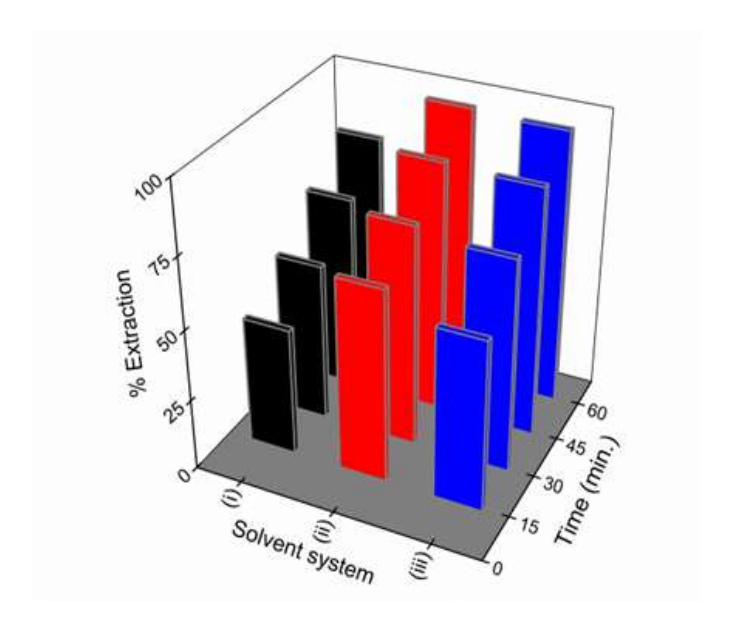


Figure 14: *trans*-Uranyl(VI) dication extraction by HL² in the solvent systems (i) MeOH–H₂O, (ii) CHCl₃–H₂O, and (iii) CH₂Cl₂–H₂O.

The acidic pH ensures the maximum extraction and no precipitation of the complex formed. The progress of extraction was followed by monitoring the 429 nm band¹⁷ in the electronic spectrum of the aqueous phase after each extraction (Figure 15). The absorption bands in the electronic spectrum of the CHCl₃ layer recorded after extraction confirm the formation of **2** in the organic phase (Figure 16). The absorbance values and the extraction data are listed in Table 7. The maximum extraction (55%) of the *trans*-(UO₂)²⁺ from the aqueous layer to the organic layer occurred in the first extraction. The amount of *trans*-uranyl(VI) dication in the aqueous phase gradually decreased with successive extractions with CHCl₃ solutions of HL². Total 91% *trans*-(UO₂)²⁺ could be removed from the aqueous phase in four extractions. After the fourth extraction there was very little change in the *trans*-uranyl(VI) dication content of the aqueous phase in the following extraction attempts.

Thus the present Schiff bases (HLⁿ) turned out to be effective extractants for the extraction of *trans*-(UO₂)²⁺ from aqueous phase. All three compounds showed

excellent extraction abilities. The maximum extents of extraction in the above mentioned two-phase extraction studies are very good (>90%) in both methods. These results are better or comparable to the previously reported extraction studies using Schiff bases. 2d,f,m

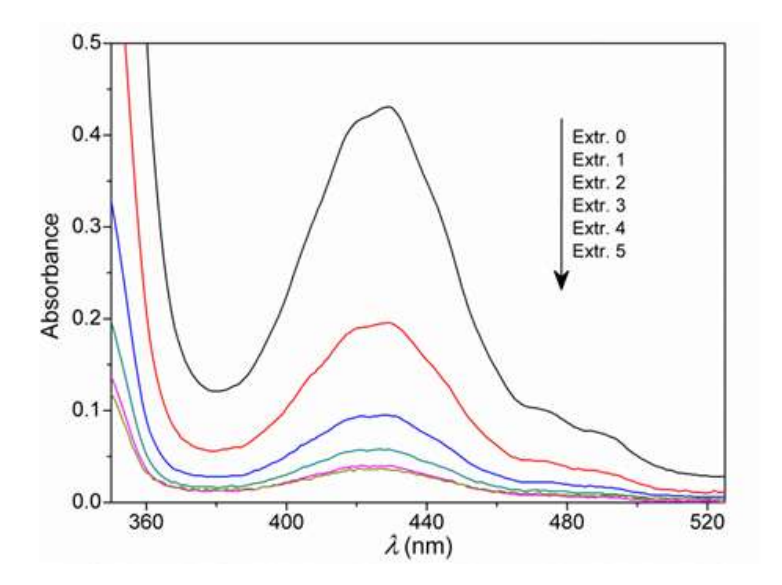


Figure 15: Electronic spectroscopic profiles of the aqueous phase (pH 6) containing UO₂(OAc)₂ recorded after sequential extractions of *trans*-uranyl(VI) dication using CHCl₃ solutions of HL².

Table 6: Extraction of *trans*- $(UO_2)^{2+}$ by gravimetric separation.

Solvent system	Time [min]	Schiff base	Extraction [%]
CH ₃ OH–H ₂ O	15	HL ¹	42
		HL^2	45
		HL ³	40
	30	HL ¹	55
		HL^2	56
		HL^3	52
	45	HL ¹	63
		HL^2	69
		HL^3	63
	60	HL ¹	81
		HL ²	81
		HL^3	79
CHCl ₃ –H ₂ O	15	HL ¹	65
		HL ²	68
		HL ³	67
	30	HL ¹	75
		HL^2	78
		HL^3	76
	45	HL^1	84
		HL^2	89
		HL ³	85
	60	HL^1	96
		HL^2	98
		HL^3	95
CH ₂ Cl ₂ -H ₂ O	15	HL^1	62
		HL^2	60
		HL^3	60
	30	HL ¹	74
		HL^2	75
		HL^3	72
	45	HL^1	86
		HL^2	88
		HL ³	85
	60	HL ¹	96
		HL^2	97
		HL^3	96

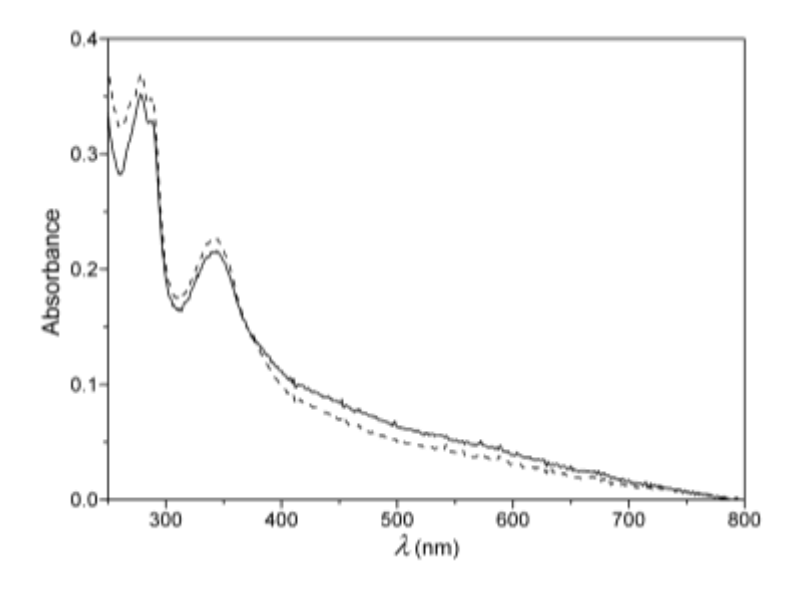


Figure 16: Electronic spectra of the CHCl₃ extract (–) and $[(UO_2)_2(\mu - OAc)_2(L^2)_2]$ (2) in CHCl₃ (----).

Table 7: Sequential liquid-liquid extraction of *trans*-(UO₂)²⁺

Extraction no.	Absorbance ^[a]	% of (UO ₂) ²⁺ ion ^[b]
0	0.431	100
1	0.196	45
2	0.095	22
3	0.058	13
4	0.040	9
5	0.036	8
[a] Measured with aqueous phase at 429 nm. [b] In aqueous phase.		

2.4. Conclusions

Stabilization and isolation of the rare $\{O_2U(\mu\text{-OAc})_2UO_2\}^{2+}$ core using the deprotonated N,N,O-donor Schiff bases N-(2-pyridyl)-N'-(5-R-salicylidene)hydrazines (HLⁿ where R = H, Me, and OMe) as ligands have been demonstrated. The discrete dinuclear complexes isolated have the general

molecular formula $[(UO_2)_2(\mu\text{-OAc})_2(L^n)_2]$. X-ray crystallographic studies revealed pentagonal-bipyramidal N₂O₅ coordination sphere around each metal center and a chair conformation of the central eight-membered U(OCO)₂U ring in each complex. In the crystal lattice, the complexes form two-dimensional and one-dimensional supramolecular structures through intermolecular regular and bifurcated hydrogen bonding interactions. The infrared and proton NMR spectroscopic characteristics of all the complexes are in good agreement with their molecular structures. All three complexes display four strong electronic absorption bands and two closely spaced reduction responses at the cathodic side of Ag/AgCl. Theoretical calculations show that the first three absorption bands are of ligand-to-metal charge transfer character, while, the highest energy band is due to a ligand centered transition and the two successive electron transfer processes are due to $U(VI)-U(VI) \rightarrow U(V)-U(VI) \rightarrow U(V)-U(V)$ reductions. Constant potential coulometric measurements confirm an overall stoichiometry of two electrons for the stepwise reductions of the two metal centers. Very effective extraction of trans-(UO₂)²⁺ from the aqueous layer has been achieved using the Schiff bases (HLⁿ) as the extractants in two-phase extraction studies.

2.5. References

- (a) J. R. Kumar, J. –S. Kim, J. –Y. Lee, H. –S. Yoon, Sep. Purif. Rev. 2011, 40, 77. (b) R. Gilligan, A. N.Nikoloski, Miner. Eng. 2015, 71, 34. (c) A. Basu, S. T. Brown, J. N. Christensen, D. J. DePaolo, P. W. Reimus, J. M. Heikoop, G. Woldegabriel, A. M. Simmons, B. M. House, M. Hartmann, K. Maher, Environ. Sci. Technol. 2015, 49, 5939. (d) D. K. Singh, S. Mondal, J. K. Chakravartty, Solvent Extr. Ion Exch. 2016, 34, 201. (e) F. Endrizzi, C. J. Leggett, L. Rao, Ind. Eng. Chem. Res. 2016, 55, 4249.
- 2. (a) A. K. Sah, C. P. Rao, P. K. Saarenketo, E. K. Wegelius, E. Kolehmainen, K. Rissanen, Eur. J. Inorg. Chem. 2001, 2773. (b) C. C. Gatto, E. S. Lang, A. Kupfer, A. Hagenbach, U. Abram, Z. Anorg. Allg. Chem. 2004, 630, 1286. (c) P. L. Arnold, A. J. Blake, C. Wilson, J. B. Love, *Inorg. Chem.* **2004**, *43*, 8206. (d) M. S. Bharara, K. Strawbridge, J. Z. Vilsek, T. H. Bray, A. E. V. Gorden, *Inorg. Chem.* **2007**, *46*, 8309. (e) M. S. Bharara, S. A. Tonks, A. E. V. Gorden, Chem. Commun. 2007, 4006. (f) M. S. Bharara, K. Heflin, S. Tonks, K. L. Strawbridge, A. E. V. Gorden, Dalton Trans. 2008, 2966. (g) H. C. Hardwick, D. S. Royal, M. Helliwell, S. J. A. Pope, L. Ashton, R. Goodacre, C. A. Sharrad, Dalton Trans. 2011, 40, 5939. (h) Z. Asadi, M. Asadi, A. Zeinali, M. Ranjkeshshorkaei, K. Fejfarova, V. Eigner, M. Dusek, A. Dehnokhalaji, J. Chem. Sci. 2014, 126, 1673. (i) M. Azam, S. I. Al-Resayes, G. Velmurugan, P. Venuvanalingam, J. Wagler, E. Kroke, Dalton Trans. **2015**, 44, 568. (j) C. Camp, L. Chatelain, V. Mougel, J. Pécaut, M. Mazzanti, Inorg. Chem. 2015, 54, 5774. (k) Y. Zhang, D. J. Fanna, N. D. Shepherd, I. Karatchevtseva, K. Lu, L. Kong, Jason R. Price, RSC Adv. **2016**, 6, 75045. (1) M. Azam, G. Velmurugan, S. M. Wabaidur, A. Trzesowska-Kruszynska, R. Kruszynski, S. I. Al-Resayes, Z. A. Al-Othman, P. Venuvanalingam, Sci. Rep. 2016, 6, 32898:1-13, doi: 10.1038/srep32898. (m) H. B. T. Jeazet, K. Gloe, T. Doert, J. Mizera, O. N. Kataeva, S. Tsushima, G. Bernhard, J. J. Weigand, L. F. Lindoy, K. Gloe, Polyhedron 2016, 103, 198. (n) L. Pavelek, V. Ladányi, M. Nečas,

- S. Vallová, K. Wichterle, *Polyhedron* **2016**, *107*, 89. (o) A. Akbari, A. Fasihizad, M. Ahmadi, B. Machura, *Polyhedron* **2017**, *128*, 188. (p) E. E. Hardy, K. M. Wyss, M. A. Eddy, A. E. V. Gorden, *Chem. Commun.* **2017**, *53*, 5718. (q) J. R. Pankhurst, N.a L. Bell, M. Zegke, L. N. Platts, C. A. Lamfsus, L. Maron, L. S. Natrajan, S. Sproules, P. L. Arnold, J. B. Love, *Chem. Sci.* **2017**, *8*, 108. (r) J. E. Niklas, B. H. Farnum, J. D. Gorden, A. E. V. Gorden, *Organometallics* **2017**, *36*, 4626.
- (a) A. –M. Stadler, J. Harrowfield, *Inorg. Chim. Acta* 2009, 362, 4298. (b)
 L. D. Popov, A. N. Morozov, I. N. Shcherbakov, Y. P. Tupolova, V. V. Lukov, V. A. Kogan, *Russ. Chem. Rev.* 2009, 78, 643. (c) N. P. Belskaya, W. Dehaen, V. A. Bakulev, *ARKIVOC* 2010, i, 275. (d) J. R. Dilworth, R. Hueting, *Inorg. Chim. Acta* 2012, 389, 3. (e) R. Narang, B. Narasimhan, S. Sharma, *Curr. Med. Chem.* 2012, 19, 569. (f) P. Zhang, L. Zhang, J. Tang, *Curr. Inorg. Chem.* 2013, 3, 101. (g) M. M. E. Shakdofa, M. H. Shtaiwi, N. Morsy, T. M. A. Abdel-rassel, *Main Group Chem.* 2014, 13, 187. (h) X. Su, I. Aprahamian, *Chem. Soc. Rev.* 2014, 43, 1963.
- (a) N. R. Sangeetha, S. Pal, Bull. Chem. Soc. Jpn. 2000, 73, 357. (b) N. R. Sangeetha, V. Kavita, S. Wocadlo, A. K. Powell, S. Pal, J. Coord. Chem. 2000, 51, 55. (c) S. N. Pal, S. Pal, Acta Crystallogr. Sect. C 2001, 57, 141. (d) S. N. Pal, K. Radhika, S. Pal, Z. Anorg Allg. Chem. 2001, 627, 1631. (e) A. Sarkar, S. Pal, Polyhedron 2006, 25, 1689–1694. (f) A. Sarkar, S. Pal, Polyhedron 2007, 26, 1205–1210. (g) A. Sarkar, S. Pal, Inorg. Chim. Acta 2008, 361, 2296–2304. (h) A. Sarkar, S. Pal, Inorg. Chim. Acta 2009, 362, 3807; i) A. Sarkar, S. Pal, Eur. J. Inorg. Chem. 2009, 5391. (j) S. K. Kurapati, U. Ugandhar, S. Maloth, S. Pal, Polyhedron 2012, 42, 161.
- (a) M. F. Zady, J. L. Wong, J. Org. Chem. 1976, 41, 2491. (b) K. Nagaraju, R. Raveendran, S. N. Pal, S. Pal, Polyhedron 2012, 33, 52. (c)
 C. Basu, S. Chowdhury, R. Banerjee, H. S. Evans, S. Mukherjee, Polyhedron 2007, 26, 3617. (d) D. Debnath, S. Roy, B. –H. Li, C. –H. Lin, T. K. Misra, Spectrochim. Acta, Part A 2015, 140, 185.

- (a) C. Panattoni, R. Graziani, G. Bandoli, B. Zarli, G. Bombieri, *Inorg. Chem.* 1969, 8, 320. (b) V. I. Spitsyn, V. V. Kolesnik, V. É. Mistryukov, I. A. Yuranov, Y. N. Mikhailov, K. M. Dunaeva, *Russ. Chem. Bull.* 1982, 31, 715. (c) I. A. Charushnikova, N. N. Krot, Z. A. Starikova, *Radiochemistry* 2008, 50, 117. (d) P. D. Bernardo, P. L. Zanonato, F. Benetollo, A. Melchior, M. Tolazzi, L. Rao, *Inorg. Chem.* 2012, 51, 9045. (e) L. B. Serezhkina, M. S. Grigor'ev, N. A. Shimin, V. V. Klepov, V. N. Serezhkin, *Russ. J. Inorg. Chem.* 2015, 60, 672.
- (a) S. K. Kurapati, U. Ugandhar, S. Maloth, S. Pal, *Polyhedron* 2012, 42, 161.
 (b) M. F. Zady, F. N. Bruscato, J. L. Wong, *J. Chem. Soc., Perkin Trans I* 1975, 2036.
- 8. CrysAlisPro, Agilent Technologies, Yarnton, Oxfordshire, UK, 2015.
- 9. *SMART v5.630 and SAINT-plus v6.45*, Bruker-Nonius Analytical X-ray Systems Inc., Madison, WI, USA, **2003.**
- 10. G. M. Sheldrick, *SADABS*, *Program for Area Detector Absorption Correction*, University of Göttingen, Göttingen, Germany, **1997**.
- 11. S. Parkin, B. Moezzi, H. Hope, J. Appl. Crystallogr. 1995, 28, 53.
- 12. G. M. Sheldrick, Acta Crystallogr. Sect. A 2008, 64, 112.
- 13. L. J. Farrugia, *J. Appl. Crystallogr.* **2012**, *45*, 849.
- 14. F. Macrae, I. J. Bruno, J. A. Chisholm, P. R. Edgington, P. M. Cabe, E. Pidcock, L. Rodriguez-Monge, R. Taylor, J. van de Streek, P. A. Wood, J. Appl. Crystallogr. 2008, 41, 466.
- (a) Z. Libuś, *J. Inorg. Nucl. Chem.* 1962, 24, 619. (b) A. Günther, G. Geipel, G. Bernhard, *FZR–IRC Annu. Rep.* 2004, 24. (c) M. Glorius, G. Bernhard, *Radiochim. Acta* 2007, 95, 151. (d) P. K. Mohapatra, D. R. Raut, A. Sengupta, *Sep. Purif. Technol.* 2014, 133, 69.
- (a) W. Kuchle, M. Dolg, H. Stoll, H. Preuss, *Mol. Phys.* **1991**, *74*, 1245–1263.
 (b) W. Kuchle, M. Dolg, H. Stoll, H. Preuss, *J. Chem. Phys.* **1994**, *100*, 7535.
- (a) Z. Libuś, *J. Inorg. Nucl. Chem.* **1962**, 24, 619. (b) A. Günther, G. Geipel, G. Bernhard, *FZR–IRC Annu. Rep.* **2004**, 24. (c) M. Glorius, H.

Moll, G. Bernhard, *Radiochim. Acta* **2007**, *95*, 151. (d) P. K. Mohapatra, D. R. Raut, A. Sengupta, *Sep. Purif. Technol.* **2014**, *133*, 69.

Syntheses, Structural Insight and Photocatalytic Applications of Di-µ-hydroxo Diuranyl(VI) Complexes §

Two new dihyroxo-bridged diuranyl(VI) complexes of the molecular formula $[(UO_2)_2(\mu\text{-OH})_2(L^n)_2]$ (1 and 2) were synthesized in good yields (~64%) by reacting equimolar amounts of [UO₂(OAc)₂]·2H₂O and 2-((2-(6-chloropyridazin-3-yl)hydrazono)methyl)-4-R-phenols (HLⁿ where n = 1 and 2 for R = H and OMe, respectively) in dimethylformamide. Both complexes were characterized by elemental analysis, various spectroscopic and cyclic voltammetric measurements. X-ray crystal structures of the two complexes crystallized as solvated species showed the rare $\{(UO_2)_2(\mu\text{-OH})_2\}^{2+}$ core where each metal center is in a distorted pentagonal-bipyramidal N₂O₅ coordination sphere assembled by the two axial oxo atoms, two equatorial bridging hydroxo-O atoms and the equatorial N,N,O-donor (Lⁿ)⁻. The solvated complexes assemble through intermolecular bifurcated N-H···(O,O) and simple O-H···O and N-H···O hydrogen bonding interactions and form supramolecular one-dimensional chainlike and three-dimensional network structures in the crystal lattices. Infrared and proton NMR spectroscopic characteristics of the two complexes corroborate their molecular structures. Electronic spectra of 1 and 2 display three strong absorptions in the range 405-301 nm. A metal centered irreversible reduction having the E_{pc} near -1.06 V (vs. Ag/AgCl) has been observed in the cyclic voltammograms of 1 and 2. Both complexes are photocatalytically active in degradation of rhodamine B (RhB) and methylene blue (MB) under visible light irradiation. Photodegradation of RhB up to a maximum of 96% and that of MB up to a maximum of 85% was achieved in 150 and 180 min, respectively using 2 as catalyst.

[§] This work has been published in *New J. Chem.* **2019**, *43*, 970–978.

3.1. Introduction

The uranyl coordination complexes and uranyl-organic-framework materials have found a variety of applications ranging from photoluminescence to photochemical reactions to photocatalysis. 1,2 These properties are a consequence of the strongly covalent U-O bond in trans-(UO₂)²⁺ which primarily dictates the uranyl coordination chemistry. Thus, in search of new and more effective transuranyl(VI) dication containing species, coordination chemistry of it has emerged as one of the actively pursued areas of inorganic chemistry.³ Photocatalysis is the phenomenon of catalyzing reactions in presence of light of suitable wavelength. Photocatalysts have gained tremendous interest primarily because of their effective use against environmental pollution problems. The significant factors on which the photocatalytic activity of a substance depends are the desired band gap, reusability, surface morphology and stability. Over the decades, TiO₂ has emerged as an excellent photocatalyst for a variety of applications such as water splitting, degradation of pollutants, organic synthesis and phototherapy.⁵ But, TiO2 is an active photocatalyst only under ultraviolet light, which somewhat confines its practical applications. Thus there is an increasing demand of band gap tunable photocatalysts for visible light driven catalytic processes.⁶

In this chapter, we have explored the coordination chemistry of *trans*-uranyl(VI) dication with 2-((2-(6-chloropyridazin-3-yl)hydrazono)methyl)-4-methylphenols (HLⁿ) (n = 1 and 2 for R = H and OMe, respectively) has been explored. In this effort, two dinuclear complexes of formula $[(UO_2)_2(\mu\text{-OH})_2(L^n)_2]$ (1 and 2 for n = 1 and 2, respectively) have been isolated (Chart 1). Visible light induced photocatalytic abilities of these two complexes have been also examined by following the photodegradation of rhodamine B (RhB) and methylene blue (MB) solutions. In the following sections, the syntheses, X-ray structures, physical properties and the photocatalytic activities of $[(UO_2)_2(\mu\text{-OH})_2(L^{1/2})_2]$ (1 and 2) have been described.

 $[(UO_2)_2(\mu\text{-OH})_2(L^n)_2]$ (1 and 2 for n = 1 and 2)

Chart 1: Chemical structure diagrams of 2-((2-(6-chloropyridazin-3-yl)hydrazono)methyl)-4-R-phenols (HLⁿ) and their corresponding complexes $[(UO_2)_2(\mu\text{-OH})_2(L^n)_2]$.

3.2. Experimental Section

3.2.1. Materials:

3-Hydrazino-6-chloropyridazine was prepared by following a reported procedure.⁷ All other chemicals and the solvents used in this work were of reagent grade available commercially and were used as received without further purification.

3.2.2. Physical Measurements:

Elemental (CHN) analysis data were obtained with the help of a Thermo Finnigan Flash EA1112 series elemental analyzer. A Shimadzu LCMS 2010 liquid chromatograph mass spectrometer was used for the purity verification of the Schiff bases (HL^{1/2}). Solid state magnetic susceptibility measurements were performed with a Sherwood Scientific balance. A Digisun DI-909 conductivity meter was used for solution electrical conductivity measurements. A Thermo Scientific Nicolet iS5 FT-IR spectrophotometer was used to record the infrared spectra. A Shimadzu UV-3600 UV-Vis-NIR spectrophotometer was used to

collect the electronic spectra. The ¹H (400 MHz) NMR spectra were recorded with the help of a Bruker NMR spectrometer. Cyclic voltammetric measurements were carried out with the help of a CH Instruments model 620A electrochemical analyzer.

3.2.3. Synthesis of the complexes $[(UO_2)_2(\mu - OH)_2(L^n)_2]$ (1 and 2):

The complexes 1 and 2 were synthesized using the following general procedure. Solid $UO_2(OAc)_2 \cdot 2H_2O$ (0.25 mmol) was added to a hot dimethylformamide solution (8 mL) of the corresponding HL^n (n = 1 or 2) (0.25 mmol) in a 25 mL beaker. The color of the mixture immediately turned to deep brown. The solution was then heated on a water bath for about 45 min and filtered hot to remove any solid present. The filtrate was kept at room temperature (298 K) for slow evaporation. In about 3–4 weeks the brown crystalline material separated was collected by filtration, washed with methanol and finally dried in vacuum.

[(UO₂)₂(μ -OH)₂(L¹)₂] (1): Yield 65%. Anal. Calcd for C₂₂H₁₈Cl₂N₈O₈U₂: C, 24.71; H, 1.70; N 10.48. Found C 24.35, H 1.76, N 10.23. Selected IR data (ν (cm⁻¹)): 3460 (O–H), 3278 (N–H), 1620 (C=N), 891, 872 (UO₂). UV–Vis data (λ max(nm) (ε(10⁴ M⁻¹cm⁻¹))): 405 (4.59)^{sh}, 367 (7.85), 301 (10.97). ¹H NMR data (δ (ppm) (J (Hz))): 11.14 (s, 1H, NH), 9.02 (s, 1H, H⁷), 7.72 (8) (d, 1H, H¹⁰), 7.46 (8) (d, 1H, H⁹), 7.41 (8) (dd \rightarrow t, 1H, H⁴), 7.00 (8) (d, 1H, H⁶), 6.98 (8) (d, 1H, H³), 6.69 (8) (dd \rightarrow t, 1H, H⁵). CV data (E_{pc} and E_{pa} (V)): –1.01 and –0.47.

[(UO₂)₂(μ -OH)₂(L²)₂] (2): Yield 63%. Anal. Calcd for C₂₄H₂₂Cl₂N₈O₁₀U₂: C, 25.52; H, 1.96, N 9.92. Found: C, 25.21; H 1.93, N 9.56. Selected IR data (ν (cm⁻¹)): 3470 (O–H), 3240 (N–H), 1618 (C=N), 899 (UO₂). UV–Vis data (ν (λmax(nm) (ε($10^4 \text{ M}^{-1}\text{cm}^{-1}$))): 405 (6.98)^{sh}, 375 (9.52), 302 (11.59). ¹H NMR data (ν (ppm) (ν (Hz))): 10.60 (s, 1H, NH), 8.97 (s, 1H, H⁷), 7.29 (3) (d, 1H, H⁶), 7.11 (s, 1H, μ -OH), 7.09 (8) (d, 1H, H¹⁰), 7.03 (8,3) (dd, 1H, H⁴), 6.92 (8) (d, 1H, H⁹), 6.87 (8) (d, 1H, H³), 3.75 (s, 3H, -OCH₃). CV data (ν (E_{pc} and E_{pa} (V)): –1.11 and –0.50.

3.2.4. X-ray Crystallography:

Single crystals suitable for X-ray data collection for both complexes were collected from the crystalline materials separated in the synthetic reaction mixtures. In each case, the crystal was taken from the mother liquor, coated with silicone oil and then mounted on a glass fibre using epoxy. Both 1 and 2 crystallized as solvated species, which are 1·H₂O·2Me₂NCHO and 2·1.5H₂O, respectively. Unit cell determination and intensity data collection for each of 1·H₂O·2Me₂NCHO and 2·1.5H₂O were performed at room temperature (298 K) on a Bruker D8 Quest diffractometer fitted with a Photon 100 CMOS area detector and an Incoatec microfocus source for graphite monochromated Mo Ka radiation ($\lambda = 0.71073$ Å). The APEX3 software package⁸ was used for data acquisition, integration and reduction. The SADABS program⁹ was employed for absorption correction. In the case of 1·H₂O·2Me₂NCHO, some residual absorption effect was treated with an additional correction using the XABS2 program. ¹⁰ Both structures were solved by direct method and refined on F^2 using full-matrix least-squares procedures. In each structure, the non-hydrogen atoms were refined anisotropically. The hydrogen atoms of the water molecules were located in difference maps and placed at idealized positions, while the remaining hydrogen atoms were included at idealized positions using a riding model. All hydrogen atoms were refined as riding atoms with relative isotropic thermal parameters of their parent atoms. The SHELX-97 programs¹¹ available in the WinGX software suite¹² were used for structure solution and refinement. Structural illustrations were prepared using the Mercury package. 13 Selected crystallographic data for 1·H₂O·2Me₂NCHO and 2·1.5H₂O are listed in Table 1. Detailed X-ray crystallographic data for 1·H₂O·2Me₂NCHO and 2·1.5H₂O have been deposited with the Cambridge Crystallographic Data Centre under the deposition numbers CCDC 1870329 and 1870330, respectively.

3.2.5 Photocatalysis:

Organic dyes rhodamine B (RhB) and methylene blue (MB) were selected for heterogeneous photodegradation experiments. The powdered complex catalyst (20 mg) was suspended in an aqueous solution of the dye (40 mL, conc. 10 ppm) and stirred for ½ h in dark to ensure proper absorption/desorption equilibrium of the dye on the catalyst surface. The mixture was then exposed to irradiation of visible light with continuous stirring. After every ½ h of interval a portion of the solution was pipetted out and filtered. The clear dye solution obtained after filtration was used for spectrophotometric analysis. The degradations of the dyes with the increase of the irradiation time were followed by measuring the changes in the absorption intensities at λ_{max} values of 554 and 664 nm for RhB and MB, respectively.

3.3. Results and Discussions

3.3.1. Synthesis and Characterization:

The Schiff bases (HL^{1/2}) were prepared in fairly high yields (~80%) by condensation reactions of equimolar amounts 3-hydrazino-6-chloropyridazine and the corresponding 5-R-salicyladehydes (R = H and OMe) in ethanol by following a procedure very similar to that reported earlier.^{7,14} Complexes having the general molecular formula [(UO₂)₂(μ-OH)₂(Lⁿ)₂] (1 (n = 1) and 2 (n = 2)) were synthesized in good yields (~64%) by treating the corresponding Schiff bases (HL^{1/2}) with UO₂(OAc)₂·2H₂O in dimethylformamide. Elemental analysis data of 1 and 2 are in good agreement with their molecular formulas. Room temperature magnetic susceptibility measurements with the powdered samples of the two complexes indicate their diamagnetic character and hence the +6 oxidation state of uranium in each. Both complexes are insoluble in most of the common organic solvents except for dimethylformamide and dimethylsulfoxide. In solution, each of the two complexes is electrically non-conducting. The non-electrolytic behavior of 1 and 2 is consistent with their molecular formulas as neutral species.

Table 1: Selected crystal data and structure refinement summary

Complex	1·H ₂ O·2Me ₂ NCHO	2·1.5H ₂ O
Chemical formula	$C_{28}H_{34}Cl_2N_{10}O_{11}U_2$	$C_{24}H_{23}Cl_2N_8O_{11.5}U_2$
Formula weight	1233.61	1154.46
Crystal system	Triclinic	Monoclinic
Space group	$P\bar{1}$	C2/c
a (Å)	7.0485(5)	15.4436(13)
b (Å)	14.7628(11)	14.7742(12)
c (Å)	18.7692(14)	15.3194(12)
α(°)	73.799(3)	90
$oldsymbol{eta}(^{\circ})$	89.767(3)	113.786(2)
γ(°)	89.067(3)	90
Volume (Å ³)	1875.2(2)	3198.5(5)
Z	2	4
ρ (g cm ⁻³)	2.185	2.397
$\mu (\mathrm{mm}^{-1})$	8.837	10.352
Reflections collected	64327	20243
Reflections unique	6603	2812
Reflections $[I \ge 2\sigma(I)]$	5938	2219
Data / parameter	6603 / 482	2812 / 219
$R1$, $wR2$ [$I \ge 2\sigma(I)$]	0.0307, 0.0710	0.0355, 0.0791
R1, wR2 [all data]	0.0351, 0.0728	0.0536, 0.0857
GoF on F^2	1.086	1.039
Max. / Min. $\Delta \rho$ (e Å ⁻³)	3.227 / -1.941	0.927 / -1.002

3.3.2. X-ray Molecular Structures:

The structures of 1·H₂O·2Me₂NCHO and 2·1.5H₂O were solved in triclinic *P*1 and monoclinic *C*2/c space groups, respectively. The asymmetric unit of the first crystal contains one complete molecule of the dinuclear complex 1, one water molecule and two dimethylformamide molecules. On the other hand, the asymmetric unit of the second crystal contains one-half of the dinuclear complex 2, one-half of a water molecule and a second water molecule having one-quarter occupancy. The two halves of the molecule of 2 are related by an inversion centre, while a two-fold axis passes through the O-atom of each water molecule. The structures of 1·H₂O·2Me₂NCHO and 2·1.5H₂O are illustrated in Figure 1. The bond lengths and bond angles associated with the metal centres for 1 and 2 are listed in Tables 2 and 3, respectively.

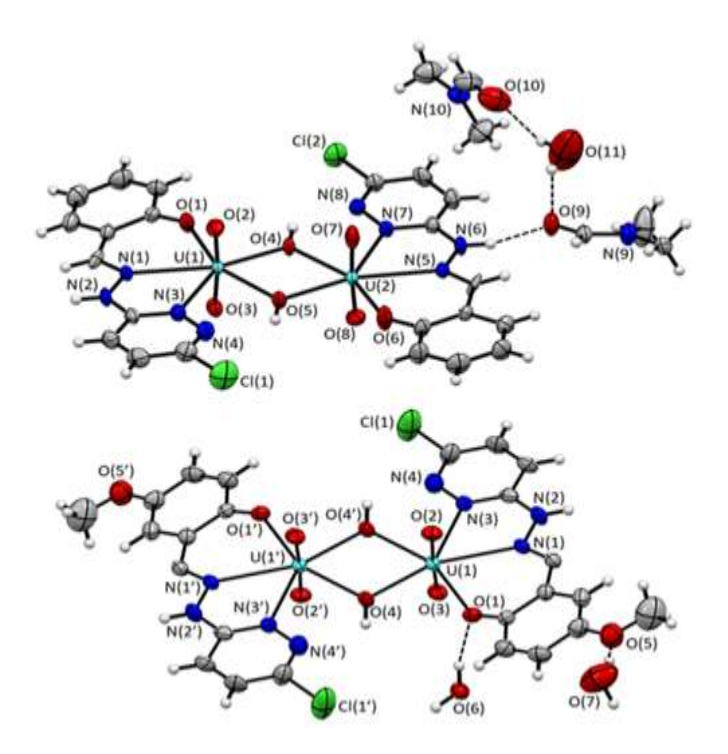


Figure 1: The structures of $[(UO_2)_2(\mu\text{-OH})_2(L^1)_2]\cdot H_2O\cdot 2Me_2NCHO$ ($\mathbf{1}\cdot H_2O\cdot 2Me_2NCHO$) (top) and $[(UO_2)_2(\mu\text{-OH})_2(L^2)_2]\cdot 1.5H_2O$ ($\mathbf{2}\cdot 1.5H_2O$) (bottom). In both structures, all the non-hydrogen atoms are represented by their 40% probability thermal ellipsoids and only the non-carbon atoms are labelled for clarity.

In the case of 1·H₂O·2Me₂NCHO, the water molecule acts as a bridge between the two dimethylformamide molecules by forming two O-H···O hydrogen bonds with the two dimethylformamide O-atoms. One end this Me₂NCHO···HOH···OHCNMe₂ ensemble is connected to the complex molecule through a N-H···O interaction involving O-atom of one Me₂NCHO and the hydrazinic N-H of the U(2) bound (L¹)- (Figure 1). On the other hand, in 2·1.5H₂O, the full occupancy water molecule is hydrogen bonded to the metal coordinated phenolate O-atom and the water molecule having the half-occupancy is hydrogen bonded to the O-atom of the methoxy substituent of $(L^2)^-$ (Figure 1). The structures of the two dinuclear complex molecules are very similar. The metal centres are in distorted pentagonal-bipyramidal N₂O₅ coordination spheres. The fused 5,6-membered chelate rings forming pyridazine-N, azomethine-N and phenolate-O donor (Lⁿ) and the two bridging hydroxo-O atoms form the pentagonal N₂O₃ plane (rms deviations 0.03–0.16 Å) and the two oxo atoms occupy the axial positions. The $U_2(\mu\text{-OH})_2$ is essentially planar (rms deviation 0.02 Å) in 1 and perfectly planar in 2. The U-O(H)-U bridge angles (113.2(2) and 112.4(2)°) in 1 are slightly larger than the bridge angle (110.6(2)°) in centrosymmetric 2. As a consequence the U···U distance in 1 (3.8821(4) Å) is little longer than that in 2 (3.8405(7) Å). It may be noted that very few structurally characterized discrete diuranyl(VI) complexes containing the $\{(UO_2)_2(\mu\text{-OH})_2\}^{2+}$ core are known. Overall, the U-OH bond lengths, U-O(H)-U bridge angles and the U···U distances in the $\{(UO_2)_2(\mu\text{-OH})_2\}^{2+}$ fragment of 1 and 2 are within the corresponding ranges reported earlier for complexes of this core.¹⁵ In 1, the average of U=O bond lengths for U(1) (1.786(5) Å) is significantly longer than that for U(2) (1.760(6) Å). This difference is most likely due to the involvement of the oxo atoms O(2) and O(3) attached to U(1) in intermolecular N-H···O hydrogen bonding interactions as acceptors (vide infra). In the centrosymmetric 2, the average of U=O bond lengths is 1.776(6) Å. Overall, the U=O bond lengths in 1 and 2 are within the range found in trans-uranyl(VI) dication complexes. 15-17 The trans-O=U=O angles (174.1(2)-176.6(3)°) are slightly off from the ideal value of 180°. The remaining bond lengths and angles associated with the uranium centres and the N,N,O-donor $(L^n)^-$ are comparable with the corresponding bond parameters reported for complexes of *trans*- $(UO_2)^{2+}$ having pentagonal-bipyramidal uranium centres and similar coordinating atom containing Schiff base ligands. ^{16,17}

3.3.3. Hydrogen Bonding and Self-assembly:

In both structures, the complex molecules and the lattice solvent molecules have several classical hydrogen bond donors such as N–H and O–H and acceptors such as O– and Cl– atoms. Thus the two structures have been scrutinized for intermolecular hydrogen bonding interactions and if there is any then how that directs the supramolecular self-assembly process. The intermolecular hydrogen bonds found are O–H···O and bifurcated O–H···O···H–N and N–H···(O,O) in $1 \cdot H_2O \cdot 2Me_2NCHO$ and O–H···O and N–H···O in $2 \cdot 1.5H_2O$. The geometric parameters for these intermolecular hydrogen bonds are listed in Table 4 and the supramolecular structures assembled by them are described below.

In 1·H₂O·2Me₂NCHO, the hydrogen bonded ensemble of the lattice solvent molecules (Me₂NCHO···HOH···OHCNMe₂) that is connected to the U(2) side of 1 via the N–H···O interaction (Figure 1) does not participate in any further intermolecular interaction. However, on the other side of the solvated dinuclear molecule, the hydrazinic N–H of the U(1) coordinated (L¹)⁻ and the U(1) bound oxo atoms O(2) and O(3) participate in three bifurcated N–H···(O,O) hydrogen bonding interactions with two neighbouring inversion symmetry related molecules in a kind of reciprocal manner. This intermolecular N–H···(O,O) interaction leads to a one-dimensional assembly of 1·H₂O·2Me₂NCHO in the crystal lattice (Figure 2).

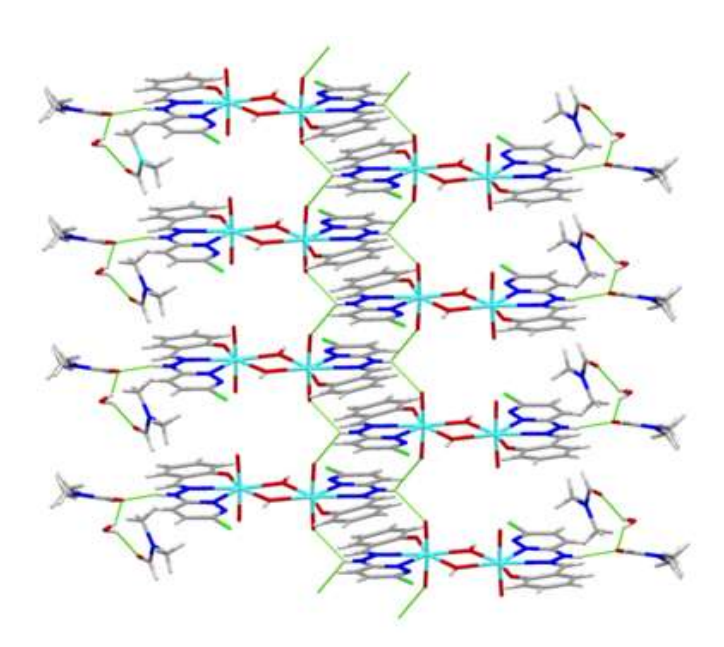


Figure 2: One-dimensional chain-like assembly of $[(UO_2)_2(\mu-OH)_2(L^1)_2]\cdot H_2O\cdot 2Me_2NCHO$ ($1\cdot H_2O\cdot 2Me_2NCHO$).

In $2\cdot1.5H_2O$, the two-fold symmetric half-occupancy water molecule acts as donor in two O–H···O hydrogen bonds involving the O–atoms of the methoxy substituents on the salicylidene moieties of $(L^2)^-$ of two complex molecules. This water molecule is not involved in any other hydrogen bonding. Formation of a one-dimensional chain like array of $2\cdot0.5H_2O$ due to the above mentioned intermolecular O–H···O interactions cannot be counted due to the positional disorder of the water molecule.

Table 2: Selected bond parameters (Å and °) for $1 \cdot H_2O \cdot 2Me_2NCHO$

	1	, – –	
U(1)-O(1)	2.220(5)	U(2)-O(4)	2.356(4)
U(1)–O(2)	1.799(5)	U(2)–O(5)	2.336(4)
U(1)–O(3)	1.773(5)	U(2)–O(6)	2.202(5)
U(1)–O(4)	2.293(4)	U(2)-O(7)	1.737(6)
U(1)–O(5)	2.335(4)	U(2)-O(8)	1.782(5)
U(1)–N(1)	2.632(5)	U(2)–N(5)	2.621(5)
U(1)–N(3)	2.584(6)	U(2)-N(7)	2.582(5)
O(1)-U(1)-O(2)	88.8(2)	O(4)–U(2)–O(5)	66.63(15)
O(1)-U(1)-O(3)	91.8(2)	O(4)-U(2)-O(6)	155.29(17)
O(1)–U(1)–O(4)	86.77(17)	O(4)-U(2)-O(7)	89.3(2)
O(1)–U(1)–O(5)	154.40(16)	O(4)-U(2-O(8)	91.6(2)
O(1)-U(1)-N(1)	69.24(17)	O(4)-U(2)-N(5)	134.53(16)
O(1)-U(1)-N(3)	130.01(18)	O(4)-U(2-N(7)	72.60(16)
O(2)-U(1)-O(3)	174.1(2)	O(5)-U(2)-O(6)	88.68(17)
O(2)-U(1)-O(4)	94.3(2)	O(5)-U(2)-O(7)	91.8(2)
O(2)–U(1)–O(5)	91.5(2)	O(5)-U(2)-O(8)	93.4(2)
O(2)-U(1)-N(1)	91.2(2)	O(5)-U(2)-N(5)	158.74(16)
O(2)-U(1)-N(3)	84.4(2)	O(5)-U(2)-N(7)	139.21(16)
O(3)–U(1)–O(4)	91.5(2)	O(6)-U(2)-O(7)	90.5(3)
O(3)–U(1)–O(5)	90.5(2)	O(6)-U(2)-O(8)	90.9(3)
O(3)–U(1)–N(1)	83.5(2)	O(6)-U(2)-N(5)	70.11(18)
O(3)-U(1)-N(3)	90.8(2)	O(6)-U(2)-N(7)	132.11(18)
O(4)-U(1)-O(5)	67.67(15)	O(7)-U(2)-O(8)	174.7(2)
O(4)-U(1)-N(1)	155.26(17)	O(7)-U(2)-N(5)	87.1(2)
O(4)-U(1)-N(3)	143.04(17)	O(7)–U(2)–N(7)	88.6(2)
O(5)–U(1)–N(1)	136.32(16)	O(8)–U(2)–N(5)	88.5(2)
O(5)-U(1)-N(3)	75.42(17)	O(8)–U(2)–N(7)	86.6(2)
N(1)-U(1)-N(3)	61.51(18)	N(5)-U(2)-N(7)	62.02(17)

Table 3 Selected bond parameters (Å and °) for $2 \cdot 1.5 H_2 O$

U(1)–O(1)	2.251(6)	U(1)–O(2)	1.775(6)
U(1)–O(3)	1.776(6)	U(1)–O(4)	2.322(5)
$U(1)-O(4')^a$	2.350(6)	U(1)–N(1)	2.612(7)
U(1)–N(3)	2.613(7)		
O(1)-U(1)-O(2)	92.6(3)	O(1)–U(1)–O(3)	87.2(3)
O(1)-U(1)-O(4)	86.1(2)	$O(1)-U(1)-O(4')^a$	155.5(2)
O(1)-U(1)-N(1)	69.6(2)	O(1)–U(1)–N(3)	129.6(2)
O(2)-U(1)-O(3)	176.6(3)	O(2)–U(1)–O(4)	92.9(3)
$O(2)-U(1)-O(4')^a$	90.7(3)	O(2)–U(1)–N(1)	82.5(3)
O(2)-U(1)-N(3)	94.6(3)	O(3)–U(1)–O(4)	90.4(3)
$O(3)-U(1)-O(4')^a$	90.8(3)	O(3)–U(1)–N(1)	94.2(3)
O(3)-U(1)-N(3)	82.9(3)	$O(4)-U(1)-O(4')^a$	69.4(2)
O(4)-U(1)-N(1)	155.0(2)	O(4)–U(1)–N(3)	143.0(2)
$O(4')^a - U(1) - N(1)$	134.9(2)	$O(4')^a - U(1) - N(3)$	74.3(2)
N(1)-U(1)-N(3)	62.0(2)		

^a Symmetry transformation used: -x + 3/2, -y + 1/2, -z

Table 4: Hydrogen bonding parameters for 1·H₂O·2Me₂NCHO and 2·1.5H₂O^a

Complex	D-H···A	D…A (Å)	∠DHA (°)
1·H ₂ O·2Me ₂ NCHO	N(6)-H(6)···O(9)	2.758(8)	163
	O(11)-H(11A)···O(9)	3.017(13)	153
	O(11)-H(11B)···O(10)	2.750(16)	142
	$N(2)$ – $H(2A)$ ···O $(2)^i$	2.964(7)	133
	N(2)– $H(2A)$ ···O (3) ⁱⁱ	3.093(8)	127
2 ·1.5H ₂ O	O(6)-H(6A)···O(1)	2.705(7)	161
	O(7)–H(7A)···O(5)	2.94(2)	158
	N(2)–H(2A)···O(6) ⁱⁱⁱ	2.844(10)	174

 $[^]a$ Symmetry transformations used: (i) $-x+1,\,-y+1,\,-z+1.$ (ii) $-x+2,\,-y+1,\,-z+1.$ (iii) $-x+1,\,-y,\,-z.$

On the other hand, the second two-fold symmetric but full occupancy water molecule participates in the maximum possible that is four hydrogen bonding interactions. These are two O–H···O interactions as donor and two N–H···O interactions as acceptor. In the former, the uranium coordinated phenolate-O atom of $(L^2)^-$ is the acceptor and in the latter, the hydrazinic N–H of $(L^2)^-$ is the donor. Thus, each full occupancy water molecule is connected to four complex molecules which are tetrahedrally oriented around the water O-atom and a butterfly-like motif is formed (Figure 3, top). Interconnection of these motifs via these four intermolecular hydrogen bonding interactions leads to an overall three-dimensional network of $2\cdot1.5\text{H}_2\text{O}$ in the crystal lattice (Figure 3, bottom).

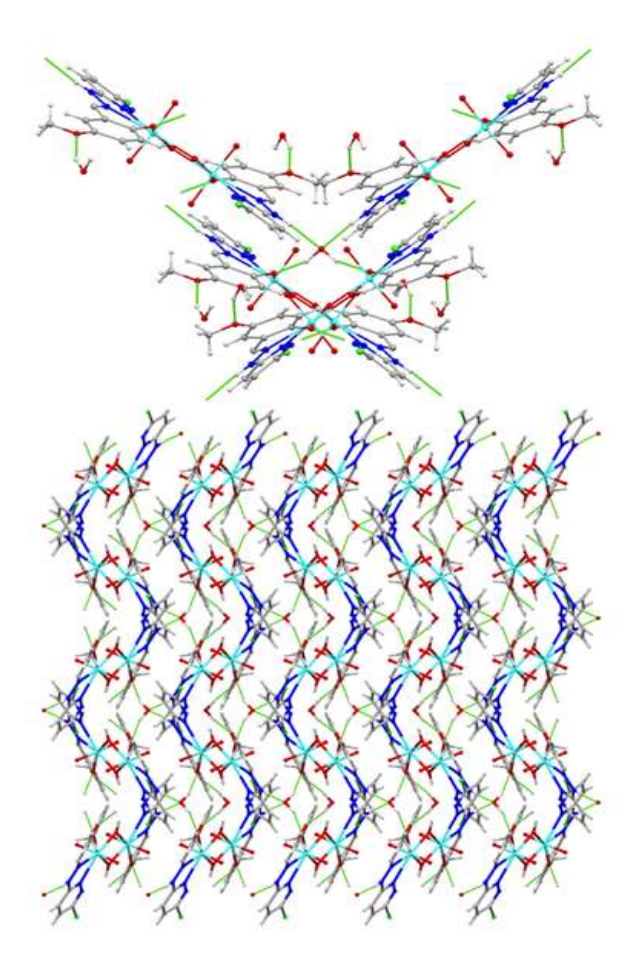


Figure 3: Butterfly-like motif (top) and the three-dimensional network of $[(UO_2)_2(\mu\text{-OH})_2(L^2)_2]\cdot 1.5H_2O$ (2·1.5H₂O) viewed along the *a*-axis (bottom).

3.3.4. Spectroscopic Characterizations:

Infrared spectra of 1 and 2 were recorded in ATR mode in the range 4000–550 cm⁻¹. A large number of bands with various intensities have been observed in each spectrum. No attempt has been made to assign all the bands except for few characteristic bands. Both complexes display a broad band at ~3465 cm⁻¹. Similar band observed for dihdroxo bridged complexes is attributed to the bridging-OH groups. 15g,18 A weak and somewhat broad band observed at ~3260 cm^{-1} is assigned to the hydrazinic-NH of $(L^n)^{-15,19}$. The sharp and strong band at ~1619 cm⁻¹ displayed by both complexes is attributed to the metal coordinated azomethine (-HC=N-) group of (Lⁿ)-. 14,17,18 The spectrum of 1 displays two closely spaced strong bands at 891 and 872 cm⁻¹, while the spectrum of 2 displays a single strong band at 899 cm⁻¹ (Figure 4). The asymmetric stretching vibration of the trans-uranyl(VI) moiety is generally observed in this region as a strong band. 15g,h,18,19 Observation of two closely spaced bands in the case of 1 is most likely due to the difference in the two average U=O bond lengths at the two uranium centres caused by participation of the oxo atoms of one metal centre in intermolecular hydrogen bonding interactions (vide supra).

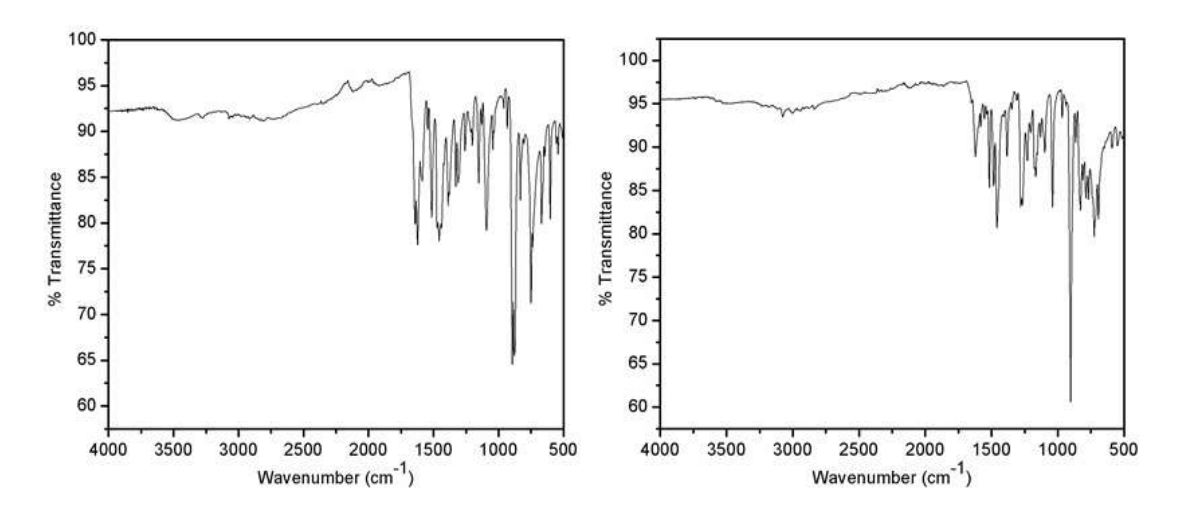


Figure 4: IR spectra of 1 (left) and 2 (right) in powder phase.

The electronic spectra of both 1 and 2 were recorded in dimethylformamide. The spectral profiles of the two complexes are very similar (Figure 5). They display a somewhat broad and strong band centered at ~370 nm (367 and 375 nm for 1 and

2, respectively), which is preceded by a shoulder at ~405 nm and followed by another strong band at ~302 nm. The free Schiff bases ($HL^{1/2}$) in dimethylformamide display two strong bands having almost equal intensities at ~350 and ~300 nm. Comparison of the spectra of the complexes with those of the Schiff bases clearly indicates that for **1** and **2** the absorption at ~302 nm is due to a ($L^{1/2}$)⁻ centered transition. Absorption bands at the longer wavelength ultraviolet region for *trans*-diuranyl(VI) dication containing species is characteristic of charge transfer transitions involving the U=O bonds. ²⁰ Thus the absorption band of **1** and **2** at ~370 nm, which is red-shifted in comparison to the corresponding absorption of the Schiff bases at ~350 nm, has most likely a combined ($L^{1/2}$)⁻ centered and *trans*-(UO_2)²⁺ centered charge transfer character. In the visible region, the shoulder at 405 nm has been assigned to primarily phenolate-to-metal charge transfer transition.

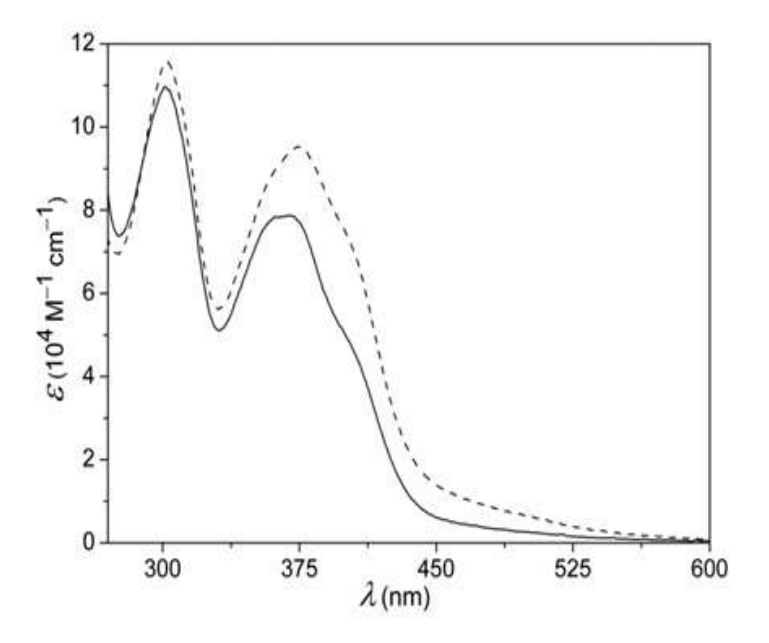


Figure 5: Electronic spectra of $[(UO_2)_2(\mu\text{-OH})_2(L^1)_2]$ (1) (—) and $[(UO_2)_2(\mu\text{-OH})_2(L^2)_2]$ (2) (- - -) in dimethylformamide.

The ¹H NMR spectra of **1** and **2** were recorded in DMSO-d₆ solutions. Each of the two spectra clearly indicates that in solution the two halves of the centrosymmetric complex molecule are equivalent. The chemical shift values with tentative assignments are provided in the experimental section under the

respective complexes. Absence of any signal assignable to the phenol proton resonance¹⁴ is consistent with the deprotonated state of the Schiff base ligand in both complexes. The hydrazinic N–H appears as a singlet at δ 11.14 and 10.60 ppm for 1 and 2, respectively. The azomethine (–HC=N–) proton (H⁷) of 1 and 2 resonates as a singlet at δ 9.02 and 8.97 ppm, respectively. A singlet observed at δ 7.11 ppm for 2 is assigned to the bridging hydroxyl group proton.²¹ However, no such signal has been observed for 1. The protons of the methoxy substituent in 2 are observed as a singlet at δ 3.75 ppm. In both complexes, the aromatic protons of (L¹)⁻ and (L²)⁻ appear with the expected splitting patterns in the ranges δ 7.71–6.69 and 7.29–6.87 ppm, respectively (Figures 6 and 7).

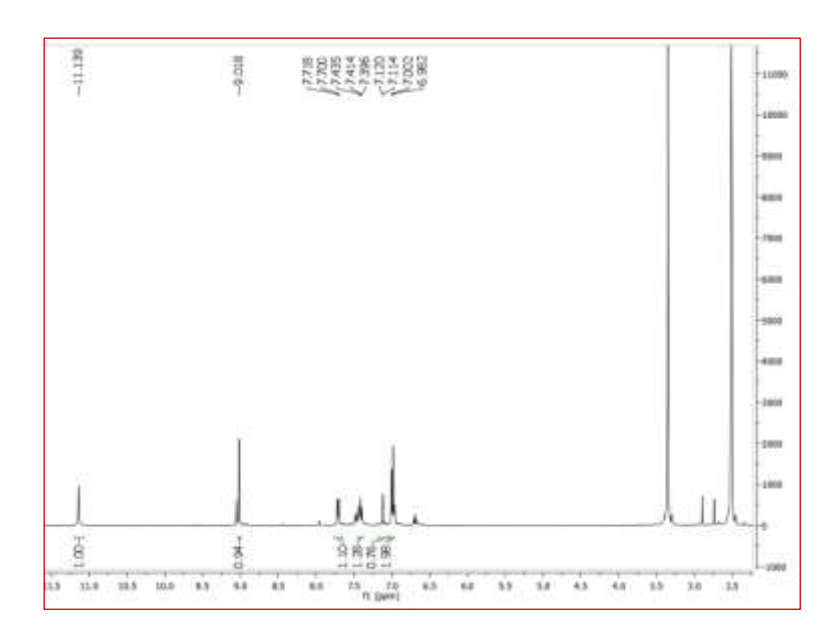


Figure 6: ¹H-NMR spectra of $[(UO_2)_2(\mu\text{-OH})_2(L^1)_2]$ (1) in DMSO-d₆

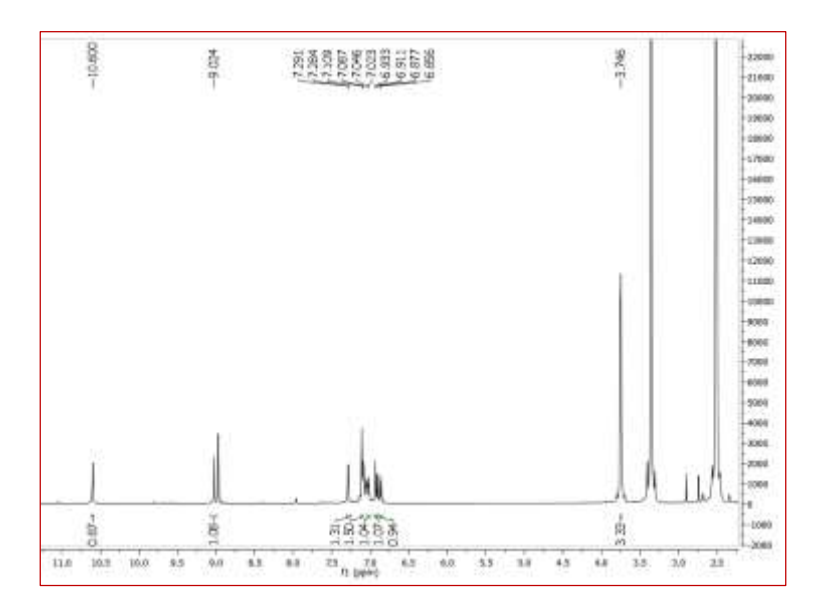


Figure 7: ${}^{1}\text{H-NMR}$ spectra of $[(UO_{2})_{2}(\mu\text{-OH})_{2}(L^{2})_{2}]$ (2) in DMSO-d₆.

3.3.5. Redox Properties:

Redox properties of 1 and 2 have been investigated by cyclic voltammetric measurements using their corresponding dimethylformamide solutions ($\sim 10^{-3}$ M) containing tetra-n- butylammonium perchlorate (TBAP) as the supporting electrolyte with a Pt-disk working electrode, a Pt-wire auxiliary electrode and an Ag/AgCl reference electrode under nitrogen atmosphere at 298 K. Under identical condition, the $E_{1/2}$ and $\Delta E_{\rm p}$ (= $E_{\rm pa}$ - $E_{\rm pc}$) values for the ferrocenium/ferrocene (Fc⁺/Fc) couple were 0.50 V and 150 mV, respectively. The cyclic voltammograms of the two complexes are very similar. They display a cathodic peak and a well separated weak anodic peak on reverse scan (Figure 8). The cathodic peak potentials (E_{pc}) are -1.01 and -1.10 V and the corresponding anodic peak potentials (E_{pa}) are -0.47 and -0.50 V for 1 and 2, respectively. The cathodic peak currents of both complexes are comparable with those of the Fc⁺/Fc couple and other known one electron transfer processes under similar conditions. 17,22 The free Schiff bases show an irreversible reduction response having relatively broader peaks and at more cathodic potentials (average $E_{\rm pc}$ and $E_{\rm pa}$ values are around -1.55 and -0.82 V, respectively) in the same experimental conditions. Comparison of the reduction responses displayed by the complexes with those of HL^{1/2} and considering that complexes of *trans*-(UO₂)²⁺ with ligands having comparable coordinating atoms are known to show uranium(VI) to uranium(V) reduction at similar potential range, the reductions observed for **1** and **2** have been assigned to a metal centered process. ^{16a,17} This assignment is further substantiated by the 90 mV cathodic shift of the E_{pc} of **2** compared to that of **1** due to the presence of the electron releasing methoxy group at *para* to the phenolate-O of the ligand (L²)⁻ in **2**.

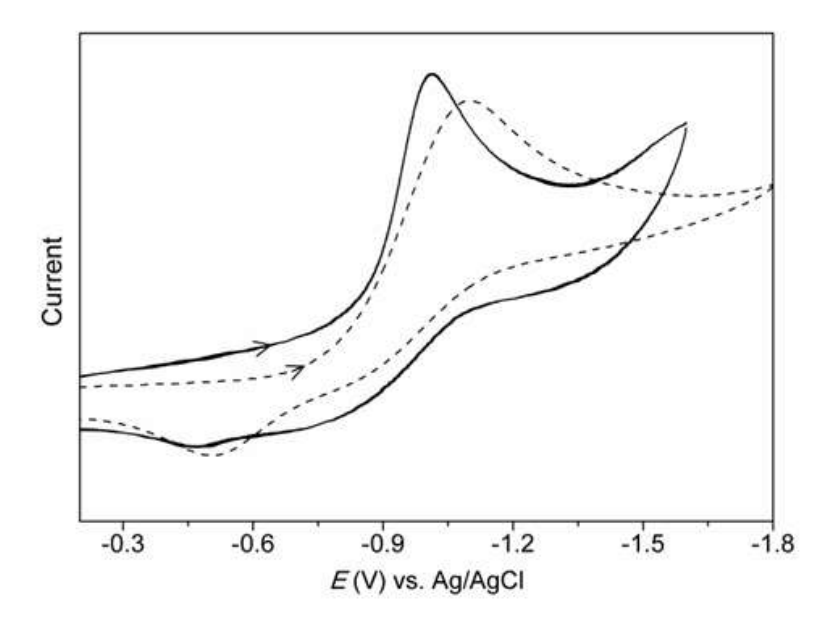


Figure 8: Cyclic voltammograms of $[(UO_2)_2(\mu\text{-OH})_2(L^1)_2]$ (1) (—) and $[(UO_2)_2(\mu\text{-OH})_2(L^2)_2]$ (2) (- - -) in dimethylformamide.

3.3.6. Photocatalytic Activities:

The electronic transition within the U=O double bond has been considered to be the key for the photocatalytic activities of the complexes of *trans*-diuranyl(VI) dication.^{1,2} The transition that gives rise to the absorption band of **1** and **2** at 367 and 375 nm, respectively has a partial *trans*-(UO₂)²⁺ centered character (*vide supra*). Appearance of this band near to the violet end of the visible light accompanied by the shoulder in the visible region at ~405 nm prompted us to examine the photocatalytic potentials of **1** and **2** by visible light irradiation. Herein we have chosen Rhodamine B (RhB) and Methylene Blue (MB) as the model pollutants for photo-degradation experiments. The photocatalytic reactions were heterogeneous in nature where the catalyst powder (**1** or **2**) was suspended

in the dye solution and stirred in presence of the white visible light. The degradation of the dye (RhB or MB) with the increase in the irradiation time was monitored spectrophotometrically. Irradiation time dependent spectral changes for RhB and MB in presence of 1 and 2 as catalyst are depicted in Figures 9–12. In the control experiments without catalysts in presence of light the variation in the absorption spectrum of either of the two dyes is insignificant. The degradation of RhB is as high as 96% in 150 min with 2 as catalyst, whereas for 1 as catalyst the degradation was 80% in a span of 180 min. In the case of MB the degradations were 71% in 210 min and 85% in 180 min for 1 and 2, respectively. Thus 2 is relatively more effective catalyst in photodegradation of both dyes (Figure 13). This difference in the activities is consistent with appearance of the first absorption band in the ultraviolet region for 2 at slightly lower energy than that in 1 and the higher extinction coefficients of this band and the ~405 nm shoulder of 2 compared to those of 1. In general, the photocatalytic dye degradation abilities of 1 and 2 are better or comparable with the previously reported uranyl containing catalysts. 1c,2a,b,e-g

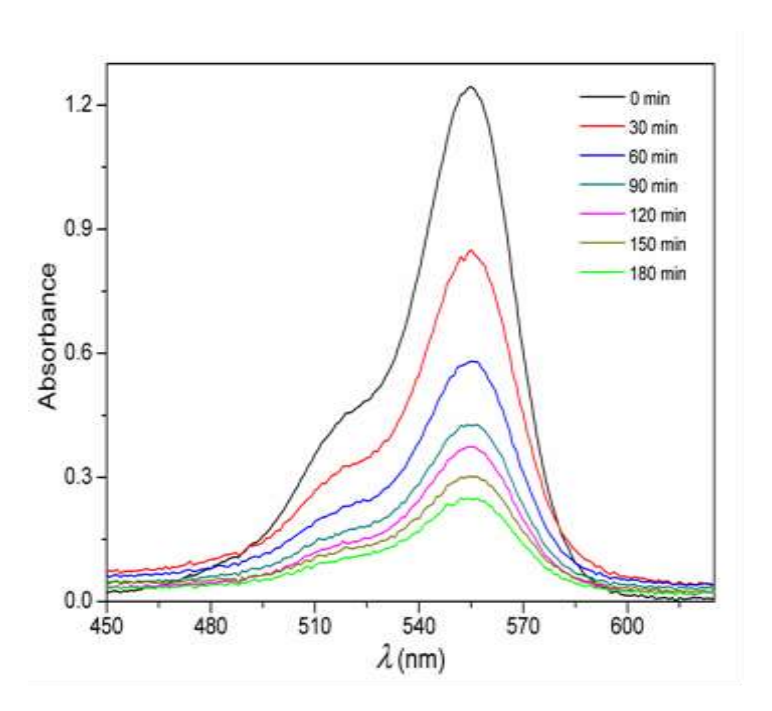


Figure 9: Degradation of Rhodamine B (RhB) under visible light irradiation in presence of $[(UO_2)_2(\mu\text{-OH})_2(L^1)_2]$ (1) as catalyst.

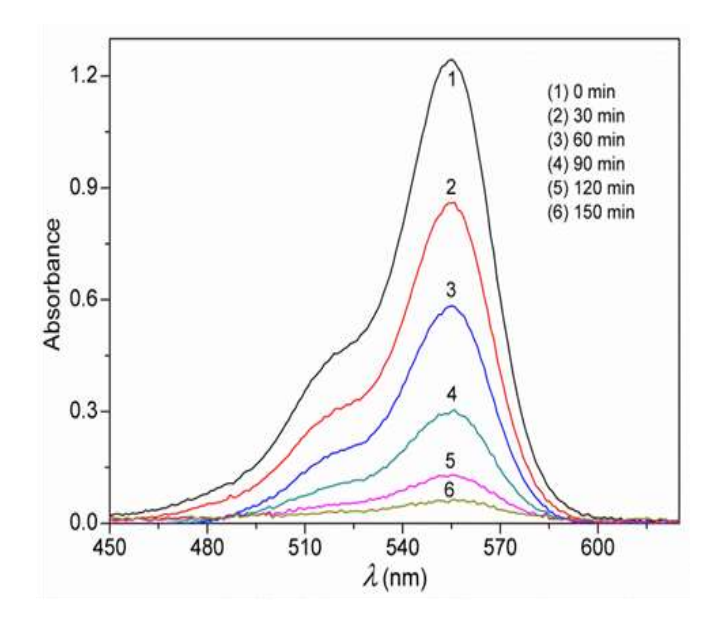


Figure 10: Photocatalytic degradation of Rhodamine B (RhB) under visible light irradiation in presence of $[(UO_2)_2(\mu\text{-OH})_2(L^2)_2]$ (2).

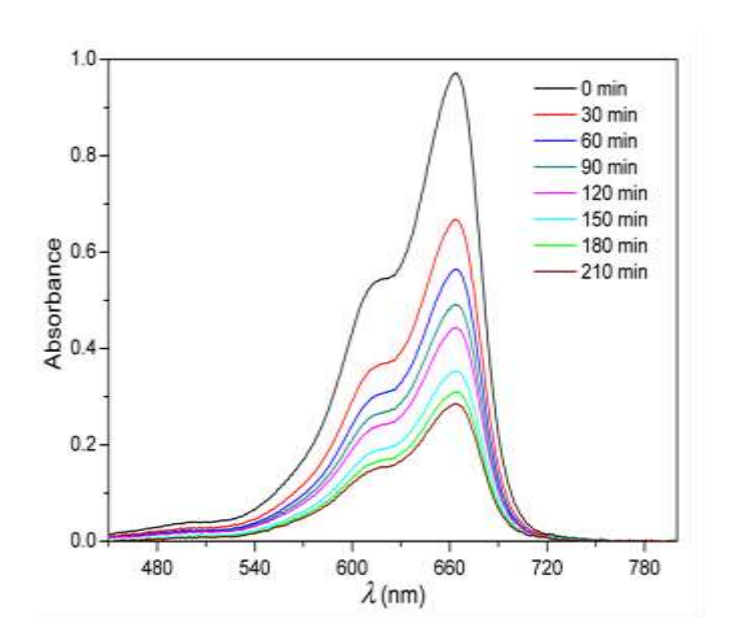


Figure 11: Degradation of Methylene Blue (MB) under visible light irradiation in presence of $[(UO_2)_2(\mu\text{-OH})_2(L^1)_2]$ (1) as catalyst.

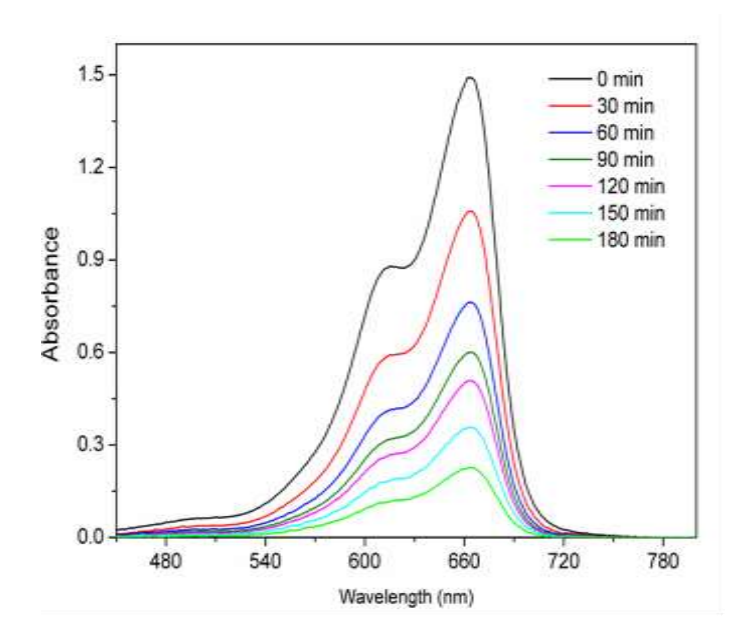


Figure 12: Degradation of Methylene Blue (MB) under visible light irradiation in presence of $[(UO_2)_2(\mu\text{-OH})_2(L^2)_2]$ (2) as catalyst.

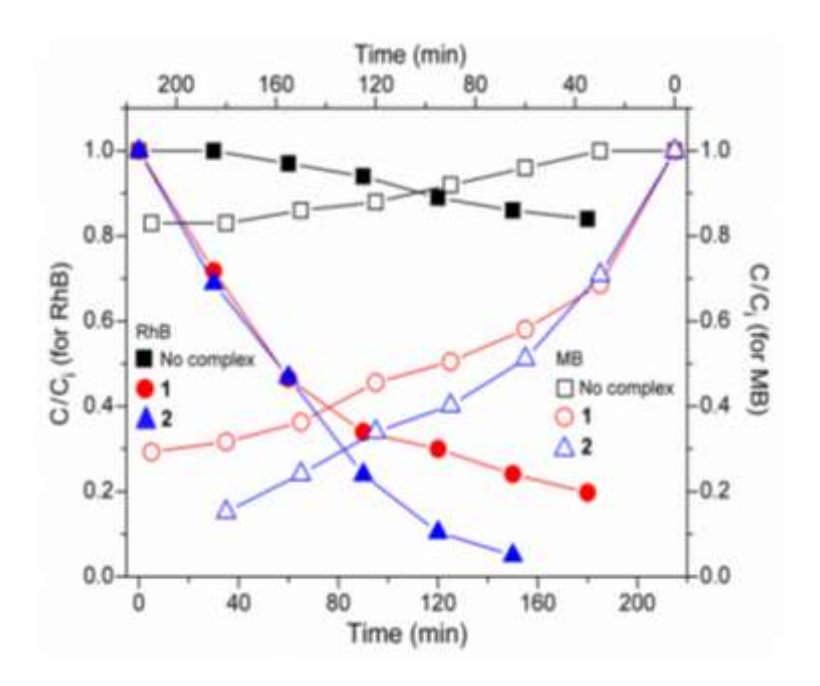


Figure 13: Change of dye (RhB and MB) concentrations with and without catalyst (1 and 2) as a function of irradiation time. C and C_i represent dye concentrations after and before irradiation, respectively.

In order to account for the reusability of **1** and **2** as catalysts they were recovered after the reactions by filtration. About 85% of the catalysts were recovered. The ¹H NMR spectra of the recovered samples were essentially identical with the spectra of the complexes before the reaction. Thus the complexes remain intact throughout the catalysis and they can be recycled and reused for further catalytic cycles.

The mechanism suggested for photocatalytic dye degradation involves primarily two processes – electron transfer and hydrogen abstraction. Upon photoexcitation of trans- $(UO_2)^{2+}$ containing species, electrons get promoted from the highest bonding molecular orbital primarily possessing coordinated oxygen character to the lowest antibonding molecular orbital localized at the uranium atom and thereby the excited trans- $(*UO_2)^{2+}$ containing species is generated. In presence of a suitable guest like the dye molecule, the hole in the highest bonding molecular orbital gets filled by an electron from the α -CH of the dye while the promoted electron still remains in the antibonding molecular orbital. As a result, dye degradation intermediate and a proton are produced.

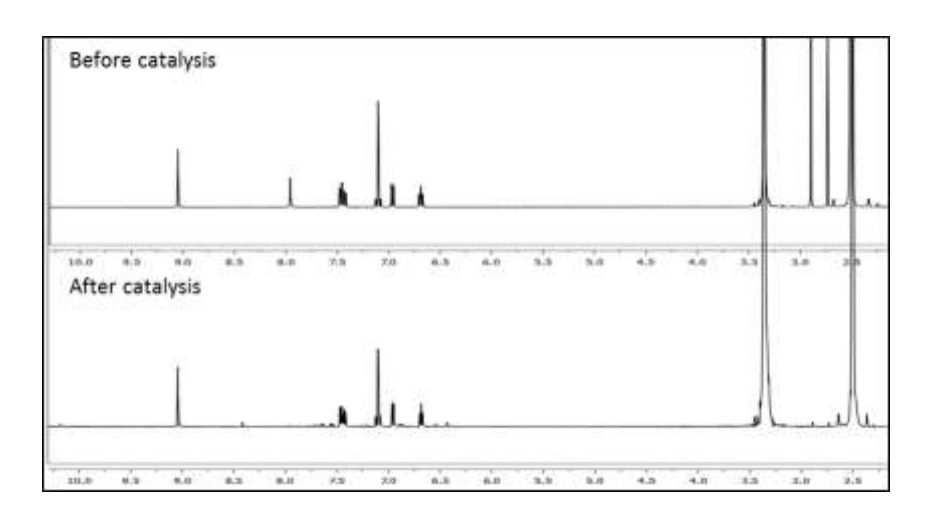


Figure 14: ¹H NMR spectra of catalyst 1 before and after photocatalysis.

Since the antibonding molecular orbital in the reduced photo-excited *trans*- $(*UO_2)^{2+}$ containing species is higher in energy the electron in it is not stable and hence reduces the dissolved oxygen to reactive oxygen species such as superoxide or peroxide. These reactive species are responsible for the oxidation

and complete degradation of the dye molecules. Thus aerobic condition is essential because in absence of oxygen the reduced photo-excited *trans*-(*UO₂)²⁺ containing species will not be oxidized back to the original *trans*-(UO₂)²⁺ containing catalyst and there will be no generation of reactive oxygen species to carry on the dye degradation process further.

3.4. Conclusions

Two complexes having the general molecular formula $[(UO_2)_2(\mu\text{-OH})_2(L^n)_2]$ containing the rare di- μ -hydroxo-diuranyl(VI) core with the Schiff base system 2-((2-(6-chloropyridazin-3-yl)hydrazono)methyl)-4-R-phenol (HLⁿ) have been synthesized. X-ray structures of the solvated complexes revealed the meridionally spanning fused 5,6-membered chelate rings forming N,N,O-donor coordination mode of (Lⁿ)⁻ and the pentagonal-bipyramidal N₂O₅ coordination sphere around the metal centers in each of the two complexes. Supramolecular self-assembly via intermolecular simple and bifuracted hydrogen bonding interactions leads to onedimensional chain-like and three-dimensional network structures in the crystal lattices of the two solvated complexes. The spectroscopic features of both complexes are consistent with their molecular structures. The redox active complexes display a metal centered one-electron reduction. Utilizing the visible region absorption shoulder and a strong absorption band close to the high-energy end of the visible light of both complexes, decent photocatalytic activities of them in degradation of organic dyes in presence of visible light have been demonstrated.

3.5. References

- (a) H. D. Burrows, T. J. Kemp, *Chem. Soc. Rev.* 1974, 3, 139. (b) H. D. Burrows, M. da Graça Miguel, *Adv. Colloid Interface Sci.* 2001, 89–90, 485. (c) K. –X. Wang and J. –S. Chen, *Acc. Chem. Res.* 2011, 44, 531. (d) R. J. Baker, *Chem. Eur. J.* 2012, 18, 16258; (e) Z. R. Ismagilov, S. V. Lazareva, *Cat. Rev. Sci. Eng.* 2013, 55, 135. (f) L. Yong, S. Jing, M. Ellen, Z. GuoQing, L. Jun, *Sci. China Chem.* 2013, 56, 1671.
- (a) Z. –T. Yu, Z. –L. Liao, Y. –S. Jiang, G. –H. Li, G. –D. Li, J. –S. Chen, *Chem. Commun.* 2004, 1814. (b) Z. –T. Yu, Z. –L. Liao, Y. –S. Jiang, G. –H. Li, J. –S. Chen, *Chem. Eur. J.* 2005, 11, 2642. (c) S. Kannan, A. E. Vaughn, E. M. Weis, C. L. Barnes, P. B. Duval, *J. Am. Chem. Soc.* 2006, 128, 14024. (d) S. Tsushima, *Inorg. Chem.* 2009, 48, 4856. (e) W. Yang, W. G. Tian, X. X. Liu, L. Wang, Z. M. Sun, *Cryst. Growth Des.* 2014, 14, 5904. (f) H. –H. Li, X. –H. Zeng, H. –Y. Wu, X. Jie, S. –T. Zheng, Z. –R. Chen, *Cryst. Growth Des.* 2015, 15, 10. (g) M. Azam, G. Velmurugan, S. M. Wabaidur, A. Trzesowska-Kruszynska, R. Kruszynski, S. I. Al-Resayes, Z. A. Al-Othman, P. Venuvanalingam, *Sci. Rep.* 2016, 6, 32898:1-13, doi: 10.1038/srep32898.
- (a) M. R. Maurya, R. C. Maurya, Rev. Inorg. Chem. 1995, 15, 1. (b) J. L. Sessler, P. J. Melfi, G. D. Pantos, Coord. Chem. Rev. 2006, 250, 816. (c) P. A. Giesting, P. C. Burns, Crystallogr. Rev. 2006, 12, 205. (d) K. –X. Wang, J. –S. Chen, Acc. Chem. Res. 2011, 44, 531. (e) R. J. Baker, Chem. Eur. J. 2012, 18, 16258. (f) K. Kiegiel, L. Steczek, G. Zakrzewska-Trznadel, J. Chem. 2013, doi: 10.1155/2013/762819. (g) A. G. Beirakhov, I. M. Orlova, Y. N. Mikhailov, Russ. J. Inorg. Chem. 2014, 59, 1679. (h) T. Loiseau, I. Mihalcea, N. Henry, C. Volkringer, Coord. Chem. Rev. 2014, 266–267, 69.
- (a) M. R. Hoffmann, S. T. Martin, W. Choi, D. W. Bahnemann, *Chem. Rev.* 1995, 95, 69. (b) H. Kirsch, *Angew. Chem. Int. Ed.* 2013, 52, 812. (c)
 T. Hisatomi, J. Kubota, K. Domen, *Chem. Soc. Rev.* 2014, 43, 7520.

- (a) A. Fujishima, T. N. Rao, D. A. Tryk, J. Photochem. Photobiol. C: Photochem. Rev. 2000, 1, 1. (b) G. Burgeth, H. Kisch, Coord. Chem. Rev. 2002, 230, 41. (c) X. Chen, S. S. Mao, Chem. Rev. 2007, 107, 2891. (c) C. L. Pang, R. Lindsay, G. Thornton Chem. Soc. Rev. 2008, 37, 2328. (d) G. S. Mital, T. Manoj, Chinese Sci. Bull. 2011, 56, 1639. (e) M. A. Lazar, S. Varghese, S. S. Nair, Catalysts 2012, 2, 572. (f) Z. F. Yin, L. Wu, H. G. Yang, Y. H. Su, Phys. Chem. Chem. Phys. 2013, 15, 4844.
- (a) S. G. Kumar, L. G. Devi, J. Phys. Chem. A 2011, 115, 13211. (b) D. Pei, J. Luan, Int. J. Photoenerg. 2012, doi:10.1155/2012/262831. (c) Y. Q. Zou, J. –R. Chen, W. –J. Xiao, Angew. Chem. Int. Ed. 2013, 52, 11701. (d) P. Kanhere, Z. Chen, Molecules, 2014, 19, 19995. (e) S. N. Tijare, S. Bakardjieva, J. Subrt, M. V. Joshi, S. S. Rayalu, S. Hishita, N. Labhsetwar, J. Chem. Sci. 2014, 126, 517. (f) R. S. Jack, G. A. Ayoko, M. O. Adebajo, R. L. Frost, Environ. Sci. Pollut. Res. 2015, 22, 7439. (g) R. Fagan, D. E. McCormack, D. D. Dionysiou, S. C. Pillai, Mater. Sci. Semicond. Process. 2016, 42, 2.
- 7. K. R. Grünwald, M. Volpe, P. Cias, G. Gescheidt, N. C. Mösch-Zanetti, *Inorg. Chem.* **2011**, *50*, 7478.
- 8. APEX3, *Program for Data Collection on Area Detectors*, Bruker AXS Inc., Madison, Wisconsin, USA, **2016**.
- 9. G. M. Sheldrick, SADABS, Program for Area Detector Absorption Correction, University of Göttingen, Göttingen, Germany, **1997**.
- 10. S. Parkin, B. Moezzi, H. Hope, J. Appl. Crystallogr. 1995, 28, 53.
- 11. G. M. Sheldrick, Acta Crystallogr. Sect. A 2008, 64, 112.
- 12. L. J. Farrugia, J. Appl. Crystallogr. 2012, 45, 849.
- F. Macrae, I. J. Bruno, J. A. Chisholm, P. R. Edgington, P. M. Cabe, E. Pidcock, L. Rodriguez-Monge, R. Taylor, J. van de Streek, P. A. Wood, *J. Appl. Crystallogr.* 2008, 41, 466.
- 14. U. M. Rafi, D. Mahendiran, A. K. Haleel, R. P. Nankar, M. Doble, A. K. Rahiman, *New J. Chem.* **2016**, *40*, 2451.

- (a) M. Åberg, Acta Chem. Scand. 1969, 23, 791; (b) J. Jiang, M. J. Sarsfield, J. C. Renshaw, F. R. Livens, D. Collison, J. M. Charnock, M. Helliwell, H. Eccles, Inorg. Chem. 2002, 41, 2799. (c) A. Fischer, G. Palladino, Acta Crystallogr. Sect. E 2005, 61, m1542. (d) B. Masci, P. Thuéry, Polyhedron 2005, 24, 229. (e) V. Cocalia, M. Smiglak, S. P. Kelley, J. L. Shamshina, G. Gurau, R. D. Rogers, Eur. J. Inorg. Chem. 2010, 2760. (f) N. D. Shepherd, Y. Zhang, I. Karatchevtseva, J. R. Price, L. Kong, N. Scales, G. R. Lumpkin, Polyhedron 2016, 113, 88. (g) K. Lyczko, L. Steczek, J. Struct. Chem. 2017, 58, 102. (h) S. Hadjithoma, M. G. Papanikolaou, E. Leontidis, T. A. Kabanos, A. D. Keramidas, Inorg. Chem. 2018, 57, 7631.
- (a) Z. Asadi, M. Asadi, A. Zeinali, M. Ranjkeshshorkaei, K. Fejfarova, V. Eigner, M. Dusek, A. Dehnokhalaji, *J. Chem. Sci.* 2014, 126, 1673. (b) M. Azam, S. I. Al-Resayes, A. Trzesowska-Kruszynska, R. Kruszynski, *Polyhedron* 2017, 124, 177. (c) X. Zhao, D. Zhang, R. Yu, S. Chen, D. Zhao, *Eur. J. Inorg. Chem.* 2018, 1185.
- 17. S. Ghosh, S. K. Kurapati, A. Ghosh, A. K. Srivastava, S. Pal, *ChemistrySelect* **2018**, *3*, 4865 and references therein.
- 18. (a) J. R. Ferraro, W. R. Walker, *Inorg. Chem.* **1965**, *4*, 1382. (b) D. L. Perry, *Inorg. Chim. Acta*, **1982**, *65*, L211.
- (a) N. R. Sangeetha, C. K. Pal, P. Ghosh, S. Pal, *J. Chem. Soc. Dalton Trans.* 1996, 3293.
 (b) A. Sarkar, S. Pal, *Polyhedron* 2006, 25, 1689.
 (c) A. Sarkar, S. Pal, *Polyhedron* 2007, 26, 1205.
 (d) S. K. Kurapati, U. Ugandhar, S. Maloth, S. Pal, *Polyhedron* 2012, 42, 161.
 (e) K. Nagaraju, R. Raveendran, S. N. Pal, S. Pal, *Polyhedron* 2012, 33, 52.
- (a) V. A. Volkovich, T. R. Griffiths, D. J. Fray, R. C. Thied, *Phys. Chem. Chem. Phys.* 2001, *3*, 5182.
 (b) P. M. Almond, T. E. Albrecht-Schmitt, *Inorg. Chem.* 2002, *41*, 1177–1183.
- 21. A. F. Oliveri, L. A. Wills, C. R. Hazlett, M. E. Carnes, I. –Y. Chang, P. H. –Y. Cheong, D. W. Johnson, *Chem. Sci.*, **2015**, *6*, 4071.

22. (a) R. Raveendran, S. Pal, Eur. J. Inorg. Chem. 2008, 5540. (b) R. Raveendran, S. Pal, J. Organomet. Chem. 2009, 694, 1482. (c) K. Nagaraju, S. Pal, Inorg. Chim. Acta 2014, 413, 102; (d) S. K. Kurapati, S. Pal, Dalton Trans. 2015, 44, 2401.

Electrocatalytic and Photocatalytic Hydrogen Evolution using a Diuranyl(VI) Complex from Neutral Aqueous Medium §

The reaction of equimolar amounts of UO₂(OAc)₂·2H₂O, 2,6-diformyl-4methylphenol and N-(hydroxyethyl)ethylenediamine in methanol affords a dinuclear trans-uranyl(VI) complex of the molecular formula $[(UO_2)_2(\mu-L)_2]$ (L²-= 2-formyl-4-methyl-6-((2-(2-oxidoethylamino)ethylimino)methyl)phenolate) in 65% yield. Detailed structural elucidation of the complex was performed by using single crystal X-ray crystallographic and spectroscopic studies. In $[(UO_2)_2(\mu-L)_2]$, the metal centers are in edge-shared pentagonal bipyramidal N₂O₅ coordination spheres assembled by the two meridional ONNO-donor bridging L²⁻ and two pairs of mutually *trans*-oriented oxo groups. The complex is redox active and displays two successive metal centered one-electron reductions at $E_{\rm pc} = -0.71$ and -1.03 V in N,N-dimethylformamide solution. The redox active complex was used as a heterogeneous catalyst for electrochemical hydrogen evolution from aqueous medium at pH 7 with a turnover frequency (TOF) of 384 h^{-1} and a Tafel slope of 274 mV dec⁻¹. The Faradaic efficiency of $[(UO_2)_2(\mu-L)_2]$ was found as 84%. Beyond electrocatalytic response, the [(UO₂)₂(μ-L)₂]-TiO₂-N719 composite also exhibited significant heterogeneous photocatalytic hydrogen evolution activity in neutral aqueous medium under visible light and provided a yield of 3439 µmol g_{cat}⁻¹ of H₂ in 4 h with a TOF of 172 h⁻¹ and apparent quantum yield (AQY) of 7.6%.

[§] This work has been published in *Inorg. Chem.* **2019**, *58*, 14410–14419.

4.1. Introduction

One of the major concerns of the present day is to have a source of clean and green energy. Hydrogen is not only an environment friendly renewable source of energy without emission of any carbon-based greenhouse gas during combustion, but it also has the highest gravimetric energy density for any known fuel till date. In nature, hydrogenase enzymes utilize iron and/or nickel cofactors to produce hydrogen from neutral aqueous medium with turnover frequency (TOF) ranging from 100 to 10,000 s⁻¹. However, the complexity of the macromolecule as well as their inefficiency to work under aerobic conditions has restricted their practical usage. Thus, immense efforts have been devoted to the development of efficient, robust and inexpensive catalysts for production of hydrogen from water.^{3,4} Hydrogen can be generated by both photocatalytic as well as electrocatalytic water splitting reactions. The platinum based electrocatalysts are considered to be ideal for hydrogen production because they have low overpotentials along with Tafel slopes as low as 30 mv dec⁻¹, but then again, they suffer the problem of high cost due to low abundance of platinum.^{5,6} Several other earth abundant 3d and 4d transition metal containing catalysts under both homogeneous and heterogeneous conditions have been shown to be quite efficient and robust in aqueous as well as non-aqueous medium.^{3,4,6}

Fujishima and Honda carried out the first photoelectrochemical water splitting reaction in 1972, using a TiO₂ electrode as anode and a platinum electrode as cathode.⁷ But the reaction has a low quantum efficiency. Among various semiconductors available, TiO₂ possesses better light harvesting capacity and low fermi energy levels to undergo water splitting reactions. However, the major drawback of it is the higher band gap (3.2 eV) which obstructs the light absorption from visible region. To overcome this drawback there is a continuous quest for design and synthesis of new photocatalysts which not only possess better light harvesting ability but also can absorb visible light which is about 40% of the total sunlight.^{3,8,9}

The application of low-valent uranium as catalyst in electrolytic water reduction has been recently reported by Meyer and group⁹ and it happens to be the first report on uranium to act as an electrocatalyst for hydrogen evolution reaction (HER). In the present chapter, the synthesis, characterization, X-ray crystal structure and spectroscopic properties of a high-valent dinuclear *trans*-uranyl(VI) complex with the molecular formula $[(UO_2)_2(\mu-L)_2]$ (H₂L is 2-hydroxy-3-((2-(2-hydroxyethylamino)ethylimino)-methyl)-5-methylbenzaldehyde where 2 Hs represent the dissociable phenolic and alcoholic protons) and its use for efficient reduction of water to hydrogen by both electrocatalytic and photocatalytic methods have been described.

Scheme 1. Synthesis of $[(UO_2)_2(\mu-L)_2]$.

4.2. Experimental Section

4.2.1. Materials:

2,6-diformyl-4-methylphenol was prepared by following a reported procedure.¹⁰ All other chemicals and solvents used in this work were of reagent grade and used as received without any further purification.

4.2.2. Physical Measurements:

Elemental (CHN) analysis data were obtained with the help of a Thermo Finnigan Flash EA1112 series elemental analyzer. Solid state magnetic susceptibility measurement was performed with a Sherwood Scientific balance. A Digisun DI-909 conductivity meter was used for solution electrical conductivity measurement. Mass spectrum was recorded with a Bruker Maxis (ESI-TOF analyzer) spectrometer. Α Thermo Scientific Nicolet iS5 FT-IR spectrophotometer was used to record the infrared (IR) spectrum in ATR mode. A Shimadzu UV-3600 UV-Vis-NIR spectrophotometer was used to collect the electronic absorption spectrum. Cyclic and differential pulse voltammetric (CV and DPV) measurements with N,N-dimethylformamide solution of $[(UO_2)_2(\mu -$ L)2] were carried out using a CH Instruments model 620A electrochemical analyzer. A Varian 720-ES ICP-OES spectrometer was used for determination of the uranium content. XPS measurements were carried out on a Thermo Scientific K-Alpha⁺ spectrometer. Gas chromatographic measurements were performed using a Perkin Elmer Clarus 590 gas chromatograph equipped with thermal conductivity detector and a molecular sieve 5Å column. Diffuse reflectance spectra were recorded using BaSO₄ as the reference on a Perkin Elmer Lambda 750 UV-Vis-NIR spectrophotometer fitted with an integrating sphere. A Newport 450 W xenon lamp was used for photocatalytic experiments.

4.2.3. Synthesis of the $[(UO_2)_2(\mu - L)_2]$:

A solution of N-(hydroxyethyl)ethylenediamine (42 mg, 41 μL, 0.4 mmol) in methanol (10 mL) was added to a methanol solution (10 mL) of 2,6-diformyl-4-methylphenol (66 mg, 0.4 mmol) and the mixture was boiled under reflux for 1 h. To the resulting solution, a solution of UO₂(OAc)₂·2H₂O (170 mg, 0.4 mmol) in methanol (10 mL) was added dropwise and the mixture was refluxed for another 3 h. A microcrystalline orange solid separated on cooling to room temperature (298 K) was collected by filtration and dried in air. For recrystallization the precipitate was dissolved in dimethylformamide–methanol (1:1) mixture and allowed to evaporate slowly. The crystalline material deposited in about 8–10

days was collected by filtration and dried in vacuum. Yield: 135 mg (65%). Anal. Calcd for $C_{26}H_{32}N_4O_{10}U_2$ (1036.61): C, 30.12; H, 3.11; N 5.40. Found: C, 30.19; H, 3.07; N, 5.48. Selected IR data (ν (cm⁻¹)): 3225 (N–H), 2831 ((O)C–H), 1676 (C=O), 1625 (C=N), 886 (UO₂). UV–Vis data (λ_{max} (nm) (ε (10³ M⁻¹cm⁻¹))): 465 (0.9), 396 (4.1), 372 (4.7). ESI-MS (m/z): 1037.3099 (Calcd. for $C_{26}H_{33}N_4O_{10}U_2^+$ = 1037.3212).

4.2.4. X-ray Crystallography:

A single crystal suitable for X-ray data collection was selected from the recrystallized sample of the complex. Unit cell determination and the intensity data collection at room temperature (298 K) were performed on a Bruker D8 Quest diffractometer fitted with a Photon 100 CMOS area detector and an Incoatec microfocus source for graphite monochromated Mo $K\alpha$ radiation ($\lambda =$ 0.71073 Å). Data acquisition, integration and reduction were done using the APEX3 software package. 11 An empirical multi-scan absorption correction was applied to the data using the SADABS program. 12 The structure was solved by direct method in $P2_1/c$ space group and refined on F^2 using full-matrix leastsquares procedures. The asymmetric unit contains one half of the dinuclear molecule. All the non-hydrogen atoms were refined using anisotropic displacement parameters, whereas the hydrogen atoms were placed at idealized positions and were refined as riding atoms. The SHELX-97 programs¹³ provided in the WinGX software suite¹⁴ were used for structure solution and refinement. Structural illustrations were prepared using the Mercury package. 15 Significant crystal and refinement data are summarized in Table 1.

Detailed X-ray crystallographic data for $[(UO_2)_2(\mu-L)_2]$ have been deposited with the Cambridge Crystallographic Data Centre under the deposition numbers CCDC 1921042.

Table 1. Selected Crystal Data for [(UO₂)₂(μ -L)₂]

Chemical formula	$C_{26}H_{32}N_4O_{10}U_2\\$		
Formula weight	1036.62		
Crystal system	Monoclinic		
Space Group	$P2_1/c$		
a (Å)	7.6504(6)		
b (Å)	7.4471(5)		
c (Å)	26.094(2)		
β (°)	98.150(3)		
$V(\mathring{A}^3)$	1471.63(19)		
Z	2		
ρ (g cm ⁻³)	2.339		
μ (mm ⁻¹)	11.052		
Reflections collected	54912		
Reflections unique	2588		
Reflections $[I \ge 2\sigma(I)]$	2276		
Data / restraints / parameters	2588 / 0 / 191		
$R1$, $wR2$ [$I \ge 2\sigma(I)$]	0.0283, 0.0584		
R1, wR2 [all data]	0.0356, 0.0603		
GOF on F^2	1.191		
Largest diff. peak / hole (e Å ⁻³)	1.008 / -1.546		

4.2.5. Electrochemical Studies:

All the electrochemical hydrogen evolution studies were done with the help of a Zahner Zanium electrochemical workstation using a three electrode system. The measurements were carried out using a $[(UO_2)_2(\mu-L)_2]$, carbon-black and Nafion coated fluorine doped tin oxide (FTO) glass plate as the working electrode, a Pt wire as the counter electrode and an Ag/AgCl reference electrode in 0.1 M phosphate buffer of pH 7 (unless otherwise mentioned) at room temperature (298 K). Sample preparation for the coating of the FTO plate was as follows: To a mixture of 4 mg of $[(UO_2)_2(\mu-L)_2]$ and 1 mg of carbon-black in 1 mL of ethanolwater (3:2 v/v) mixture, 10 μ L of 5 wt% Nafion was added and the whole mixture was kept under sonication for 2 h. 30 μ L of this mixture was then coated

on a FTO plate of area 0.2 cm^2 . The coating on the FTO plate surface was then dried by an IR lamp. The area of the electrode was maintained 0.2 cm^2 for all the electrochemical experiments unless otherwise mentioned. The open circuit potential was used as the initial potential for all the cyclic voltammetric measurements using the surface coated FTO electrode. All electrode potentials were converted to reversible hydrogen electrode (RHE) scale using the equation $E_{\text{RHE}} = E_{\text{Ag/AgCl}} + 0.059 \text{pH} + 0.2$.

4.2.6. Preparation of Dye Adsorbed Composite Photocatalyst:

N719 dye (1.19 mg, 1 μ mol) was dissolved in a mixture of ethanol-acetonitrile (20 mL, 1:1 v/v). To this solution, [(UO₂)₂(μ -L)₂] (5.5 mg, 5.3 μ mol) and TiO₂ (100 mg, 1.25 mmol) were added and the mixture was stirred at room temperature (298 K) under dark for 24 h. The solvent was then evaporated by rota-vaporization and the solid obtained was dried in vacuum at 50–60 °C. The product thus obtained was tested for photocatalytic activity. The same experimental conditions and procedures were used for preparation of all other composite photocatalysts having different dyes such as 4-hydroxycoumarin and Coumarin 343.

4.2.7. Photocatalytic Studies:

The photocatalytic hydrogen production experiments were carried out in a quartz reactor. The photocatalyst (10 mg) was added to an aqueous solution (20 mL) of triethanolamine (TEOA) (10 vol%) and the mixture was sonicated for complete dispersion of the catalyst. The pH of the mixture in the reactor was maintained at 7 using 1 M hydrochloric acid and it was purged with nitrogen for 30 min. The mixture was then stirred and irradiated with light from a 450 W xenon lamp. The hydrogen production rate was analyzed by sampling the evolved gas at periodic intervals (every 1 h) using online gas chromatography.

4.3. Results and Discussions

4.3.1. Synthesis and Characterization:

The complex $[(UO_2)_2(\mu-L)_2]$ was synthesized in good yield (65%) by reacting $UO_2(OAc)_2 \cdot 2H_2O$ with in situ prepared 2-hydroxy-3-((2-(2hydroxyethylamino)ethylimino)methyl)-5-methylbenzaldehyde (H₂L) from 2,6diformyl-4-methylphenol and N-(hydroxyethyl)ethylenediamine in methanol under reflux conditions (Scheme 1). The molecular formula of the complex is in good agreement with the elemental analysis data. The complex is insoluble in common organic solvents and is sparingly soluble in dimethylformamide and dimethylsulfoxide. In solution, it is electrically non-conducting. Room temperature magnetic susceptibility measurement indicates its diamagnetic character. The non-electrolytic and diamagnetic nature of the complex is consistent with its neutral molecular formula and the +6 oxidation state of the metal center.

4.3.2. X-ray Molecular Structures:

The structure of the dinuclear $[(UO_2)_2(\mu-L)_2]$ is illustrated in Figure 1. Selected bond parameters are listed in Table 2. The two halves of the dinuclear molecule are related by an inversion center. Coordination of the metal centers by the two meridionally spanning L^{2-} through their bridging ethoxide-O, secondary amine-N, azomethine-N and phenolate-O atoms results in the formation of fused 5,5,6-membered chelate rings and two edge-shared pentagonal N_2O_3 planes (rms deviation 0.99 Å). Four oxo groups occupy the axial sites of the two metal atoms and complete the edge-shared pentagonal-bipyramidal N_2O_5 coordination spheres around the two uranium atoms. It may be noted that not many structurally characterized discrete diuranyl(VI) complexes having such edge-shared pentagonal-bipyramidal molecular structure are known. The four-membered bridging U_2O_2 unit is perfectly planar and the $U\cdots U$ distance and the U-O-U and O-U-O angles are 3.9067(5) Å and 111.2(2) and 68.8(2)°, respectively. The U(1)-O(1) and U(1)-O(1') bond lengths are comparable with the uranium(VI) to bridging alkoxide-O distances observed before. Overall the U=O

U–O(phenolate), U–N(azomethine) and U–N(amine) bond lengths in $[(UO_2)_2(\mu-L)_2]$ are within the ranges reported for uranium(VI) complexes having similar coordinating atoms.^{17–19}

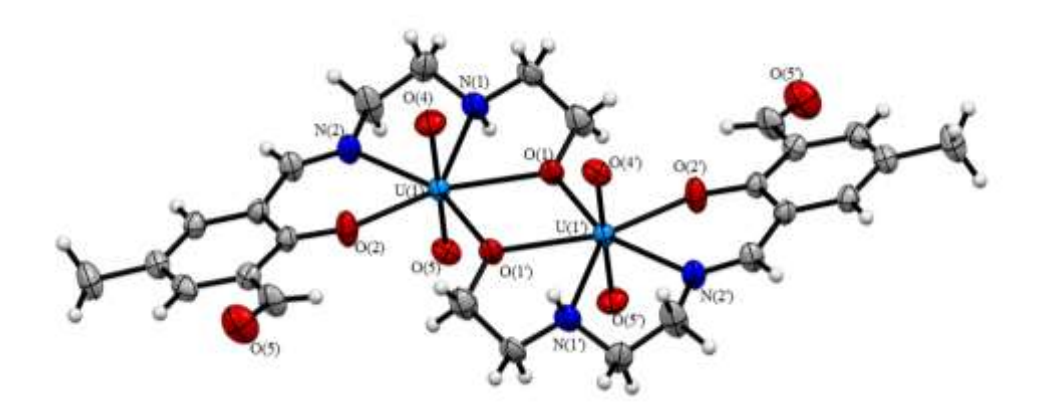


Figure 1: The ORTEP of $[(UO_2)_2(\mu-L)_2]$ (top) and the edge-shared pentagonal bipyramidal N_2O_5 coordination spheres. In the ORTEP, all the non-hydrogen atoms are represented by their 40% probability thermal ellipsoids and only the non-carbon atoms are labeled for clarity.

The dinuclear complex molecule contains two types of potential hydrogen bond donors, the formyl C–H and the secondary amine N–H groups, and several O-atoms that can act as hydrogen bond acceptors. Thus the structure was further scrutinized for intermolecular hydrogen bonding interactions and the resulting supramolecular self-assembled structure. Interestingly, the formyl group is coplanar with rest of the six-membered chelate ring forming fragment of L^{2–} and the formyl C(13)–H is oriented towards O(2), the metal coordinated phenolate-O (Figure 1). This orientation indicates that instead of any intermolecular interaction it participates in an intramolecular C–H···O hydrogen bonding interaction. Here the H···O distance is 2.53 Å and the C···O distance and the C–H···O angle are 2.835(8) Å and 99°, respectively. On the other hand, out of the two amine groups only one (N(1)–H) participates in an intermolecular strong N–H···O interaction with O(4), one of the two metal bound oxo groups. Here the N···O and H···O distances are 3.041(8) and 2.18 Å, respectively while the N–H···O angle is 157°. Due to this hydrogen bonding there is a small difference

(by 0.016 Å) in the two U=O lengths (Table 2). This intermolecular N-H···O interaction leads to a one-dimensional array of the complex molecules in the crystal lattice (Figure 2).

Table 2. Selected Bond Parameters (Å and $^{\circ})$ for [(UO2)2($\mu\text{-}L)2$]

			/- _
U(1)–O(1)	2.396(4)	$U(1)-O(1')^a$	2.339(4)
U(1)–O(2)	2.229(5)	U(1)–O(3)	1.761(5)
U(1)–O(4)	1.777(5)	U(1)–N(1)	2.554(5)
U(1)-N(2)	2.574(5)		
$O(1)-U(1)-O(1')^a$	68.80(17)	O(1)–U(1)–O(2)	157.15(16)
O(1)-U(1)-O(3)	90.2(2)	O(1)-U(1)-O(4)	90.17(19)
O(1)-U(1)-N(1)	65.43(16)	O(1)-U(1)-N(2)	131.24(16)
$O(1')^a - U(1) - O(2)$	88.39(16)	$O(1')^a - U(1) - O(3)$	93.8(2)
$O(1')^a - U(1) - O(4)$	90.82(19)	$O(1')^a - U(1) - N(1)$	134.19(16)
$O(1')^a - U(1) - N(2)$	159.11(16)	O(2)–U(1)–O(3)	89.9(2)
O(2)-U(1)-O(4)	91.6(2)	O(2)-U(1)-N(1)	137.27(17)
O(2)-U(1)-N(2)	71.58(17)	O(3)–U(1)–O(4)	175.1(2)
O(3)–U(1)–N(1)	84.6(2)	O(3)-U(1)-N(2)	92.1(2)
O(4)-U(1)-N(1)	91.2(2)	O(4)-U(1)-N(2)	84.0(2)
N(1)-U(1)-N(2)	66.34(17)	$U(1)-O(1)-U(1')^a$	111.20(17)

^aSymmetry transformation used to generate the equivalent atom: -x + 1, -y + 1, -z + 1.

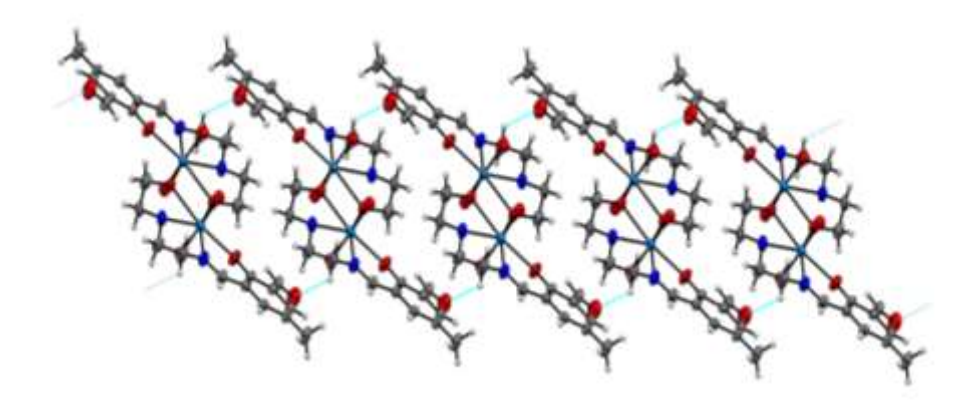


Figure 2: One-dimensional chain-like assembly of $[(UO_2)_2(\mu-L)_2]$.

4.3.3. Spectroscopic Characterization:

For further confirmation of the molecular formula and the molecular weight of the bulk sample, $[(UO_2)_2(\mu-L)_2]$ was subjected to the mass spectrometric measurement using its N,N-dimethylformamide solution. The spectrum displays the molecular ion (MH^+) as the base peak with the expected isotopic pattern at the m/z value of 1037.3099 (Figure 3).

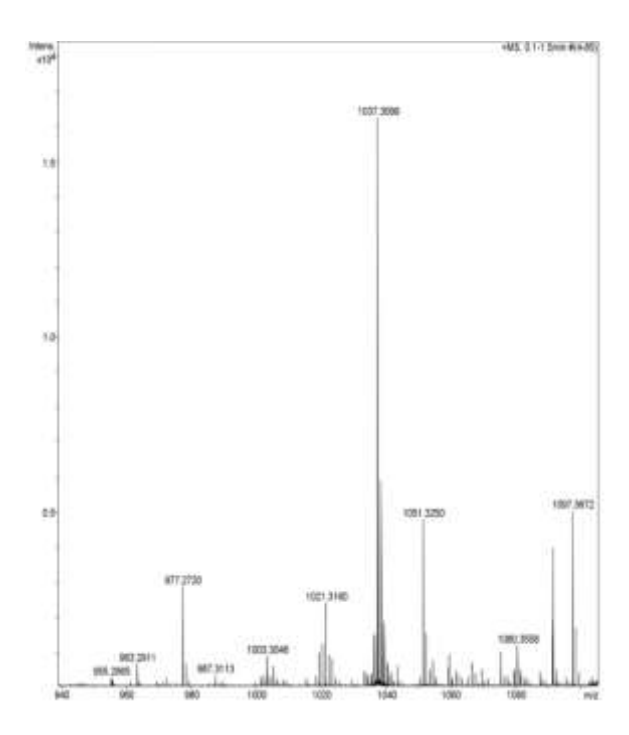


Figure 3: ESI mass spectrum of $[(UO_2)_2(\mu-L)_2]$ in dimethylformamide.

Infrared spectrum of $[(UO_2)_2(\mu-L)_2]$ displays several bands with various intensities in the range $4000-500~\rm cm^{-1}$ (Figure 4). Except for a few characteristic bands, no attempt was made to assign the remaining bands. The medium intensity band at $3225~\rm cm^{-1}$ is attributed to the secondary amine N–H stretch and it is followed by the C–H stretching band of the free aldehyde at $2831~\rm cm^{-1}.^{20}$ The sharp band at $1675~\rm cm^{-1}$ reveals the presence of the uncoordinated carbonyl (C=O) functionality. The azomethine (HC=N) stretch appears as a strong sharp band at $1625~\rm cm^{-1}.^{17g,19a,c}$ The characteristic strong band at $886~\rm cm^{-1}$ is assigned to the asymmetric stretching vibration of the *trans*-UO₂ moiety. 17f,g,19a,c

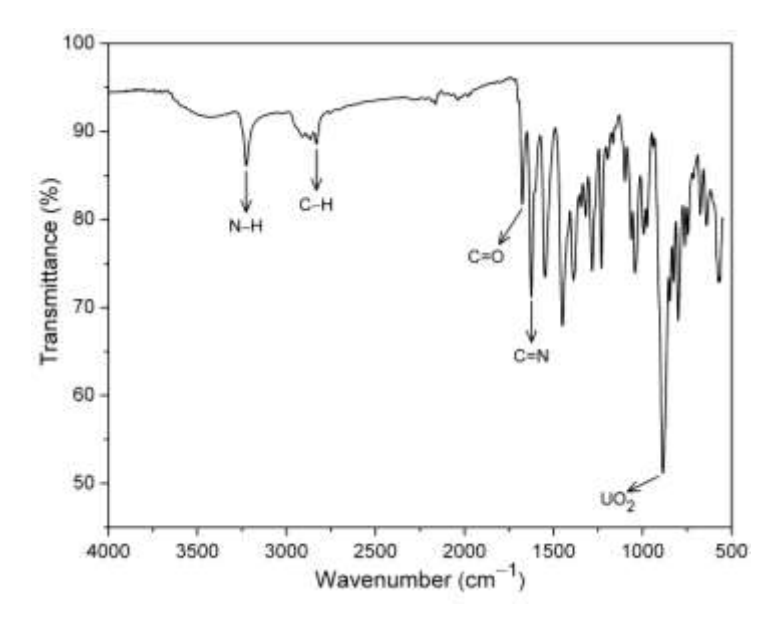


Figure 4: Infrared spectrum of $[(UO_2)_2(\mu-L)_2]$ in powder phase.

The electronic spectrum of $[(UO_2)_2(\mu-L)_2]$ was taken in *N,N*-dimethylformamide solution. The spectrum shows a broad shoulder at ~465 nm followed by one more shoulder at ~396 nm and an absorption maximum at 372 nm (Figure 5). The molar extinction coefficients of these absorptions are in three orders of magnitude. Similar absorptions for *trans*-uranyl(VI) complexes with Schiff base ligands have been shown to be due to electronic transitions from the filled porbitals of metal coordinated O-atoms to the empty f-orbitals of the uranium(VI) center. 17g,19a,c,21

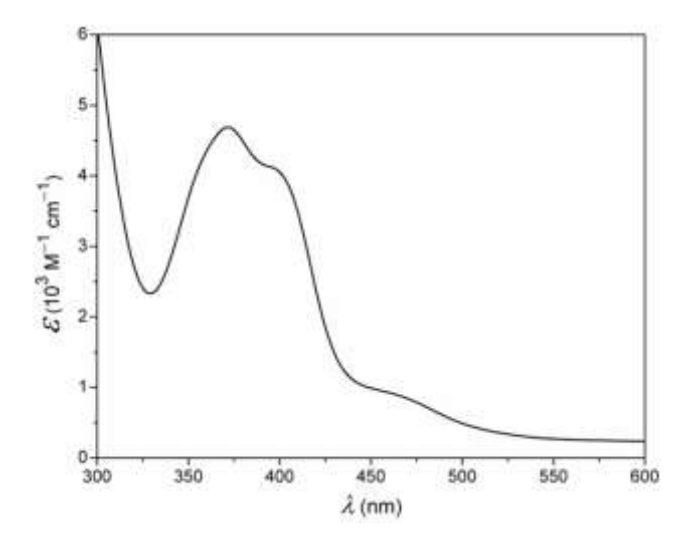


Figure 5: Electronic spectrum of $[(UO_2)_2(\mu-L)_2]$ in dimethylformamide.

4.3.4. Redox Properties:

The electron transfer characteristics of $[(UO_2)_2(\mu-L)_2]$ have been examined by cyclic and differential pulse voltammetry. The measurements were carried out at 298 K with ~1 mM N,N-dimethylformamide solution of the complex containing n-Bu₄NClO₄ (0.1 M) as the supporting electrolyte using a glassy-carbon working electrode, a Pt-wire auxiliary electrode and an Ag/AgCl reference electrode under nitrogen atmosphere. Under identical conditions, cyclic voltammogram (CV) of a ~1 mM N,N-dimethylformamide solution of ferrocene (Fc) displayed the Fc⁺/Fc couple at $E_{1/2} = 0.61 \text{ V}$ ($\Delta E_p = 100 \text{ mV}$). The CV of ferrocene and the CV and the differential pulse voltammogram (DPV) of the complex are illustrated in Figure 6. The complex displays an irreversible reductions at $E_{\rm pc} = -0.71$ and a quasireversible reduction at $E_{1/2} = -0.93 \text{ V}$ ($\Delta E_p = 200 \text{ mV}$). For the second reduction the cathodic peak current (i_{pc}) is significantly larger than the anodic peak current (i_{pa}) . Nevertheless, the i_{pc} values of both of these two reductions are comparable with the peak currents (i_{pa} and i_{pc}) of ferrocene. This similarity of peak currents suggests that each of the two reductions of the complex is one electron in nature. In the DPV, the reduction peaks are relatively well resolved and they appear at – 0.56 and -0.86 V with comparable peak currents. Complexes of trans-uranyl(VI) complexes with Schiff bases are known to display $U(VI) \rightarrow U(V)$ reduction in the similar potential range. ^{17g,19} Thus the two reductions observed for the present complex are attributed to $U(VI)-U(VI) \rightarrow U(V)-U(VI) \rightarrow U(V)-U(V)$ processes.

4.3.5. Electrocatalytic Hydrogen Evolution:

The electrochemical hydrogen evolution experiments were performed using 0.1 M phosphate buffer at pH 7. The CV recorded using $[(UO_2)_2(\mu-L)_2]$, carbon-black and Nafion mixture coated FTO working electrode shows a single broad reduction response at -0.32 V (vs RHE) followed by a sharp increase in the cathodic current which indicates the initiation of the hydrogen evolution reaction (HER) on the working electrode (Figure 7). Chromatographic analysis of the evolved gas collected in the electrolysis experiments confirmed the HER (Figure 9). Considering that $[(UO_2)_2(\mu-L)_2]$ in N,N-dimethylformamide solution displays

two successive one-electron reductions (E_{pc} values are about 300 mV apart), the broad reduction observed with the surface coated FTO electrode is attributed to a two-electron process. This two-electron reduced complex catalyst coated on the electrode surface can then produce hydrogen and go back to the original oxidized form.

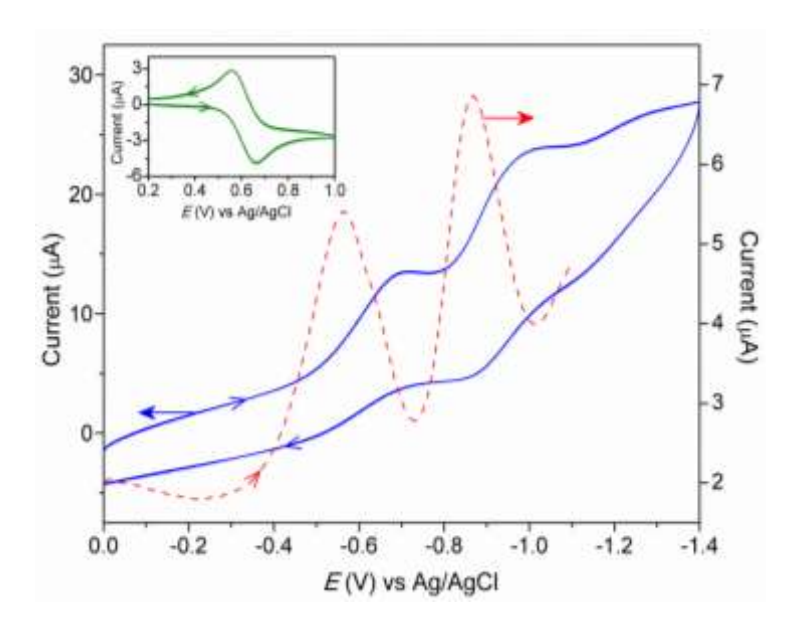


Figure 6: Cyclic (_____) and differential pulse (_____) voltammograms of $[(UO_2)_2(\mu-L)_2]$ in Me₂NCHO under the experimental conditions described in the text. Inset: Cyclic voltammogram (_____) of ferrocene under identical conditions.

Controlled experiments were performed with blank FTO as well as with carbon-black and Nafion coated FTO. A negligible increment in the cathodic current confirms the fact that HER activity does not take place in absence of [(UO₂)₂(μ -L)₂] (Figure 7). Also to further confirm the fact that the production of hydrogen is due to water reduction only, the electrocatalytic process was carried out in acetonitrile medium instead of phosphate buffer keeping the remaining conditions same. There was no increment in the catalytic current when the medium was only acetonitrile (Figure 7). However, subsequent additions of phosphate buffer (pH 7) into the acetonitrile medium led to the increase in the catalytic current (Figure 8).

To get a better measure of the electrocatalytic activity of $[(UO_2)_2(\mu - L)_2]$ in HER the Tafel equation $\eta = a + b \times \log(i)$ (where $\eta = \text{overpotential}$, i = measured

current density, b = Tafel slope and a = constant) has been employed (Figure 10). A low η , a large exchange current density (i_0 , current density at $\eta = 0$) and a low b indicates better hydrogen evolution and hence a better catalytic activity. ^{4,22} In the present case, the values of η (corresponding to a current density of 1 mA cm⁻²), i_0 and b are found to be 0.73 V, 2.07 x 10⁻⁶ A cm⁻² and 274 mV dec⁻¹, respectively. These values clearly show a decent catalytic activity of [(UO₂)₂(μ -L)₂] towards electrocatalytic hydrogen production at neutral pH.

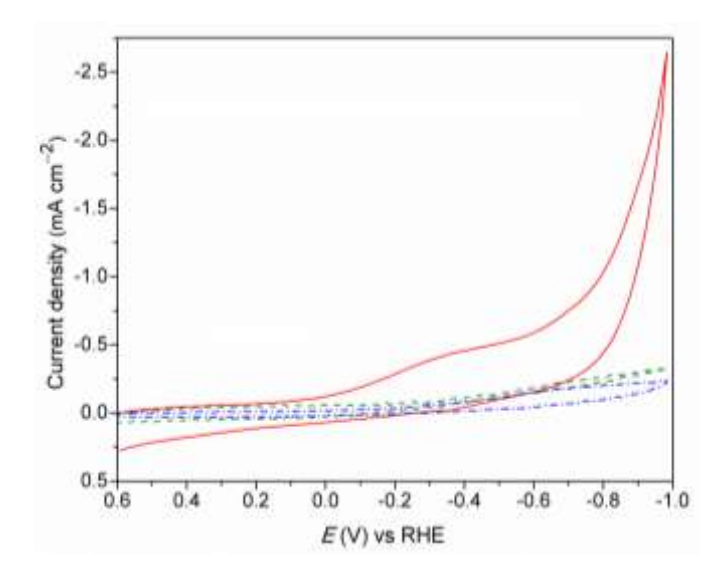


Figure 7: Cyclic voltammograms at a scan rate of 100 mV s⁻¹ using carbon-black/Nafion/[(UO₂)₂(μ -L)₂]/FTO electrode (____) and carbon-black/Nafion/FTO electrode (____) in phosphate buffer of pH 7, and carbon-black/Nafion/[(UO₂)₂(μ -L)₂]/FTO electrode (____) in acetonitrile.

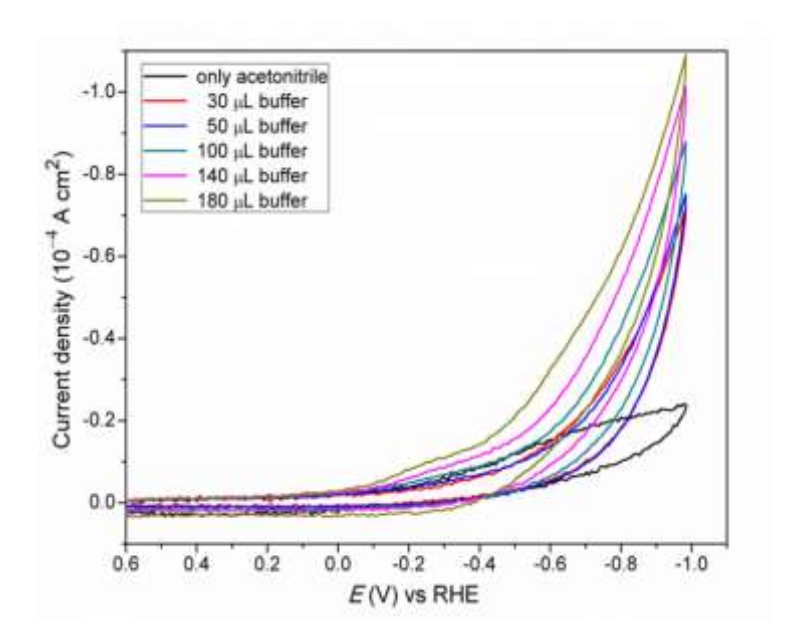


Figure 8: Electrocatalytic hydrogen evolution in acetonitrile with subsequent addition of phosphate buffer of pH 7.

The effectiveness of $[(UO_2)_2(\mu-L)_2]$ as HER electrocatalyst has been evaluated by determining the Faradaic efficiency and the TOF value. Constant current electrolysis (CCE) was performed to determine the Faradaic efficiency of $[(UO_2)_2(\mu-L)_2]$ in HER. The Faradaic efficiency was calculated as 84%. The turnover frequency (TOF) was determined by using the equation TOF = I/Q, where I is the steady state current (in A) in the constant potential electrolysis (CPE) plot and Q is the charge (in C) calculated from the reduction peak in the CV recorded in non-catalytic conditions (acetonitrile medium) with $[(UO_2)_2(\mu-L)_2]$, carbon-black and Nafion mixture coated FTO working electrode. The value of TOF obtained is 384 h⁻¹. Comparison of both Faradaic efficiency and the TOF values of $[(UO_2)_2(\mu-L)_2]$ with the corresponding values of the previously reported metal centered HER catalysts clearly indicates that the present catalyst is quite noteworthy.^{4,22}

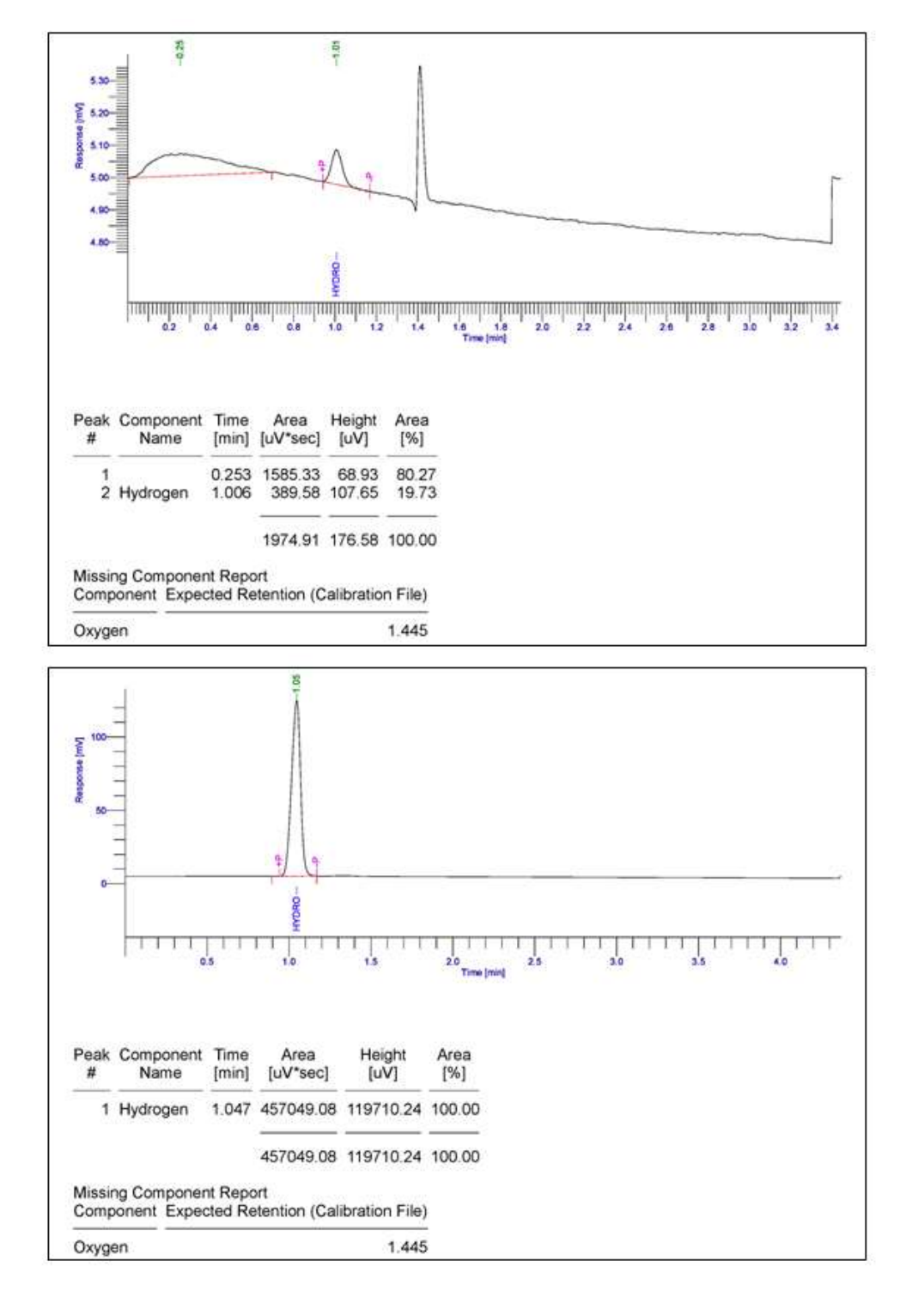


Figure 9: Chromatograms of the gas evolved in electrolysis (top) and hydrogen (bottom). In the first chromatogram, the oxygen peak is due to slight contamination by air during sample collection from the headspace.

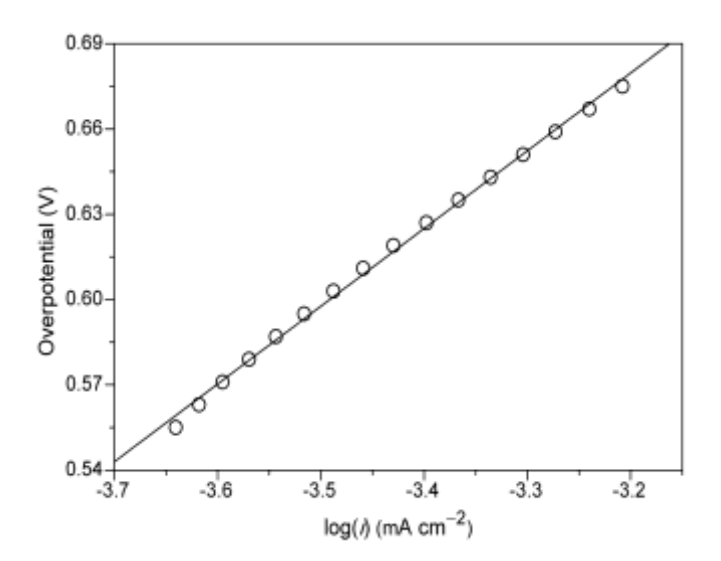


Figure 10: Tafel plot of $[(UO_2)_2(\mu-L)_2]$ in 0.1M phosphate buffer.

Calculation of Turnover Frequency (TOF).²³ The TOF (s⁻¹) can be calculated with the following equation: TOF = I/2mF, where, I is the current (= 1.76 x 10⁻⁵ A, the steady state value in the constant potential electrolysis (CPE) plot in Figure 12), F is the Faraday constant (in C mol⁻¹), m is the number of active sites (in mol) and 2 is the number of electrons required to form one hydrogen molecule from two protons.

The number of active sites m can be calculated using the equation, m = Q/2F, where, Q (1.65 x 10^{-4} C) is the charge calculated by integrating the current vs time plot (within the potential range -0.201 to -0.849 V) generated from the cyclic voltammogram trace (in Figure 7) recorded using $[(UO_2)_2(\mu-L)_2]$ /carbon-black/Nafion/FTO as the working electrode under non-catalytic conditions (CH₃CN medium rather than phosphate buffer) and the factor $\frac{1}{2}$ is for the 2 electron reduction of the catalyst $[(UO_2)_2(\mu-L)_2]$.

Now, putting Q/2F for m in the equation for TOF (in h^{-1}) we get:

TOF = (I/2*m*F) x 3600 = (I/Q) x 3600 = {(1.76 x
$$10^{-5})/(1.65 x 10^{-4})} x 3600 = 384 h-1$$

Quantitative Hydrogen Evolution Experiment. The quantitative estimation of the evolved hydrogen was done using a locally constructed electrolysis setup²⁴

where the working electrode and the counter electrode are placed in two separate chambers (Figure 11). Bulk electrolysis at constant current of $-500~\mu A$ was carried out for 5 h using the two electrode system and 0.1 M phosphate buffer of pH 7 as the electrolyte. Surface modified FTO with surface area $0.5~cm^2$ was used as the working electrode (cathode) and a spiral platinum wire was used as the counter electrode (anode). The loading of the catalyst on FTO was maintained at 1 mg/cm². During electrolysis hydrogen bubbles were formed at the surface modified FTO electrode which gradually accumulated in the graduated tube by displacing the electrolyte. The set up was constructed in such a way that the bubbles formed at the counter electrode could no way interfere with those formed on the working electrode.



Figure 11: Set-up for quantitative hydrogen evolution.

Calculation of the Faradaic Efficiency.²⁵ From the above mentioned quantitative estimation of hydrogen using $[(UO_2)_2(\mu-L)_2]$ /carbon-black/Nafion/FTO electrode, it was found that 0.18 mL h⁻¹ of hydrogen was evolved at ambient temperature and pressure. Therefore, the number of moles of hydrogen evolved in 1 h = 0.18/22400 mol = 8.03 x 10⁻⁶ mol.

The controlled experiment was performed using carbon-black/Nafion/FTO electrode keeping all other experimental conditions identical. The total amount of hydrogen evolved in 5 h was ~0.025 mL.

Therefore, in terms of number of moles, the amount of hydrogen evolved in 1 h = $0.025/(5 \times 22400) \text{ mol} = 0.22 \times 10^{-6} \text{ mol}.$

Thus, the amount of hydrogen actually evolved = $(8.03-0.22) \times 10^{-6} \text{ mol} = 7.81 \times 10^{-6} \text{ mol}$

The ideal number of moles of hydrogen expected to be evolved $H_2(ideal) = Q/nF$, where Q is the total charged employed, n is the number of electrons involved for H_2 production and F is the Faraday constant. The value of n for HER is 2 as it is a two electron process and since we employed $-500 \, \mu A$ current, $H_2(ideal)$ in 1 h = $(0.5 \times 10^{-3} \times 3600)/(2 \times 96500) = 9.32 \times 10^{-6} \, mol$.

The expression used to calculate the Faradaic Efficiency is as follows:

Faradaic Efficiency =
$$\frac{\text{Moles of hydrogen evolved experimentally}}{\text{Moles of hydrogen evolved ideally}} \times 100$$

=
$$\{(7.81 \times 10^{-6}) / (9.32 \times 10^{-6})\} \times 100 = 83.7\%$$

Another important feature which defines a good catalyst is its stability and robustness under the given experimental conditions. Constant potential electrolysis (CPE) was performed to gain insights into the stability of the present catalyst. CPE was conducted at the onset potential of -1.1 V for a period of 12 h. The current was constant with negligible change for the whole range of 12 h confirming the robust nature as well as the durability of the catalyst (Figure 12). The CVs taken before and after CPE were almost identical to each other with a slight decrease in the current density, indicating no significant change of the catalyst. ICP analysis of the electrolyte after 12 h of CPE showed presence of approximately 0.4% of the total metal content on the electrode surface and therefore confirms negligible leaching of the catalyst and very good electrochemical stability of $[(UO_2)_2(\mu-L)_2]$ for showing HER activity. Thus both electrolysis (CPE and CCE) experiments clearly indicate the high stability and competence of $[(UO_2)_2(\mu-L)_2]$ as HER catalyst.

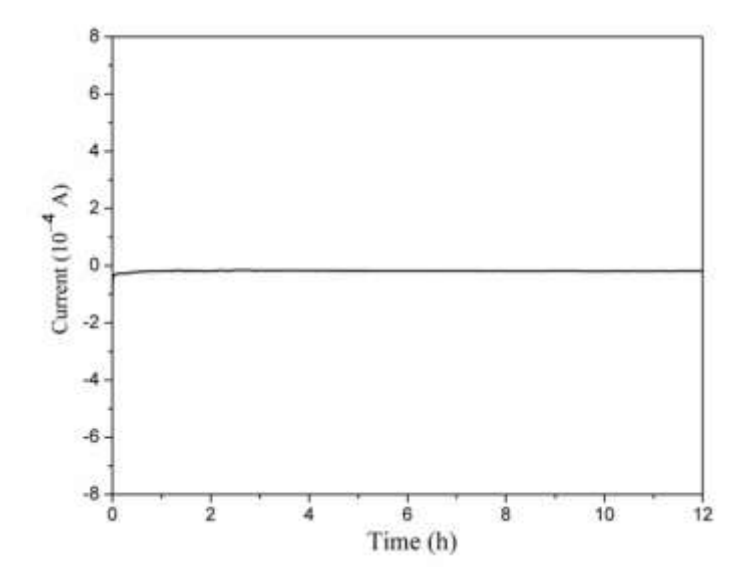


Figure 12: Constant potential electrolysis (CPE) using the surface coated FTO electrode in 0.1 M phosphate buffer of pH 7 for 12 h at a constant potential of −1.1 V (vs Ag/AgCl).

To understand whether HER causes any change of the catalyst $[(UO_2)_2(\mu-L)_2]$, the surface analyses of the $[(UO_2)_2(\mu-L)_2]$, carbon-black and Nafion mixture coated FTO electrode were done before electrolysis as well as after running 500 CV cycles by X-ray photoelectron spectroscopy (XPS). Both spectra are presented in Figure 13. There is essentially no difference between the two spectral profiles. The binding energies of the two major peaks in each spectrum reveal the presence of uranium only in +6 oxidation state. For a better comparison, both curves were fitted and the best fits led to the same number of satellite peaks in each of them. In the two deconvoluted spectra, there are little variations in the relative intensities of the resolved peaks and small differences (within 0.1–0.7 eV) in the peak maxima. However, absence of any new peak in the spectrum obtained after CV cycles indicates that there is effectively no significant alteration in the composition of the complex catalyst due to HER.

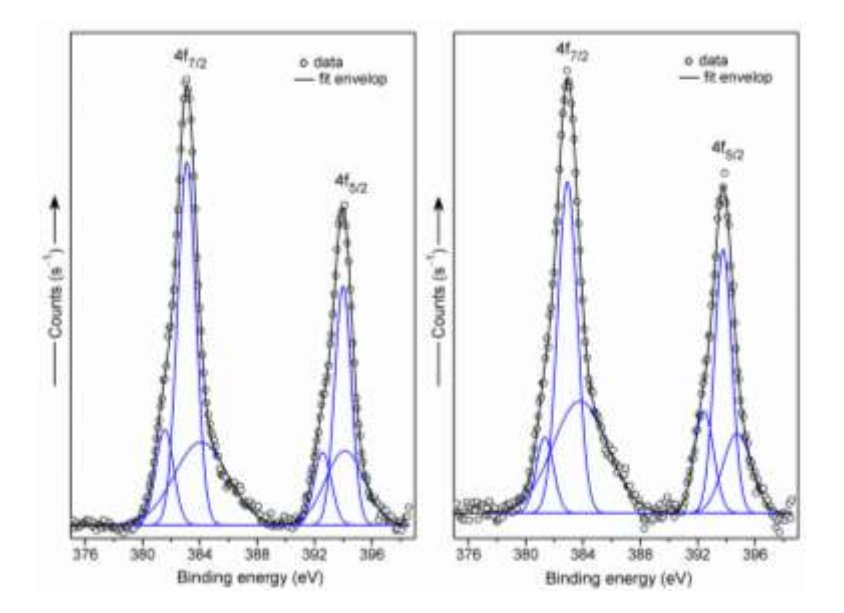


Figure 13: XPS spectra of surface coated FTO electrode before (left) and after (right) 500 cyclic voltammetry cycles.

4.3.6. Photocatalytic Hydrogen Production:

One of the major prerequisites for a good composite photocatalyst for hydrogen evolution from water is that it should absorb in the visible region. We have prepared some binary and ternary composite materials using TiO_2 as catalyst, $[(UO_2)_2(\mu - L)_2]$ as co-catalyst and the dyes N719, 4-hydroxycoumarin and coumarin 343 as photosensitizers. The diffuse reflectance spectroscopy was used to study the absorption features of these composite materials. All the spectra are illustrated in Figure 14. The dye sensitized composite materials display broad absorption bands in the wavelength range of 370–650 nm and hence they can be activated in the visible region, which in turn attributes potential light harvesting ability to them for solar energy conversion. The band gap energies of the complex $[(UO_2)_2(\mu - L)_2]$ and the composites have been calculated by using the Tauc plots (Figure 15). The value for the complex has been obtained as 1.78 eV, whereas for the composite materials it spans a narrow range of 2.50–2.66 eV.

The hydrogen production activity of a dye sensitized composite photocatalyst depends not only on the type of dye being used but also on the photocatalytic

reaction conditions such as dye/co-catalyst loading, nature of the sacrificial electron donor (SED), wavelength of the illuminating light, and time.^{7,8}

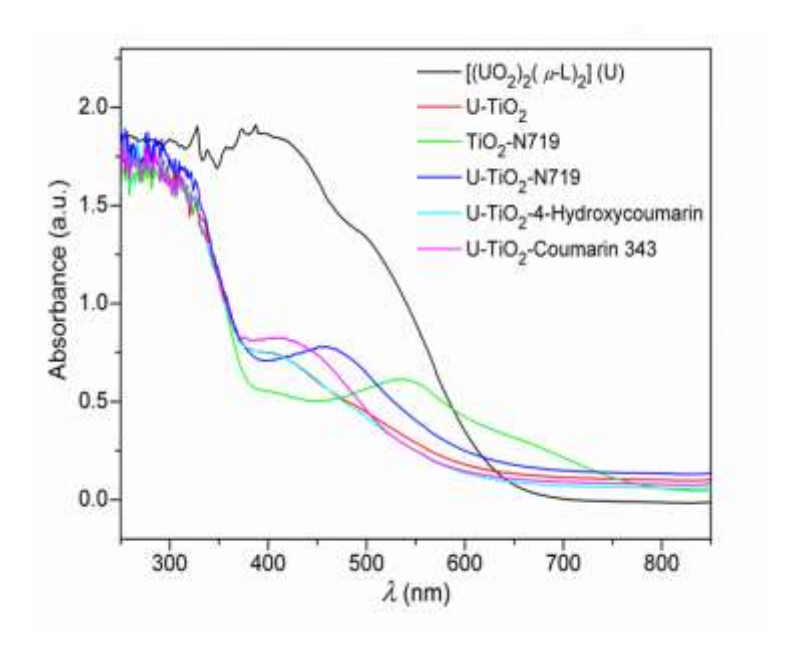


Figure 14: Diffuse reflectance spectra (DRS) of different catalyst composites.

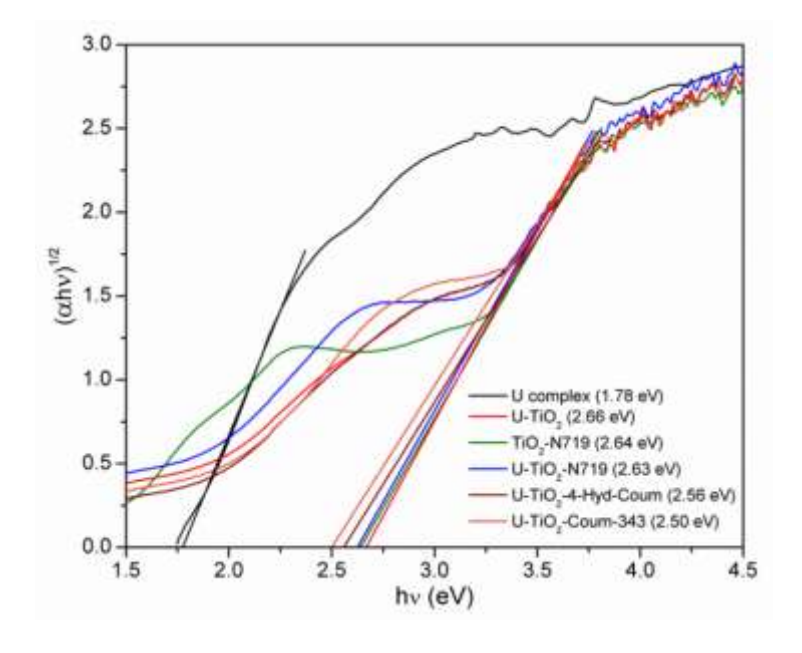


Figure 15: Tauc plots for different catalyst composites.

Herein we have used the above described binary and ternary composite materials with triethanolamine (TEOA) as the SED for the photocatalytic hydrogen evolution experiments at neutral pH under visible light irradiation for a period of

4 h. The results are summarized in Table 3 and Figure 16. The composite U-TiO₂ (U represents the co-catalyst [(UO₂)₂(μ -L)₂]) without any dye showed very little photocatalytic activity. Almost similar results were observed for the composites U-TiO₂-coumarin 343 and U-TiO₂-4-hydroxycoumarin. In these three cases, the H₂ yields and the AQY values were obtained within the ranges 449–708 μ mol g_{cat}⁻¹ and 1.0–1.6%, respectively (Table 3). The TON values for the two dye containing ternary composites were obtained as 108 and 142. In comparison, the binary composite TiO₂-N719 exhibited considerable amount of H₂ production (2117 μ mol g_{cat}⁻¹) with much higher TON (423) and AQY (4.7%) values. However, the maximum H₂ yield of 3439 μ mol g_{cat}⁻¹ with a TON and AQY values as high as 688 and 7.6%, respectively were obtained with the U-TiO₂-N719 composite. These values indicate a very decent photocatalytic hydrogen production ability of the U-TiO₂-N719 combination.^{7,8}

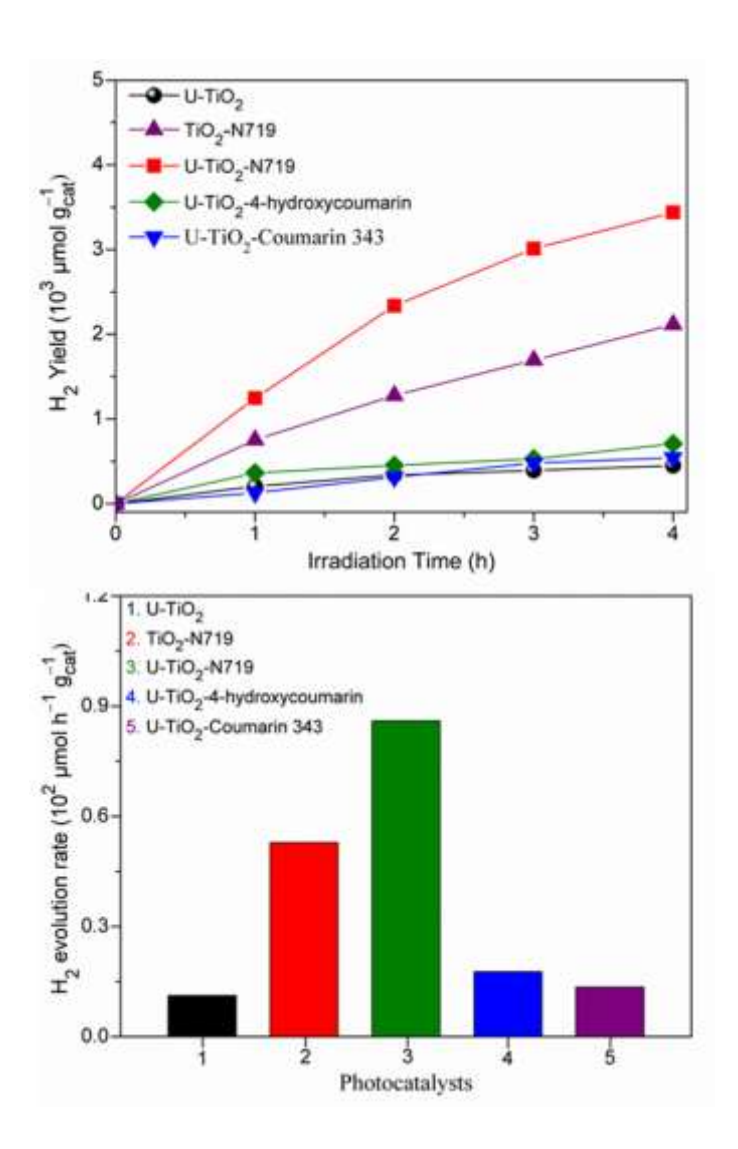


Figure 16: Kinetic profile (top) and the bar graph representation (bottom) of the photocatalytic hydrogen production activity under the reaction conditions as described in the text.

Composite	$H_2 ext{ Yield}^a$ ($\mu ext{mol } g_{ ext{cat}}^{-1}$)	TON	AQY (%)
U-TiO ₂	449	-	1.0
TiO ₂ -N719	2117	423	4.7
U-TiO ₂ -N719	3439	688	7.6
U-TiO ₂ -4-hydroxycoumarin	708	142	1.6
U-TiO ₂ -Coumarin 343	541	108	1.2

Table 3. Photocatalytic Hydrogen Evolution Activity of the Composites

"Reaction conditions: 10 mg of composite in 20 mL of 10 vol% TEOA aqueous solution at pH 7 (attained by using 1 M aqueous HCl solution) under 4 h of light irradiation ($\lambda > 420$ nm).

The turnover number (TON) was calculated according to the following equation.²⁷

Turnover Number (TON) =
$$\frac{2 \text{ x No. of evolved hydrogen molecules } (\mu \text{mol } g_{\text{cat}}^{-1})}{\text{No. of dye molecules adsorbed } (\mu \text{mol } g_{\text{cat}}^{-1})}$$

The apparent quantum yields (AQY) have been measured under the same photoreaction conditions. An optical power/energy meter (Newport, Model: 842-PE) was used for determination of the number of incident photons ($N_{photons}$). The values of $N_{photons}$ and AQY (%) was calculated using the following equations. ^{27,28}

Here, P represents power of the light (0.16 J s⁻¹ cm⁻²) in an area of 11.17 cm², λ is the wavelength of the light (420 nm), t is the duration of irradiation (4 h), h is the Planck's constant (6.626 x 10⁻³⁴ J s) and c is the velocity of light (3 x 10⁸ m s⁻¹).

$$N_{photons} = \frac{P\lambda t}{hc} \qquad N_{photons} = \frac{0.16 \times 11.17 \times 420 \times 10^{-9} \times 4 \times 3600}{6.626 \times 10^{-34} \times 3 \times 10^{8}}$$
$$= 5.44 \times 10^{22}$$

$$AQY = \frac{2 \times No. \text{ of evolved hydrogen molecules}}{No. \text{ of incident photons}} \times 100$$

The photoactivity of a dye sensitized semiconductor is strongly influenced by the attachment modes between the dye, semiconductor and the co-existing species (such as the SED and the co-catalyst) in the suspension systems, which dominate the charge generation, separation, transfer and recombination. All three ternary composites used in this work contain the same co-catalyst [(UO₂)₂(μ-L)₂] and all the reactions were performed in aqueous TEOA (SED) solution under long-term (4 h) irradiation. The superior photocatalytic activity of U-TiO₂-N719 combination compared to the other two composites is most likely due to the effective surface binding of the carboxyl anchoring groups of N719 (a Ru(II)-complex having visible light absorption capability within 400–600 nm) onto the semiconductor TiO₂. In all probability, the low efficiency of each of the other two composites containing the dyes 4-hydroxycoumarin and coumarin 343 results from the low injection yields of photoinduced electrons across the dye-semiconductor interface due to relatively poor attachment of the dye to TiO₂.

A possible reaction sequence for the photocatalytic hydrogen production has been given in Scheme 2. Upon visible light irradiation of N719, the Ru-dye, electron transfer takes place from HOMO to LUMO and the excited species Ru-dye* is formed (eq. 1). Oxidation of Ru-dye* by the semiconductor TiO₂ results into the formation of the oxidized dye Ru-dye⁺ and the reduced species TiO₂(e⁻) (eq. 2). In the third step (eq. 3), the co-catalyst U(VI)-complex gets reduced to U(V) containing species with regeneration of the semiconductor catalyst TiO₂. The U(V) containing species then reduces the water molecule to hydrogen (eq. 4). The oxidized Ru-dye⁺ takes up the electron from sacrificial electron donor (TEOA) (eq. 5) and drives the process of photocatalytic hydrogen generation.

Ru-Dye
$$\xrightarrow{hv}$$
 Ru-Dye* (1)
Ru-Dye* + TiO₂ $\xrightarrow{}$ Ru-Dye* + TiO₂(e⁻) (2)
TiO₂(e⁻) + U(VI)O₂ $\xrightarrow{}$ TiO₂ + U(V)O₂ (3)
U(V)O₂ + H₂O $\xrightarrow{}$ U(VI)O₂ + 1/2H₂ + OH⁻ (4)
Ru-Dye* + TEOA $\xrightarrow{}$ Ru-Dye + TEOA* (5)

Scheme 2. A possible mechanism for the photocatalytic evolution of hydrogen.

4.4. Conclusions

A dinuclear trans-uranyl(VI) complex of formula $[(UO_2)_2(\mu-L)_2]$ has been reported. X-ray crystal structure reveals the meridional fused 5,5,6-membered chelate rings forming ONNO-coordination mode of the bridging ligands L^{2-} and the formation of edge-shared pentagonal N₂O₃ plane around each trans-UO₂²⁺ unit. In the crystal lattice, the dinuclear molecules form a supramolecular chainlike structure via intermolecular N···H-O hydrogen bonding interactions. The spectroscopic features of the complex are consistent with its X-ray molecular structure. The complex exhibited decent activity in electrocatalytic as well as photocatalytic hydrogen evolution reaction in neutral aqueous medium. In the electrocatalytic process, the complex exhibits a Faradaic efficiency of 84% with a TOF as high as 384 h⁻¹. On the other hand, using the complex-TiO₂-N719 composite in photocatalytic hydrogen production under visible light irradiation a TOF of 172 h⁻¹ with an apparent quantum yield of 7.6% has been obtained. To the best of our knowledge, $[(UO_2)_2(\mu-L)_2]$ is the first trans-uranyl(VI) complex that can act as both electrocatalyst and photocatalyst for the hydrogen evolution reaction in neutral aqueous medium.

4.5. References

- (a) W. Lubitz, W. Tumas, *Chem. Rev.* 2007, 107, 3900. (b) S. Dutta, *J. Ind. Eng. Chem.*, 2014, 20, 1148. (c) I. Staffell, D. Scamman, A. V. Abad, P. Balcombe, P. E. Dodds, P. Ekins, N. Shah, K. R. Ward, *Energy Environ. Sci.* 2019, 12, 463.
- 2. (a) M. Frey, *ChemBioChem* **2002**, *3*, 153. (b) Evans, D. J.; Pickett, C. J. Chemistry and the hydrogenases. *Chem. Soc. Rev.* **2003**, *32*, 268.
- (a) A. A. Ismail, D. W. Bahnemann, Sol. Energy Mater. Sol. Cells 2014, 128, 85. (b) S. Rajaambal, K. Sivaranjani, C. S. Gopinath, J. Chem. Sci. 2015, 127, 33. (c) T. Jafari, E. Moharreri, A. S. Amin, R. Miao, W. Song, S. L. Suib, Molecules 2016, 21, 900. (d) K. Takanabe, ACS Catal. 2017, 7, 8006. (e) Z. Wang, C. Li, K. Domen, Chem. Soc. Rev. 2019, 48, 2109.
- (a) V. S. Thoi, Y. Sun, J. R. Long, C. J. Chang, Chem. Soc. Rev. 2013, 42, 2388.
 (b) M. Zeng, Y. Li, J. Mater. Chem. A 2015, 3, 14942.
 (c) X. Zou, Y. Zhang, Chem. Soc. Rev. 2015, 44, 5148.
- 5. K. Kunimatsu, T. Senzaki, M. Tsushima, M. Osawa, *Chem. Phys.Lett.* **2005**, *401*, 451 and references therein.
- 6. A. Z. Haddad, S. P. Cronin, M. S. Mashuta, R. M. Buchanan, C. A. Grapperhaus, *Inorg. Chem.* **2017**, *56*, 11254.
- 7. A. Fujishima, K. Honda, *Nature* **1972**, 238, 37.
- (a) K. Maeda, M. Eguchi, W. J. Youngblood, T. E. Mallouk, *Chem.Mater*.
 2008, 20, 6770. (b) T. Peng, D. Ke, P. Cai, K. Dai, L. Ma, L. Zan, *J. Power Sources* 2008, 180, 498. (c) R. Abe, K. Shinmei, K. Harac, B. Ohtani, *Chem. Commun.* 2009, 3577. (d) P. D. Tran, L. Xi, S. K. Batabyal, L. H. Wong, J. Barber, J. S. C. Loo, *Phys. Chem. Chem. Phys.* 2012, 14, 11596. (e) A. Tanaka, S. Sakaguchi, K. Hashimoto, H. Kominami, *ACS Catal.* 2013, 3, 79. (f) R. Abe, K. Shinmei, N. Koumura, K. Hara, B. Ohtani, *J. Am. Chem. Soc.* 2013, 135, 16872. (g) B. N. Mongal, A. Tiwari, C. Malapaka, U. Pal, *Dalton Trans.* 2019, doi: 10.1039/C9DT01506J.
- (a) R. J. Abe, *Photochem. Photobiol. C* 2010, 11, 179. (b) X. B. Chen, S. H. Shen, L. J. Guo, S. S. Mao, *Chem. Rev.* 2010, 110, 6503. (c) Y. Qu, X.

- Duan, Chem. Soc. Rev. 2013, 42, 2568. (d) X. H. Zhang, T. Y. Peng, S. S Song, J. Mater. Chem. A 2016, 4, 2365. (e) H. Junge, N. Rockstroh, S. Fischer, A. Brückner, R. Ludwig, S. Lochbrunner, O. Kühn, M. Beller, Inorganics 2017, 5, doi:10.3390/inorganics5010014.
- D. P. Halter, F. W. Heinemann, J. Bachmann, K. Meyer, *Nature* **2016**, 530, 317.
- 11. R. R. Gagné, C. L. Spiro, T. J. Smith, C. A. Hamann, W. R. Thies, A. K. Shiemke, *J. Am. Chem. Soc.* **1981**, *103*, 4073.
- 12. APEX3: *Program for Data Collection on Area Detectors*, Bruker AXS Inc., Madison, Wisconsin, USA, **2016**.
- 13. G. M. Sheldrick, *SADABS: Program for Area Detector Absorption Correction*, University of Göttingen, Göttingen, Germany, **1997**.
- 14. G. M. Sheldrick, Acta Crystallogr. Sect. A 2008, 64, 112.
- 15. L. J. Farrugia, J. Appl. Crystallogr. 2012, 45, 849.
- F. Macrae, I. J. Bruno, J. A. Chisholm, P. R. Edgington, P. M. Cabe, E. Pidcock, L. Rodriguez-Monge, R. Taylor, J. van de Streek, P. A. Wood, *J. Appl. Crystallogr.* 2008, 41, 466.
- (a) M. Åberg, Acta Chem. Scand. 1969, 23, 791. (b) J. Jiang, M. J. Sarsfield, J. C. Renshaw, F. R. Livens, D. Collison, J. M. Charnock, M. Helliwell, H. Eccles, Inorg. Chem. 2002, 41, 2799. (c) B. Masci, P. Thuéry, Polyhedron 2005, 24, 229. (d) K. Lyczko, L. Steczek, J. Struct. Chem. 2017, 58, 102. (e) S. Hadjithoma, M. G. Papanikolaou, E. Leontidis, T. A. Kabanos, A. D. Keramidas, Inorg. Chem. 2018, 57, 7631. (f) X. Zhao, D. Zhang, R. Yu, S. Chen, D. Zhao, Eur. J. Inorg. Chem. 2018, 1185. (g) S. Ghosh, A. K. Srivastava, S. Pal, New J. Chem. 2019, 43, 970.
- 18. C. J. Burns, A. P. Sattelberger, *Inorg. Chem.* **1988**, 27, 3692.
- (a) Z. Asadi, M. Asadi, A. Zeinali, M. Ranjkeshshorkaei, K. Fejfarova, V. Eigner, M. Dusek, A. Dehnokhalaji, *J. Chem. Sci.* 2014, 126, 1673. (b) C. Camp, L. Chatelain, V. Mougel, J. Pécaut, M. Mazzanti, *Inorg. Chem.* 2015, 54, 5774. (c) S. Ghosh, S. K. Kurapati, A. Ghosh, A. K. Srivastava, S. Pal, *ChemistrySelect* 2018, 3, 4865.

- 20. W. Kemp, *Organic Spectroscopy*; 2nd Ed., Macmillan: Hampshire, **1987**, pp 46–51.
- 21. (a) V. A. Volkovich, T. R. Griffiths, D. J. Frayand, R. C. Thied, *Phys. Chem. Chem. Phys.* **2001**, *3*, 5182. (b) P. M. Almond, T. E. Albrecht-Schmitt, *Inorg. Chem.* **2002**, *41*, 1177.
- 22. (a) Y. –H. Fang, Z. –P. Liu, ACS Catal. 2014, 4, 4364. (b) T. Shinagawa,
 A. T. Garcia-Esparza, K. Takanabe Sci. Rep. 2015, 5, 13801.
- 23. J. Mahmood, F. Li, S.M. Jung, M. S. Okyay, I. Ahmad, S. J. Kim, N. Park, Y. H. Jeong, J. B. Baek, *Nature Nanotech.* **2017**, *12*, 441.
- 24. S. Mukhopadhyay, J. Debgupta, C. Singh, A. Kar, S. K. Das, *Angew. Chem. Int. Ed.* **2018**, *57*, 1918.
- 25. B. C. Patra, S. Khilari, R. N. Manna, S. Mondal, D. Pradhan, A. Pradhan, A. A. Bhaumik, *ACS Catal.* **2017**, *7*, 6120.
- 26. E. S. Ilton, P. S. Bagus, Surf. Interface Anal. 2011, 43, 1549.
- 27. A. Kudo, Y. Miseki, Chem. Soc. Rev. 2009, 38, 253.
- 28. F. Raziq, Y. Qu, X. Zhang, M. Humayun, J. Wu, A. Zada, H. Yu, X. Sun, L. Jing, *J. Phys. Chem. C* **2016**, *120*, 98.

Catecholase Activity of Chiral Diuranyl(VI) Complexes: Experimental and Computational Study

Four chiral dinuclear uranyl(VI) complexes with the general molecular formulas $[(UO_2)_2(R/S-L^1)_2(H_2O)_2]\cdot 2MeCN$ (1·2MeCN and 2·2MeCN) and $[(UO_2)_2(R/S-L^1)_2(H_2O)_2]\cdot 2MeCN$ L^2 ₂(Me₂NCHO)₂] (3 and 4) (where, $(R/S-L^1)^{2-} = (R/S)-2-((1-\text{oxidopropan-}2-\text$ $(R/S-L^2)^{2-} = (R/S)-1-((1-\text{oxidopropan}-2-\text{oxidopropan})^2$ ylimino)methyl)-phenolate and ylimino)methyl)naphthalen-2-olate) were synthesized in 70–75 % yields. The complexes were characterized by elemental analyses, mass spectrometric, magnetic susceptibility and solution electrical conductivity measurements. Single crystal X-ray diffraction studies confirmed the dinuclear structure and pentagonal-bipyramidal NO₆ coordination sphere around the metal atoms in 1–4. In each complex, the metal centers of the two trans-UO₂²⁺ units reside in a NO₄ pentagonal plane constituted by the two alkoxide end bridging ONO-coordinating (L^{1/2})²⁻ and the two O-coordinating solvent (H₂O or Me₂NCHO) molecules. Spectroscopic (IR, UV–Vis and ¹H-NMR) features of the complexes corroborate well with their X-ray molecular structures. Complexes 3 and 4 exhibit good catecholase-like activity (oxidation of 3,5-di-tert-butylcatechol (3,5-DTBC) to 3,5-di-tert-butylquinone (3,5-DTBQ)) in Me₂NCHO solution with TOF as high as 3686 and 3774 h⁻¹. For both complexes, the catalytic reaction follows a radical pathway, as is confirmed by a sharp EPR signal at g = 1.99. A computational study of the reaction mechanism suggests a η^2 -syn type conformation of the adduct between the substrate and each of the two catalysts 3 and 4, which is favorable for an effective catalysis. On the other hand, an unfavorable η^1 -anti conformation of the substrate-catalyst adduct has been found for both 1 and 2. This conformation results in inactivity of both 1 and 2 towards the catecholase activity.

5.1. Introduction

There is a continuous quest for developing simple and effective small molecule catalysts having the potential to mimic the activities of various metalloenzymes. Catecholase also known as tyrosinase and polyphenol oxidase is a copper containing enzyme¹ and it is primarily present in various plant bodies. Over the years a diverse range of catalysts containing various transition metal ions have been developed which successfully mimic the catecholase activity.² Although the original enzyme is a member of type III copper proteins^{1,3} having hydroxybridged dicopper(II) center, mechanistic pathway for the catecholase activity of model catalysts containing not only Cu^{II} but also Mn^{II}, Mn^{III}, Fe^{II}, Co^{II}, Ni^{II} and Zn^{II} has been widely investigated.^{2,4} Exhaustive mechanistic study of these biomimetic catalysts reveals that the catalytic pathway may either follow a metal centered redox pathway⁵ or a ligand centered radical process, where the oxidation state of the metal remains unaltered.⁶

Since the transition metals have already been exploited to a great deal for preparing biomimetic catalysts, we have explored the possibility of developing model catalysts containing actinides as the active center. Recently, the *trans*-uranyl(VI) chemistry has attracted tremendous attention due to its unique (O=U=O) bonding⁷ as well as its application in various catalytic fields.^{7a,8} But to the best of our knowledge, no *trans*-uranyl(VI) based catalyst has been developed so far that can act as a model for a biomimetic reaction such as catecholase activity. Herein, we report two pairs of enantiomeric diuranyl(VI) complexes of the general molecular formula [(UO₂)₂(R/S-L^{1/2})₂(solvent)₂] (1–4) with the Schiff bases (R/S)-(1-hydroxypropan-2-ylimino)methyl)phenol (H₂R/S-L¹) and (R/S)-(1-hydroxypropan-2-ylimino)methyl)naphthalen-2-ol (H₂R/S-L²) (Chart 1) and their applications as catalysts in the oxidation reaction of 3,5-di-tert-butylcatechol (3,5-DTBC) to 3,5-di-tert-butylquinone (3,5-DTBQ). To our surprise 1 and 2 (having H₂O as the coordinated solvent) do not show any catecholase-mimetic behavior, whereas both 3 and 4 (having Me₂NCHO as the coordinated solvent)

exhibit decent catecholase activities with comparable turnover frequencies (TOF). A comprehensive computational study has been carried out for a better understanding of the reasons responsible for the disparity in the catalytic behaviors of the two pairs of enantiomers. In the following account, synthesis, physical properties, X-ray crystal structures and catecholase activities of **1–4** and a possible mechanistic pathway explaining the inactivity of **1** and **2** and activity of **3** and **4** as catalysts in the oxidation of 3,5-DTBC to 3,5-DTBQ are described.

$$H_3C$$
OH
 H_2O

Chart 1: Chemical structure diagrams of $(R/S-H_2L^1)$ (top left) and $(R/S-H_2L^2)$ (top right) and their corresponding complexes (bottom).

5.2. Experimental Section

5.2.1. Materials:

The enantiopure (R/S)-(1-hydroxypropan-2-ylimino)methyl)phenol $(H_2R/S-L^1)$ and (R/S)-(1-hydroxypropan-2-ylimino)methyl)naphthalen-2-ol $(H_2R/S-L^2)$ were prepared in 70–85% yields by condensation reactions of equimolar amounts of enantiopure (R/S) 2-aminopropan-1-ol with salicylaldehyde and 2-hydroxynapthaldehyde, respectively in methanol by following a procedure very

similar to those reported for analogous Schiff bases.⁹ All other chemicals and solvents used in this work were of reagent grade and used as received without further purification.

5.2.2. Physical Measurements:

Elemental (CHN) analyses were performed on a Thermo Finnigan Flash EA1112 series elemental analyzer. Magnetic susceptibilities were measured using a Sherwood Scientific balance. A Digisun DI-909 conductivity meter was used to measure the solution electrical conductivities. A Thermo Scientific Nicolet 380 or a Bruker Tensor-II FT-IR spectrophotometer was used to record the infrared spectra. Electronic spectra were collected using a Shimadzu UV-3600 UV-Vis-NIR spectrophotometer. The ¹H (400 MHz) NMR spectra were recorded on a Bruker NMR spectrometer. High resolution mass spectra were recorded with a Bruker Maxis (ESI-TOF analyzer) spectrometer. A CH Instruments model 620A electrochemical analyzer was used for cyclic and differential pulse voltammetric measurements. Electron spin resonance (EPR) experiment was done with the help of a JEOL JES-FA200 spectrometer.

5.2.3. Syntheses of $[(UO_2)_2(R/S-L^1)_2(H_2O)_2]\cdot 2MeCN$ (1·2MeCN and 2·2MeCN):

A methanol solution (10 mL) of UO₂(OAc)₂·2H₂O (85 mg, 0.2 mmol) was added dropwise to a hot methanol solution (10 mL) of enantiopure (*R/S*)-H₂L¹ (36 mg, 0.2 mmol) and the mixture was refluxed for 5 h. The yellow solid precipitated was collected by filtration and dried in vacuum. The precipitate was then dissolved in acetonitrile (~8 mL) and the resulting solution was allowed to evaporate slowly at room temperature in air. The yellow crystalline solvated complex separated in 6–7 days was collected by filtration and dried in air.

[(UO₂)₂(R-L¹)₂(H₂O)₂]·2MeCN (**1**·2MeCN): Yield: 71 mg (70%). Anal. Calcd (%) for C₂₄H₃₂N₄O₁₀U₂: C, 28.47; H, 3.19; N 5.53. Found: C, 28.12; H, 3.08; N 5.26. Selected IR data (ν (cm⁻¹)): 2360 (C=N), 1620 (C=N), 894 (UO₂). UV–Vis data (λ _{max} (nm) (ε (10³ M⁻¹ cm⁻¹))): 460 (1.42), 389 (6.31), 340 (14.13) ¹H NMR data (δ (ppm) (J (Hz))): 9.46 (s, 1H, H⁷), 7.64 (6,1) (dd, 1H, H⁵), 7.60 (1) (dd \rightarrow t,

1H, H³), 7.09 (8) (d, 1H, H²), 6.73 (1) (dd \rightarrow t, 1H, H⁴), 6.37 (8,1) (dd, 1H, H^{9a}), 5.84 (8,2) (dd, 1H, H^{9b}), 4.82 (m, 1H, H⁸), 1.84 (4) (d, 3H, Me). CV data (E_{pc} (V)): -0.60, -1.22. ESI-MS (m/z) calcd for {[(UO₂)₂(R-L¹)₂(H₂O)₂] + H}⁺, {[(UO₂)₂(R-L¹)₂(H₂O)] + H}⁺, and {[(UO₂)₂(R-L¹)₂] + H}⁺: 931.2681, 913.2576, and 895.2470, found 931.2442, 913.2335, 895.2249 (base peak).

[(UO₂)₂(S-L¹)₂(H₂O)₂]·2MeCN (**2**·2MeCN): Yield: 73 mg (72%). Anal. Calcd (%) for C₂₄H₃₂N₄O₁₀U₂: C, 28.47; H, 3.19; N 5.53. Found: C, 28.19; H, 3.06; N 5.28. Selected IR data (ν (cm⁻¹)): 2363 (C=N), 1620 (C=N), 893 (UO₂). UV–Vis data (λ _{max} (nm) (ε (10⁴ M⁻¹ cm⁻¹))): 460 (0.78), 388 (3.42), 340 (7.59). ¹H NMR data (δ (ppm) (J (Hz))): 9.45 (s, 1H, H⁷), 7.64 (6,1) (dd, 1H, H⁵), 7.60 (1) (dd \rightarrow t, 1H, H³), 7.09 (8) (d, 1H, H²), 6.73 (1) (dd \rightarrow t, 1H, H⁴), 6.37 (8,2) (dd, 1H, H^{9a}), 5.84 (8,2) (dd, 1H, H^{9b}), 4.82 (m, 1H, H⁸), 1.83 (4) (d, 3H, Me). CV data (E_{pc} (V)): -0.61, -1.22. ESI-MS (m/z): calcd for {[(UO₂)₂(R-L¹)₂(H₂O)₂] + H}⁺, {[(UO₂)₂(R-L¹)₂(H₂O)] + H}⁺, and {[(UO₂)₂(R-L¹)₂] + H}⁺: 931.2681, 913.2576, and 895.2470, found 931.2593, 913.2495, 895.2421 (base peak).

5.2.4. Syntheses of $[(UO_2)_2(R/S-L^2)_2(Me_2NCHO)_2]$ (3 and 4):

To a hot methanol solution (10 mL) of enantiopure (*R/S*)-H₂L³ (46 mg, 0.2 mmol) a methanol solution (10 mL) of UO₂(OAc)₂·2H₂O (85 mg, 0.2 mmol) was added dropwise and the mixture was refluxed for 6 h. An orange solid precipitated was filtered and dried in vacuum. It was then dissolved ~4 mL dimethylformamide (Me₂NCHO) and the solution obtained was allowed to evaporate in air at room temperature. The orange crystalline complex separated in about 14–15 days was collected by filtration and dried in vacuum.

[(UO₂)₂(R-L²)₂(Me₂NCHO)₂] (**3**): Yield: 85 mg (75%). Anal. Calcd (%) for C₃₄H₄₀N₄O₁₀U₂: C, 35.80; H, 3.53; N 4.91. Found: C, 35.92; H, 3.49; N 4.98. Selected IR data (ν (cm⁻¹)): 2849 ((O)C–H), 1641 (C=O), 1605 (C=N), 895 (UO₂). UV–Vis data (λ_{max} (nm) (ε(10^3 M⁻¹cm⁻¹))): 460 (1.58), 405 (5.53), 365 (8.09), 304 (16.8). ¹H NMR data (δ (ppm) (J (Hz))): 10.35 (s, 1H, H¹¹), 8.43 (8)

(d, 1H, H⁵), 8.16 (8) (d, 1H, H⁴), 7.87 (8) (d, 1H, H⁸), 7.57 (6) (t, 1H, H⁷), 7.47 (8) (d,1H, H³), 7.29 (6) (t, 1H, H⁶), 6.43 (8,2) (dd, 1H, H^{13a}), 5.94 (8,3) (dd, 1H, H^{13b}), 5.10 (m, 1H, H¹²), 1.87 (8) (d, 3H, Me). CV data (E_{pc} (V)): -0.61, -1.23. ESI-MS (m/z): calcd for {[(UO₂)₂(R-L³)₂(Me₂NCHO)₂] + H}⁺ 1141.3838, found: 1141.3610.

[(UO₂)₂(S-L²)₂(Me₂NCHO)₂] (**4**): Yield: 80 mg (70%). Anal. Calcd (%) for C₃₄H₄₀N₄O₁₀U₂: C, 35.80; H, 3.53; N 4.91. Found: C, 35.72; H, 3.56; N 4.85. Selected IR data (ν (cm⁻¹)): 2848 ((O)C–H), 1643 (C=O), 1613 (C=N), 895 (UO₂). UV–Vis data (λ _{max} (nm) (ε (10³ M⁻¹cm⁻¹))): 460 (1.47), 406 (5.6), 365 (7.89), 304 (16.55). ¹H NMR data (δ (ppm) (J (Hz))): 10.36 (s, 1H, H¹¹), 8.44 (4) (d, 1H, H⁵), 8.16 (8) (d, 1H, H⁴), 7.88 (8,1) (dd, 1H, H⁸), 7.57 (1) (dd \rightarrow t, 1H, H⁷), 7.45 (8) (d,1H, H³), 7.29 (6) (t, 1H, H⁶), 6.44 (10,2) (dd, 1H, H^{13a}), 5.94 (8,3) (dd, 1H, H^{13b}), 5.10 (m, 1H, H¹²), 1.86 (8) (d, 3H, Me). CV data (E_{pc} (V)): –0.59, –1.21. ESI-MS (m/z): calcd for {[(UO₂)₂(R-L³)₂(Me₂NCHO)₂] + H}⁺ 1141.3838, found: 1141.6219.

5.2.5. X-ray Crystallography:

Single crystals suitable for X-ray data collection $1 \cdot \text{MeCN}$, $2 \cdot \text{MeCN}$, 3, and 4 were collected from the corresponding recrystallized samples isolated during their syntheses. Unit cell determination and the intensity data collection for all four the complexes were performed at 298 K on a Bruker D8 Quest diffractometer fitted with a Photon 100 CMOS area detector and an Incoatec microfocus source for graphite monochromated Mo $K\alpha$ radiation ($\lambda = 0.71073$ Å). Data acquisition, integration and reduction were performed using the APEX3 software package. In each case, the structure was solved by direct method and refined on F^2 using full-matrix least-squares procedures. All the non-hydrogen atoms were refined with anisotropic thermal parameters. For $1 \cdot \text{MeCN}$ and $2 \cdot \text{MeCN}$, the coordinated water molecule hydrogen atoms were located in the corresponding difference maps and refined with geometric and thermal restraints. The remaining hydrogen atoms in $1 \cdot \text{MeCN}$ and $2 \cdot \text{MeCN}$ and all the hydrogen

atoms in **3** and **4** were placed in idealized positions and refined using a riding model. The SHELX-97 programs¹¹ accessible in the WinGX software suite¹² were used for structure solution and refinement. The Mercury package¹³ was used for structural illustrations. Significant crystal and refinement data for all the four structures are summarized in Tables 1 and 2.

5.2.6. Catecholase Activity:

The catalytic activities of **3** and **4** towards oxidation of 3,5-DTBC to 3,5-DTBQ were investigated at room temperature under aerobic conditions. The substrate (50-500 equivalents) was added to the Me₂NCHO solution (10 mL) of the catalyst $(1 \times 10^{-4} \text{ M})$. The progress of the reaction was followed spectrophotometrically by monitoring the increase in the absorption of the characteristic quinone band at 400 nm at every 5 min. for a total period of 1 h.

5.2.7. Detection of H_2O_2 :

Iodometric test was done to detect the formation of H_2O_2 that is formed during the catalytic reaction. In the reaction mixture (10 mL), the catalyst-substrate concentration ratio was maintained as 1:100. After 1 h, an equal volume of water was added to the reaction mixture and the quinone formed was extracted using dichloromethane as the organic layer. The aqueous layer was acidified with H_2SO_4 (0.1 M) to pH 2 to quench further oxidation followed by addition of 1 ml of 10% KI solution and three drops of 3% ammonium molybdate solution. In presence of H_2O_2 and excess iodide, the reaction $H_2O_2 + 3I^- + 2H^+ \rightarrow 2H_2O + I_3^-$ takes place. Appearance of the characteristic I_3^- peak at 353 nm confirms the generation of H_2O_2 .¹⁴

Table 1: Selected crystallographic data for **1**⋅2MeCN and **2**⋅2MeCN

Complex	1·2MeCN	2·2MeCN
Chemical formula	$C_{24}H_{32}N_4O_{10}U_2$	$C_{24}H_{32}N_4O_{10}U_2$
Formula weight	1012.59	1012.60
Crystal system	Orthorhombic	Orthorhombic
Space group	$P2_12_12_1$	$P2_12_12_1$
a (Å)	9.1862(3)	9.1280(3)
b (Å)	17.8581(7)	17.7349(6)
c (Å)	19.7352(8)	19.5818(6)
α (°)	90	90
β(°)	90	90
γ(°)	90	90
Volume (Å ³)	3237.5(2)	3169.98(18)
Z	4	4
ρ (g cm ⁻³)	2.077	2.122
$\mu (\mathrm{mm}^{-1})$	10.045	10.259
Reflections collected	30520	26060
Reflections unique	5697	5569
Reflections $[I \ge 2\sigma(I)]$	5132	5130
Data / restraints / paramete	Data / restraints / parameters 5697 / 6 / 375	
$R1$, $wR2$ [$I \ge 2\sigma(I)$]	0.0344, 0.0796	0.0209, 0.0438
R1, wR2 [all data]	0.0400, 0.0817	0.0245, 0.0448
GoF on F^2	1.044	0.972
Absolute structure parameter 0.020(7)		0.012(7)
Max. / Min. $\Delta \rho$ (e Å ⁻³)	2.457 / -0.860	1.040 / -0.686

 $\textbf{Table 2:} \ \textbf{Selected crystallographic data for 3 and 4} \\$

Complex	3	4		
Chemical formula	$C_{34}H_{40}N_4O_{10}U_2$	$C_{34}H_{40}N_4O_{10}U_2$		
Formula weight	1140.76	1140.76		
Crystal system	Monoclinic	Monoclinic		
Space group	$P2_1$	$P2_1$		
a (Å)	13.5636(5)	13.5437(6)		
b (Å)	9.1354(3)	9.1327(4)		
c (Å)	15.9187(6)	15.9077(8)		
α(°)	90	90		
eta (°)	109.6930(10)°	109.593(2)°		
γ(°)	90	90		
Volume (Å ³)	1857.10(12)	1853.70(15)		
Z	2	2		
ρ (g cm ⁻³)	2.040	2.044		
$\mu (\mathrm{mm}^{-1})$	8.768	8.785		
Reflections collected	20966	26507		
Reflections unique	6434	6483		
Reflections $[I \ge 2\sigma(I)]$	6258	6273		
Data / restraints	/6434 / 1 / 451	6483 / 1 / 451		
parameters				
$R1$, $wR2$ [$I \ge 2\sigma(I)$]	0.0151, 0.0324	0.0237, 0.0544		
<i>R</i> 1, <i>wR</i> 2 [all data]	0.0161, 0.0326	0.0251, 0.0550		
GoF on F^2	1.034	1.017		
Absolute structu	re0.022(4)	0.059(6)		
parameter				
Max. / Min. $\Delta \rho$ (e Å ⁻³)	0.307 / -0.675	1.647 / -0.993		

5.2.8. Theoretical Calculations:

All the theoretical calculations were performed using B3LYP functional in Gaussian09 suite of program. The geometries of all the structures were optimized using LANL2DZ-ECP basis set for uranium and 6-31g(d,p) basis set for carbon, hydrogen, oxygen and nitrogen atoms. The electronic transitions were calculated using time-dependent DFT method and polarized continuum model with Me2NCHO as solvent.

5.3. Results and Discussions

5.3.1. Synthesis and Characterization:

Complexes with the general molecular formula $[(UO_2)_2(R/S-$ L¹)₂(H₂O)₂]·2CH₃CN $(1.2CH_3CN$ and 2·2CH₃CN) and $[(UO_2)_2(R/S L^2$ ₂(Me₂NCHO)₂ (3 and 4) were synthesized in good yields (70–75%) by refluxing the methanol solution of UO₂(OAc)₂·2H₂O and the corresponding Schiff base (H₂Lⁿ) for 5–6 h. Elemental analysis data of all four complexes match very well with their molecular formulas. The room temperature magnetic susceptibility measurements suggest the diamagnetic character of all four complexes and hence the +6 oxidation state of the uranium centers in them. All the complexes are highly soluble in Me₂NCHO and Me₂SO. Complexes 1 and 2 are also soluble in MeCN. In solution, each of the four complexes is electrically non-conducting. The non-electrolytic character supports the neutral molecular formula of each of the four complexes.

5.3.2. X-ray Molecular Structures:

The structures of 1.2MeCN and 2.2MeCN were solved in orthorhombic $P2_12_12_1$ space group whereas the structures of the unsolvated complexes 3 and 4 were solved in monoclinic $P2_1$ space group. The structures of 1.2MeCN and 2.2MeCN are illustrated in Figure 1 and that of 3 and 4 are illustrated in Figure 2. The bond lengths associated with the uranium centres for all the complexes are listed in Table 3. The asymmetric units of both 1.2MeCN and 2.2MeCN contain one

dinuclear complex molecule and two acetonitrile molecules which are hydrogen bonded with the two metal coordinated water molecules. The O···N distances and the O-H···N angles are within 2.889(8)-2.939(13) Å and 157(7)-162(4)°, respectively. The asymmetric unit of each of 3 and 4 has one dinuclear complex molecule. In all four dinuclear molecules, the uranium atoms are in edge-shared NO₆ pentagonal bipyramids. The phenolate-O, azomethine-N and the bridging alkoxide-O coordinating meridional tridentate $(L^{1/2})^{2-}$ ligands and the O-atoms of the solvent molecules constitute the two edge-shared NO₄ pentagonal planes (rms deviations, 0.07-0.11 Å) around the uranium atoms of the two trans-(UO₂)²⁺ moieties and form the edge-shared pentagonal bipyramids. The small fold angles $(2.8(2)-4.2(2)^{\circ})$ at the common edge $(O(2)\cdots O(4))$ suggest that the edge-shared pentagonal planes are essentially coplanar. The U···U distances in 1–4 are very similar (3.8816(3)–3.9207(5) Å). The U(1)–O(4) and U(2)–O(6) bond lengths are comparable with the uranium(VI) to bridging alkoxide-O distances observed before. ¹⁶ Overall U=O, U-O(phenolate) and U-N(azomethine) bond lengths in 1-4 are within the ranges reported for uranium(VI) complexes having similar coordinating atoms. 8e,f,16.17a

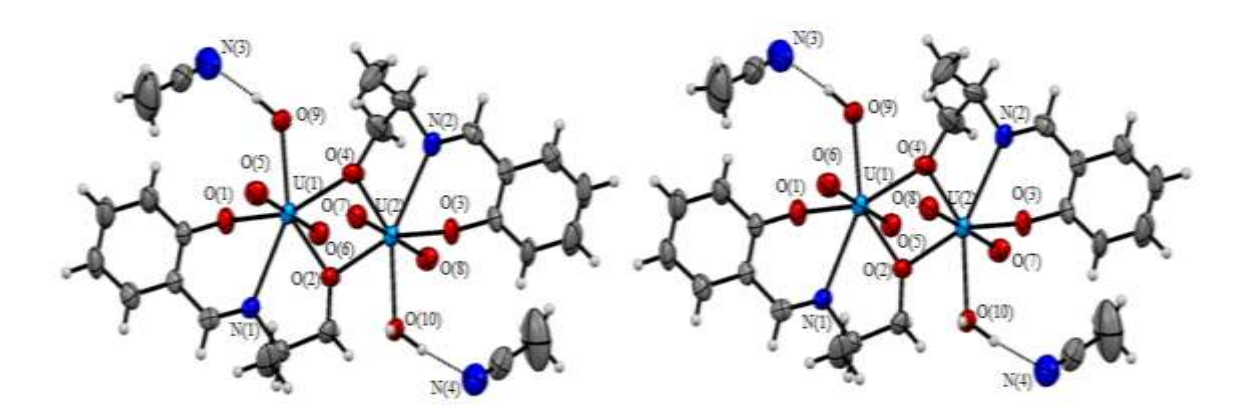


Figure 1: Molecular structures of $[(UO_2)_2(R-L^1)_2(H_2O)_2]\cdot 2MeCN$ (1·2MeCN) (left) and $[(UO_2)_2(S-L^1)_2(H_2O)_2]\cdot 2MeCN$ (2·2MeCN) (right). All the non-hydrogen atoms in each structure are represented by their 40% probability thermal ellipsoids.

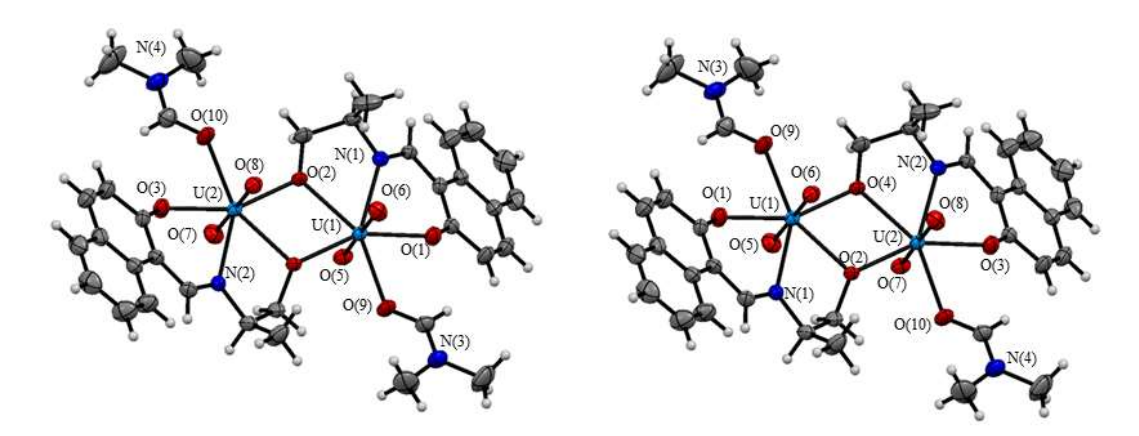


Figure 2: Molecular structures of $[(UO_2)_2(R-L^2)_2(Me_2NCHO)_2]$ (3) (left) and $[(UO_2)_2(S-L^2)_2(Me_2NCHO)_2]$ (4) (right). All the non-hydrogen atoms in each structure are represented by their 40% probability thermal ellipsoids.

Table 3: Selected bond lengths (Å) for 1·2MeCN, 2·2MeCN, 3 and 4

Complex	1.2CH ₃ CN	2 .2CH ₃ CN	3	4
U(1)–O(1)	2.302(5)	2.282(3)	2.281(3)	2.281(4)
U(1)–O(2)	2.381(5)	2.369(3)	2.364(3)	2.365(4)
U(1)–O(4)	2.347(5)	2.333(3)	2.364(2)	2.359(4)
U(1)–O(5)	1.790(6)	1.770(4)	1.775(3)	1.787(4)
U(1)–O(6)	1.798(7)	1.777(4)	1.778(3)	1.774(5)
U(1)–O(9)	2.494(6)	2.471(4)	2.428(3)	2.433(5)
U(1)-N(1)	2.575(7)	2.544(5)	2.534(3)	2.536(5)
U(2)–O(2)	2.372(6)	2.352(4)	2.339(2)	2.337(3)
U(2)–O(3)	2.302(6)	2.288(3)	2.284(3)	2.286(4)
U(2)–O(4)	2.370(5)	2.353(3)	2.379(3)	2.382(4)
U(2)–O(7)	1.794(6)	1.770(4)	1.779(3)	1.793(5)
U(2)–O(8)	1.754(7)	1.774(4)	1.775(3)	1.779(4)
U(2)–O(10)	2.471(5)	2.452(4)	2.453(3)	2.450(4)
U(2)–N2)	2.588(7)	2.568(4)	2.524(3)	2.518(5)

5.3.3. Self-assembly via Hydrogen Bonding

Both 1:MeCN and 2:MeCN contain the classical hydrogen bond donor coordinated H₂O molecules and several acceptors such as phenolate-O, alkoxide-O and oxo groups. In contrast, 3 and 4 do not have any such donor. Thus the structures of the two solvated complexes were only scrutinized for hydrogen bond assisted self-assembly patterns. The geometric parameters for the hydrogen bonds found in the two structures are listed in Table 4. As mentioned in the previous section, two MeCN molecules in each of 1 MeCN and 2 MeCN are involved in strong O-H···N hydrogen bonds with the two coordinated water molecules on two sides of the dinuclear molecule (Figure 1). The remaining hydrogen atom of each water molecule is involved in strong inter dinuclear O-H···O hydrogen bonding interaction, where the metal coordinated phenolate-O (O(1) or O(3)) acts as the acceptor. The O···O distances and the O–H···O angles are in the ranges 2.658(5)-2.719(9) Å and 166(6)-172(9)°, respectively. Because of these O-H···O hydrogen bonds both 1·MeCN and 2·MeCN form onedimensional linear supramolecular structures along a-axis in the corresponding crystal lattices (Figure 3).

Table 4: Hydrogen bonding parameters for 1·MeCN and 2·MeCN^a

Complex	D–H···A	D…A (Å)	∠DHA (°)
1·MeCN	O(9)–H(9c)···N(3)	2.939(13)	158(7)
	$O(9)$ – $H(9d)$ ··· $O(3)^i$	2.719(1)	170(8)
	O(10)-H(10d)···O(1) ⁱⁱ	2.665(1)	172(9)
	O(10)-H(10e)···N(4)	2.908(1)	157(7)
2.MeCN	$O(9)-H(9c)\cdots O(3)^{i}$	2.691(5)	166(6)
	O(9)–H(9d)···N(3)	2.921(8)	162(4)
	O(10)-H(10d)···N(4)	2.889(8)	159(4)
	O(10)-H(10e)···O(1) ⁱⁱ	2.658(5)	168(6)

^a Symmetry transformations used: (i) x - 1, y, z. (ii) x + 1, y, z.

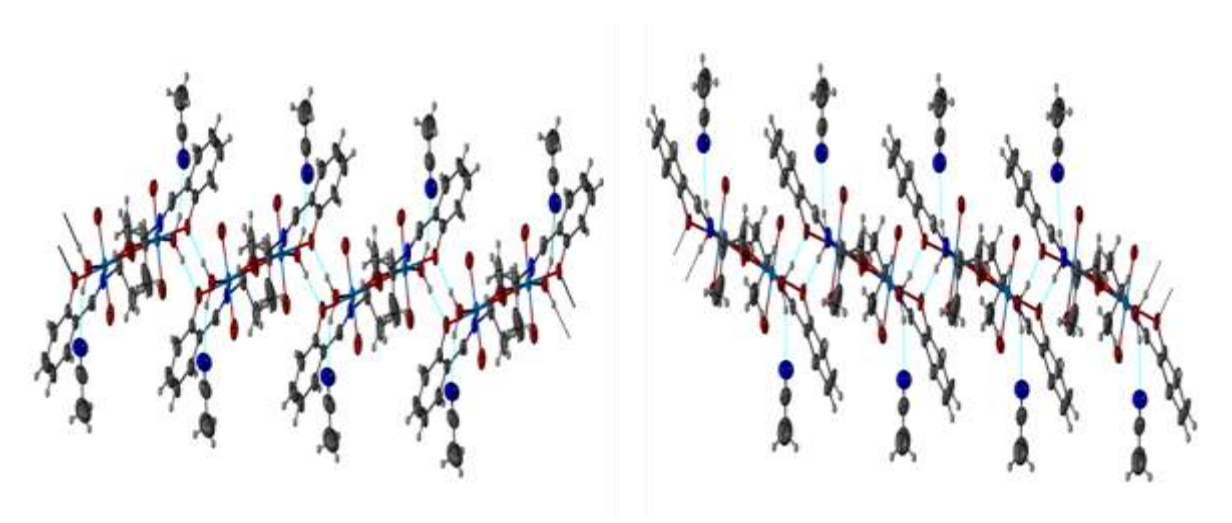


Figure 3: One dimensional assembly of 1-MeCN (left) and 2-MeCN (right).

5.3.4. Spectroscopic Characterization:

Infrared spectra of all the complexes were recorded from 4000 to 550 cm⁻¹. The spectra are shown in Figures 4 and 5. A broad band near 3000 cm⁻¹ is due to the presence of coordinated H₂O molecules in 1.2CH₃CN and 2.2CH₃CN. The presence of acetonitrile in the crystal lattice of 1·2MeCN and 2·2MeCN is indicated by the C≡N stretching band at ~2362 cm⁻¹. For complex 3 and 4, the C−H stretching band of the aldehyde of the coordinated Me₂NCHO molecule appears at 2848 cm⁻¹. This is followed by the (C=O) stretch of the Me₂NCHO at 1643 cm⁻¹. All the complexes display a band in the range 1605–1620 cm⁻¹ which is attributed to the azomethine −HC=N stretching.¹⁷ The strong sharp band ~894 cm⁻¹ for all four complexes is assigned to the asymmetric stretching vibration of the uranyl moiety.^{8e,f,17a} No attempts were made to assign rest of the bands.

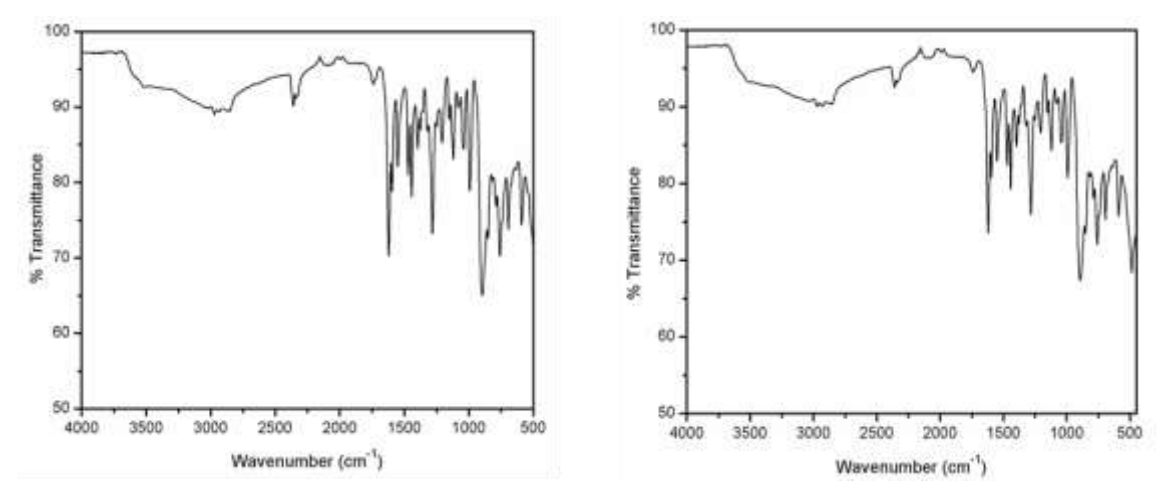


Figure 4: Infrared spectra of $[(UO_2)_2(R-L^1)_2(H_2O)_2]\cdot 2MeCN$ (1·2MeCN) (left) and $[(UO_2)_2(S-L^1)_2(H_2O)_2]\cdot 2MeCN$ (2·2MeCN) (right) in powder phase.

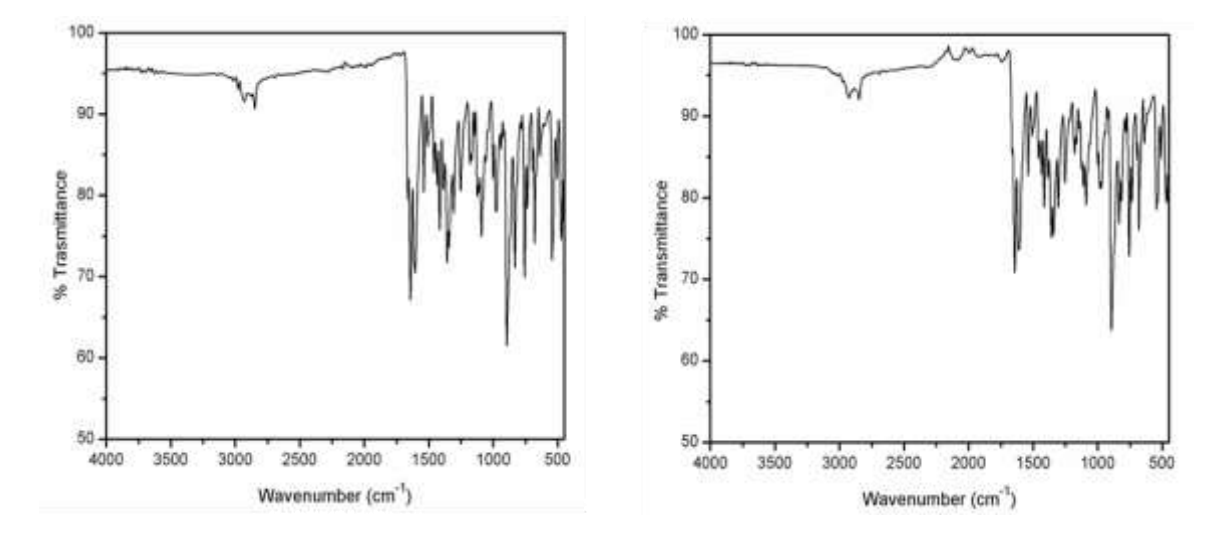


Figure 5: Infrared spectra of $[(UO_2)_2(R-L^2)_2(Me_2NCHO)_2]$ (3) (left) and $[(UO_2)_2(S-L^2)_2(Me_2NCHO)_2]$ (4) (right) in powder phase.

The electronic spectra of all the complexes were recorded in Me₂NCHO in 800 to 200 nm range. The spectral profiles are illustrated in Figure 6. Complexes 1·2MeCN and 2·2MeCN display a broad band at ~460 nm followed by a strong shoulder at ~389 nm and an very intense band at 340 nm. In case of complexes 3 and 4, the highest energy intense absorption is at ~304 nm, which is preceded by a strong band at 365 nm, a shoulder at 405 nm and another shoulder at ~460 nm. Comparing with previously reported literatures having similar metal–ligand coordination it can be concluded that for both pair of enantiomers the highest

energy transition is due to ligand centered transitions whereas the lower energy absorptions in the range 365–460 nm are due to ligand to metal charge transfer transitions. ^{17a,b, 18}

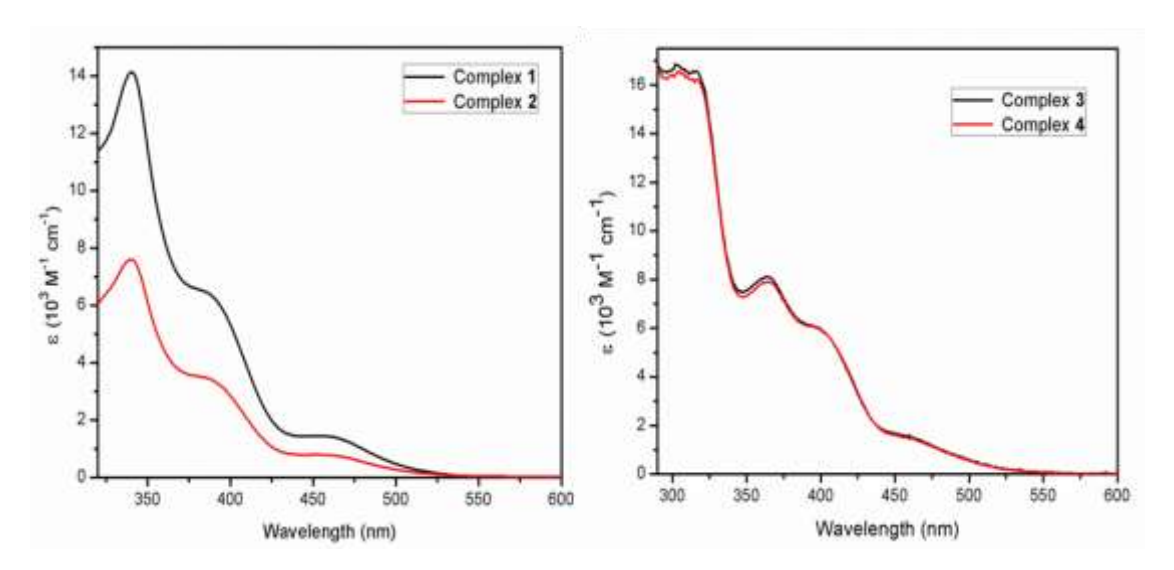


Figure 6: Electronic spectra of $[(UO_2)_2(R/S-L^1)_2(H_2O)_2]\cdot 2MeCN$ (1·2MeCN and 2·2MeCN) (left) and $[(UO_2)_2(R/S-L^2)_2(Me_2NCHO)_2]$ (3 and 4) (right) in Me₂NCHO.

DMSO-d₆ solutions of all the complexes were used for recording the 1H NMR spectra (Figures 7–10). The absence of the singlet corresponding to the phenolic and the alcoholic proton in all the spectra clearly indicates the deprotonated dianionic state of the ligands ($(R/S-L^1)^{2-}$ and $(R/S-L^2)^{2-}$). The singlet at δ 9.46 ppm for 1.2MeCN and 2.2MeCN and that at δ 10.36 ppm for δ and δ is attributed to the azomethine (-HC=N-) proton (δ in δ 1.2MeCN and δ 2.2MeCN and δ in δ and δ in δ 2.2MeCN appear in the range δ 6.73–7.65 ppm whereas in case of δ and δ they appear within δ 7.29–8.43 ppm with the expected splitting patterns. The two aliphatic protons δ in δ 2.2MeCN and δ 2.2MeCN and δ 3 and δ 4 appear as a doublet of doublet at δ 6.44 and δ 4.84 ppm, respectively. The single proton at the chiral carbon δ 1.2MeCN and δ 2.2MeCN and δ 3 and δ 4 appears as a multiplet at δ 4.82 and δ 1.85 ppm due to the coupling with the proton (δ in δ at the adjacent chiral carbon.

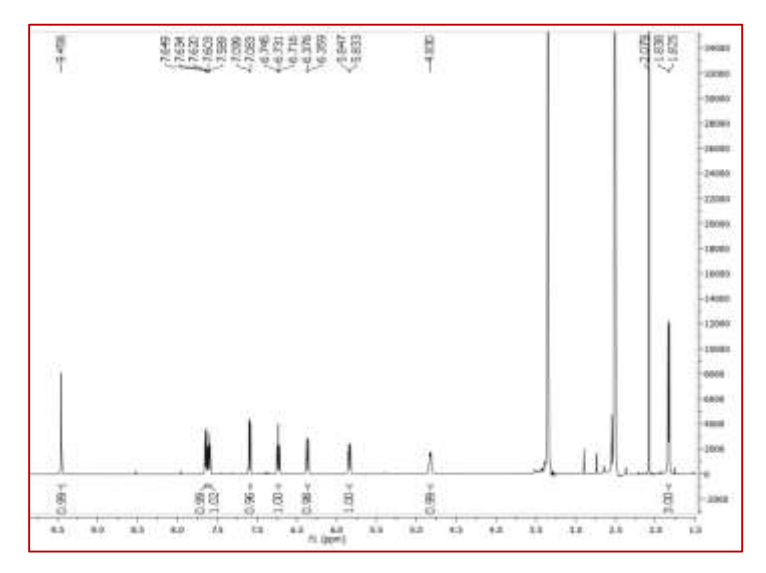


Figure 7: 1 H-NMR spectra of $[(UO_{2})_{2}(R-L^{1})_{2}(H_{2}O)_{2}]\cdot 2MeCN$ (**1**·2MeCN) in DMSO-d₆.

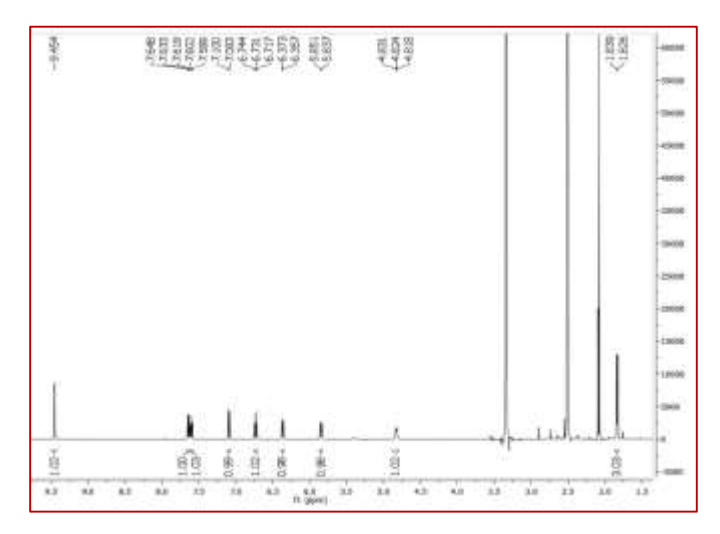


Figure 8: 1 H-NMR spectra of $[(UO_{2})_{2}(S-L^{1})_{2}(H_{2}O)_{2}]\cdot 2MeCN$ (**2**·2MeCN) in DMSO-d₆.

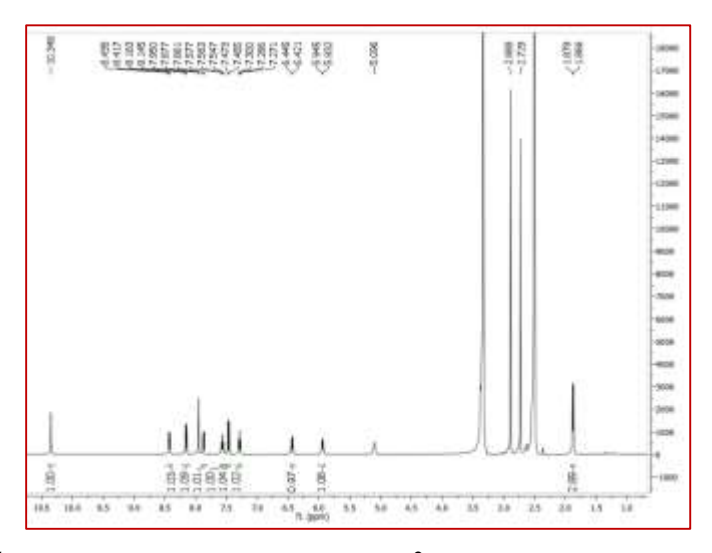


Figure 9: ${}^{1}\text{H-NMR}$ spectra of $[(UO_2)_2(R-L^2)_2(Me_2NCHO)_2]$ (3) in DMSO-d₆.

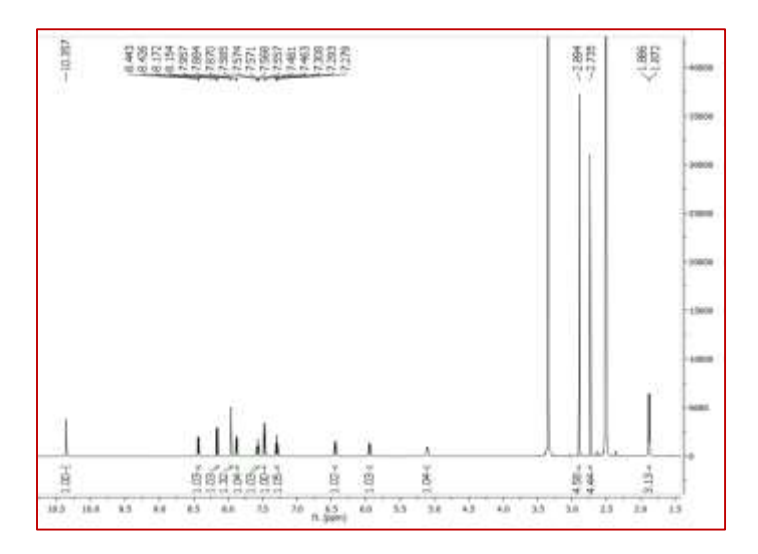


Figure 10: ${}^{1}\text{H-NMR}$ spectra of $[(UO_2)_2(S-L^2)_2(Me_2NCHO)_2]$ (4) in DMSO-d₆.

5.3.5. Redox Behavior:

Redox properties of all the complexes have been studied in Me₂NCHO solution (10^{-3} M) using a Pt-disk working electrode, a Pt-wire auxiliary electrode and an Ag/AgCl reference electrode under nitrogen atmosphere at 298 K with tetra-n-butylammonium perchlorate (TBAP) as the supporting electrolyte. The redox responses of all the four complexes are quiet similar (Figure 11). Each of them displays two irreversible cathodic responses. The E_{pc} of the first response is within -0.77 to -0.82 V, followed by the second response with the E_{pc} in the range of -1.16 to -1.24 V. Cyclic voltammogram of a ~ 1 mM Me₂NCHO

solution of ferrocene (Fc) was taken under identical conditions reveals that the peaks corresponds to one electron reductions. 8e,f,17a,b,19 Thus the observed reductions are assigned to $U(VI)U(VI) \rightarrow U(V)U(VI) \rightarrow U(V)U(V)$ processes.

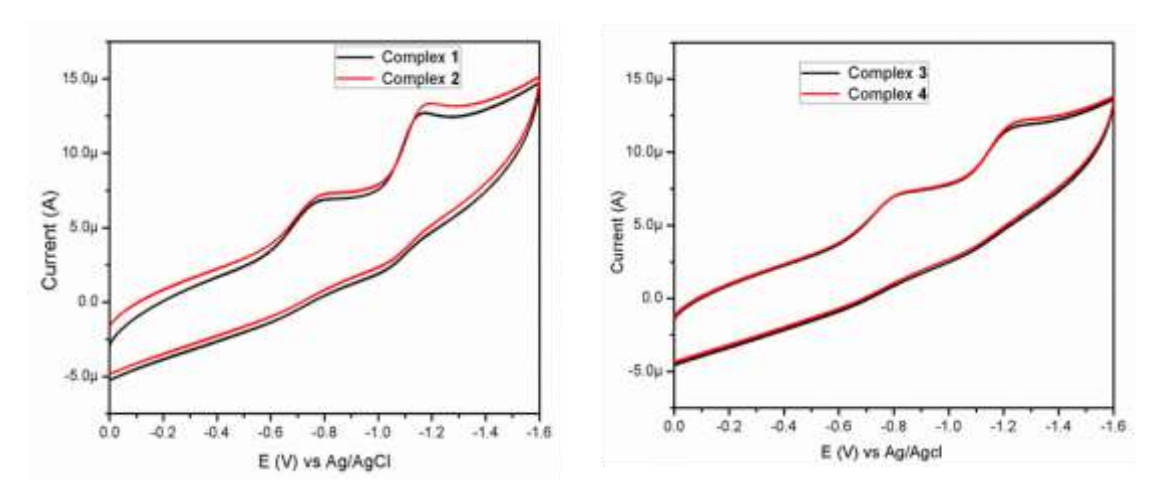


Figure 11: Cyclic Voltammograms of $[(UO_2)_2(R/S-L^1)_2(H_2O)_2]\cdot 2CH_3CN$ (1·2CH₃CN and 2·2CH₃CN) (left) and $[(UO_2)_2(R/S-L^2)_2(Me_2NCHO)_2]$ (3 and 4) (right) in Me₂NCHO.

5.3.6. Catecholase activity:

The catalytic activity of the complexes towards catechol oxidation was studied in Me₂NCHO. Solutions (10 mL) of the complex catalysts **3** and **4** (1 x 10^{-4} M) were treated with 0.01 mole of 3,5-DTBC. The catecholase activity was monitored for 1 h using UV-Vis spectroscopic measurements at an interval of every 5 mins after the addition of the substrate 3,5-DTBC. Initially, the spectrum of the complex was recorded and it displayed a hump at ~400 nm.

Upon addition of 3,5-DTBC into the Me₂NCHO solution of the catalyst (**3** or **4**), the intensity of the characteristic 3.5-DTBQ band at 400 nm gradually increases with time (Figure 12). This increase confirms the oxidation of 3,5-DTBC to 3,5-DTBQ. The solution of pure 3,5-DTBC in absence of **3** or **4** does not show any band at 400 nm even after a period of 12 h.

In case of both 1 and 2 as catalyst, no such increase in the 400 nm band was observed during a period of 1 h (Figure 13). No increment of the characteristic

3.5-DTBQ band clearly indicates the inactivity of 1 and 2 towards catecholase activity.

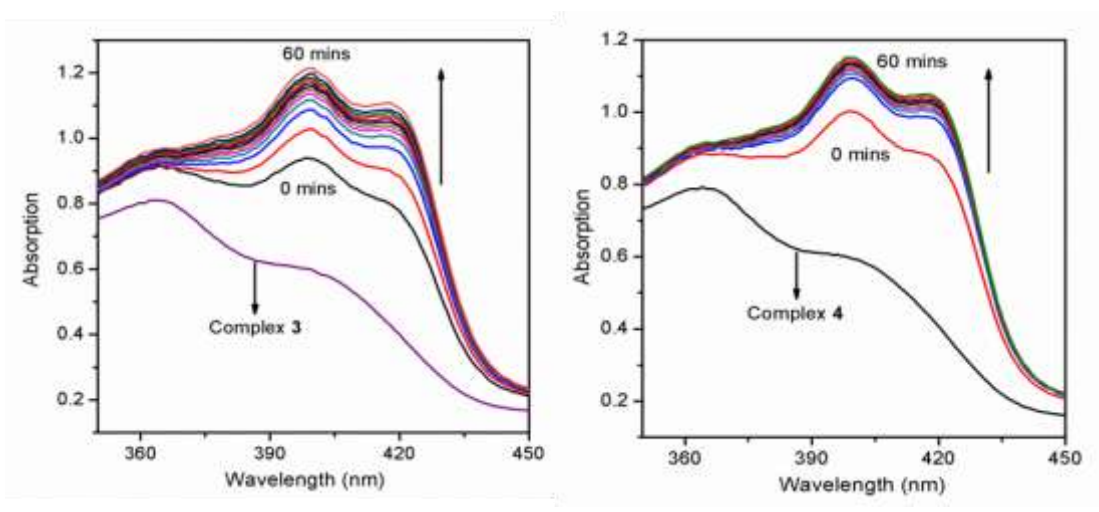


Figure 12: Catalysts **3** and **4** showing catecholase activity over a period of 60 mins.

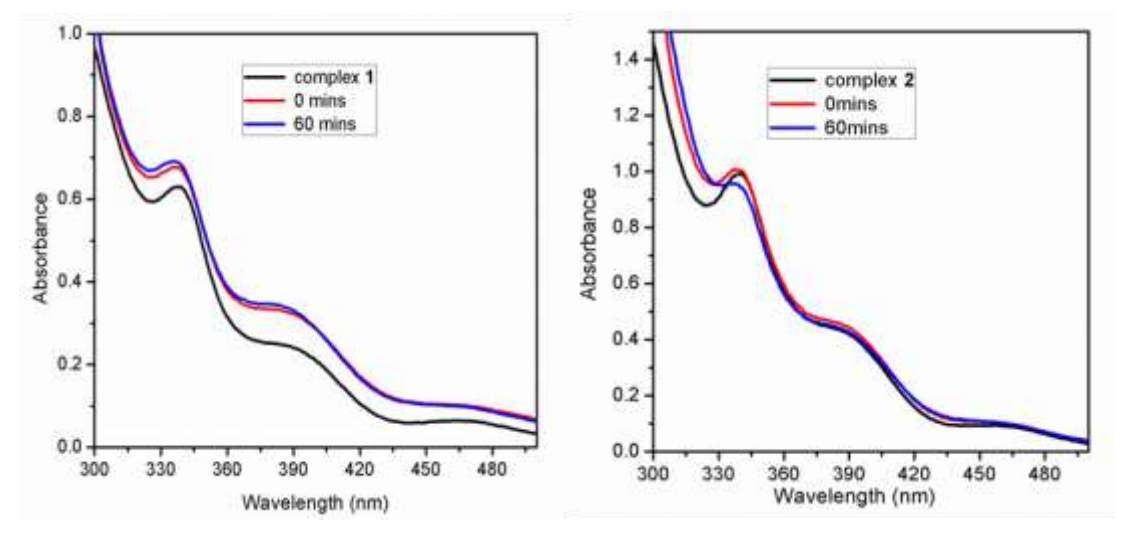


Figure 13: Catalyst **1** and **2** showing no catecholase activity over a period of 60 mins.

To understand the efficiency of catalysts 3 and 4 kinetic studies were performed (Figures 14 and 15). The catalyst concentration was fixed at 1×10^{-4} M whereas the substrate concentration was varied from 50 to 500 equivalents with respect to the catalyst. The kinetic parameters are listed in Table 5. All the experiments were done under aerobic condition at room temperature. For each set of

catalyst–substrate combination the UV–Vis spectra were recorded over a period of 1 h. The experiments were done following initial slope methods and since the complexes show saturation kinetics, Michaelis–Menten approach was used to determine the rate constant (k_{cat} i.e the turnover number). From the Lineweaver–Bruke plot of 1/V vs 1/[S] and using the equation 1/V = $\{K_M/V_{max}\}\{1/[S]\}$ + 1/V_{max}, the kinetic parameters V_{max} , k_{cat} and K_M were calculated.

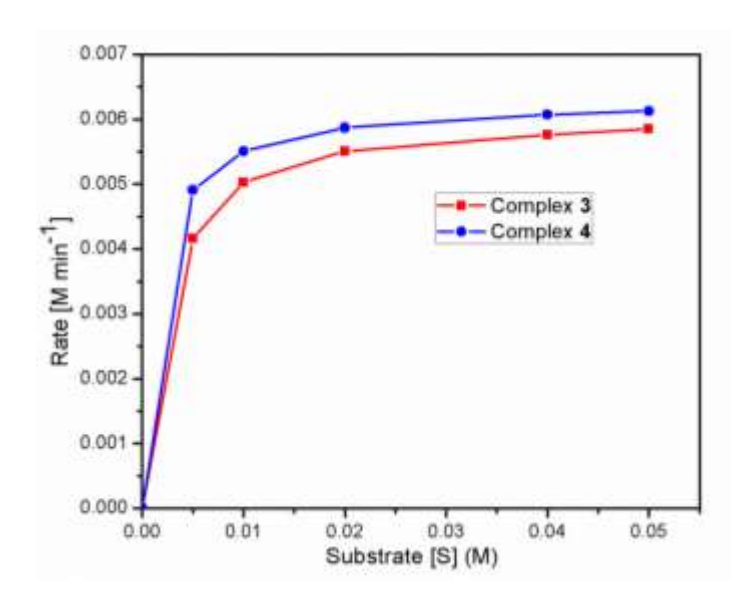


Figure 14: Initial rates vs substrate concentration for the oxidation of 3,5–DTBC to 3,5–DTBQ by complexes **3** and **4** in Me₂NCHO.

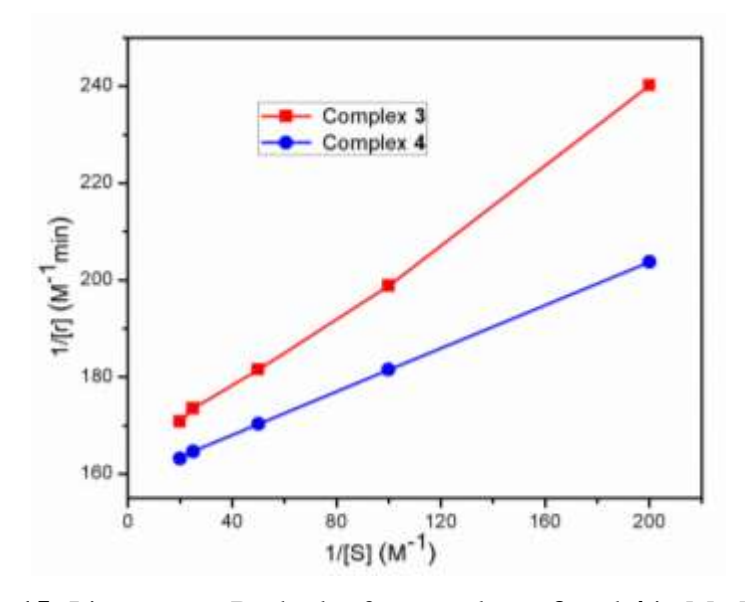


Figure 15: Lineweaver-Burk plot for complexes 3 and 4 in Me₂NCHO.

Table 5: Kinetics Data for Complexes 3 and 4.

catalyst	$V_{max} (Ms^{-1})$	K _M (M)	kcat (h ⁻¹)
3	6.14×10^{-3}	2.346×10^{-3}	3685.71
4	6.29×10^{-3}	1.409×10^{-3}	3774.23

The ESI-MS spectra of the complexes as well as that of the catechol-complex mixture were recorded to get an insight of the mechanistic pathway. The spectra of 3 and 4 display a base peak at 1141.3610 amu and 1141.6219 amu, respectively corresponding to the monocationic $\{[(UO_2)_2(R/S-L^2)_2(Me_2NCHO)_2]\}$ +H} $^+$ (m/z_{cald} = 1141.3833). ESI-MS spectra of the complexes also display peaks at 1068.3080 amu for 3 and at 1068.5615 amu for 4 corresponding to the mono solvated species $\{[(UO_2)_2(R/S-L^2)_2(Me_2NCHO)] + H\}^+$ $(m/z_{cald} = 1068.3232)$. However no peak at 994.2705 amu is observed for either of 3 and 4 suggesting that at no time both the solvent molecules get detached from the two metal centers. The spectra of [3/4 + 3.5-DTBC] taken after 10 min of mixing reveal a peak at 1312.4498 for 3 and at 1312.7181 amu for 4 (Figures 16 and 17). These peaks indicate the formation of the catalyst-substrate adduct $[3/4 + 3.5-DTBC^{-1}+$ Na + H]⁺ (m/z_{cald} = 1312.4671) where the monoanionic substrate has a monodentate binding mode of $[3/4 + 3.5-DTBC^{-1}+ Na + H]^{+}$ (m/z_{cald} = 1312.4671). The peaks at m/z = 243.1315 and 243.2509 amu in the spectra (Figure 18) of [3/4 + 3.5-DTBC] corresponds to the $[3.5-DTBQ-Na]^+$ aggregate.

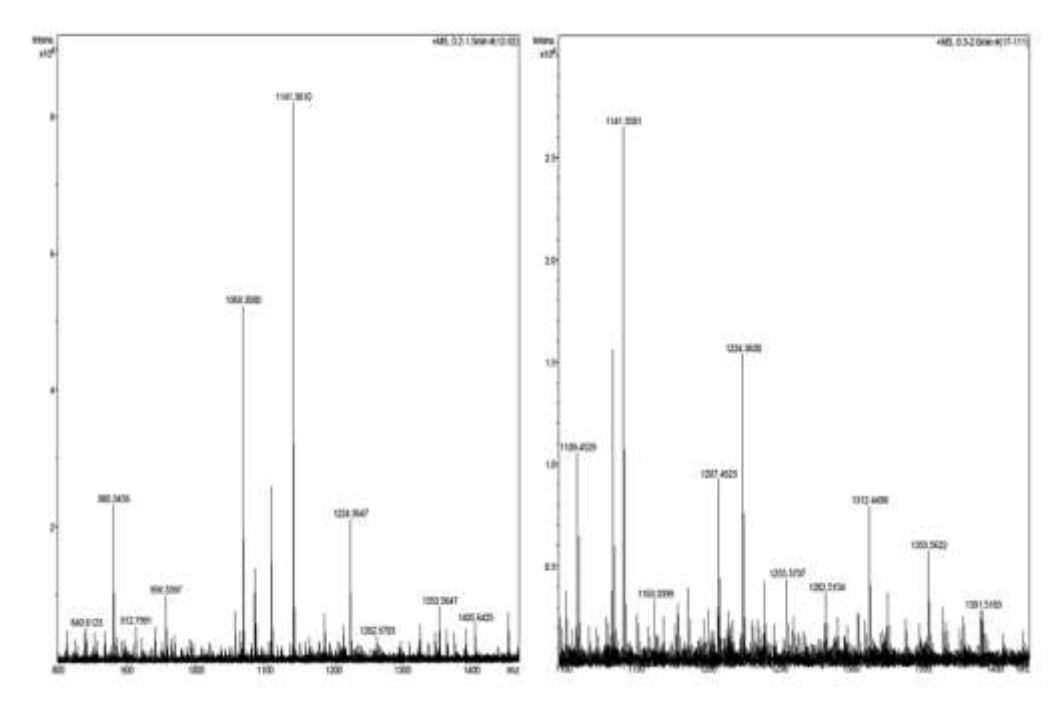


Figure 16: ESI-MS spectra of catalyst **3** and 3,5–DTBC (1:100) immediately after mixing (left) and after 10 min of mixing (right).

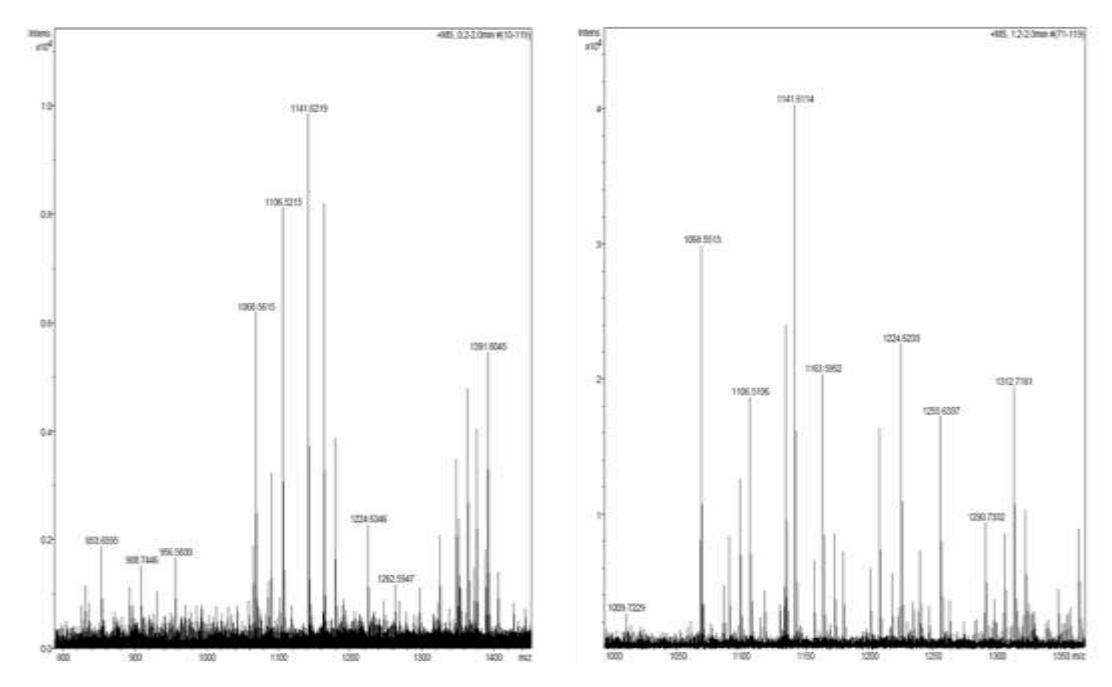


Figure 17: ESI-MS spectra of catalyst **4** and 3,5–DTBC (1:100) immediately after mixing (left) and after 10 min of mixing (right).

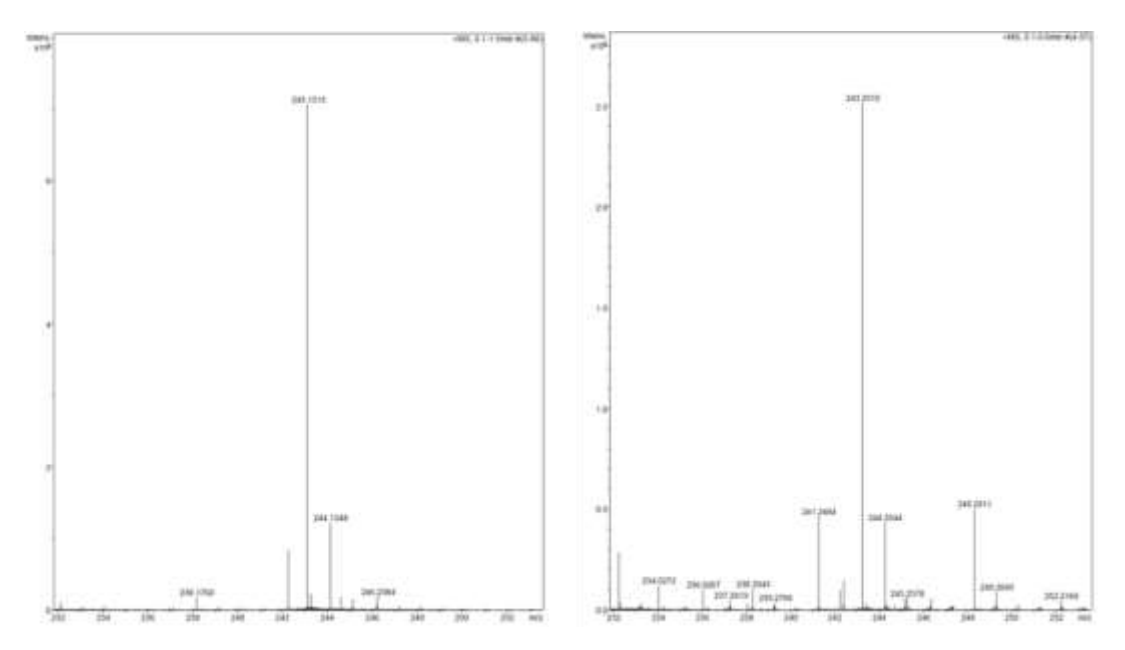


Figure 18: ESI-MS spectrum showing the formation of 3,5-DTBQ by catalyst **3** (left) and catalyst **4** (right).

The electron paramagnetic resonance (EPR) spectra of frozen (70 K) Me₂NCHO solutions of the catalyst–substrate (1:100) mixtures show a sharp signal at g = 1.99 (Figure 19). Catalysts **3** and **4** are EPR silent owing to their diamagnetic character. Thus the appearance of the EPR signal in the spectrum of each catalyst–substrate mixture clearly indicates towards the formation of radical intermediate during the oxidation of 3,5-DTBC to 3,5-DTBQ.

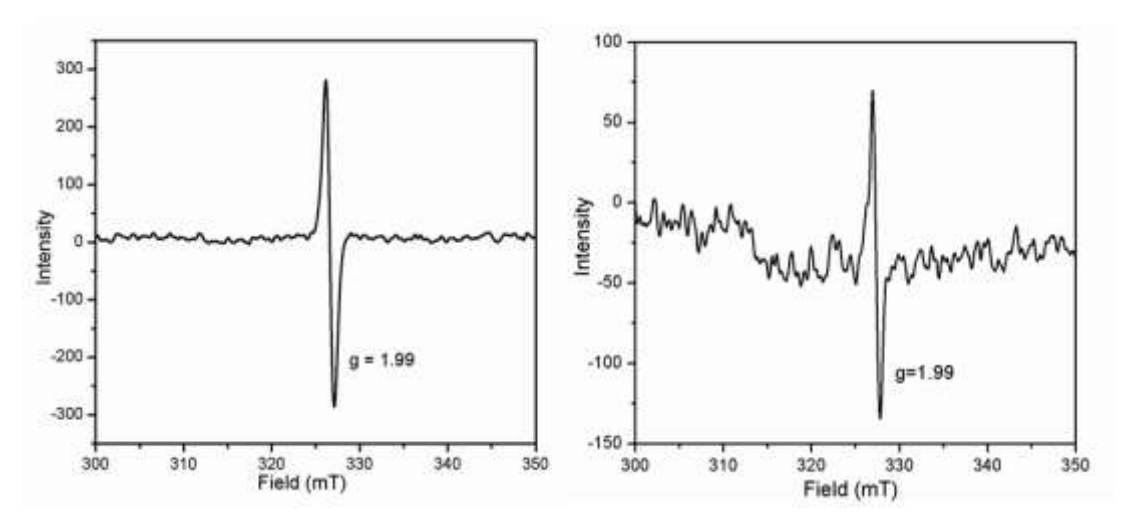


Figure 19: EPR spectra of 1:100 mixtures of **3**–substrate (left) and **4**–substrate (right) in Me₂NCHO at 70 K.

5.3.7. Computational Study:

To get a further insight into the mechanistic pathway of the catecholase activity and to understand the underlying reasons for the catalytic inactivity of complexes 1 and 2, computational study for complexes 1 and 3 was performed. As per the ESI-MS spectrum of 3, the oxidation of 3,5-DTBC to 3,5-DTBQ is initiated by the loss of one of the coordinated solvent molecule from the catalyst and simultaneous coordination of one of the hydroxyl oxygen to the respective uranium center. In view of the experimental results, the theoretical studies were $[(UO_2)_2(R-L^1)_2(H_2O)(3.5-DTBC)]$ conducted $[(UO_2)_2(R L^2$ ₂(DMF)(3,5-DTBC)] as the optimized structures (referred to as **A** and **B** respectively). The optimized configurations of these structures reveal that in case of complex A, only the coordinated –OH hydrogen of the substrate 3,5-DTBC is involved in strong H-bonding with the nearest bridging alkoxide-O at a distance of 1.82 Å. This type of interaction leads to η^1 -anti binding mode of the substrate with respect to the catalyst (Figure 20). On the other hand, in case of complex **B**, the coordinated -OH hydrogen of 3.5-DTBC are involved in strong hydrogen bonding with the nearby phenolate-O (1.70 Å) and the other –OH is involved in a relatively weak hydrogen bond with the adjacent bridging alkoxide-O (2.72 Å) due to the η^2 -syn type conformation of 3,5-DTBC with respect to the catalyst (Figure 20). The binding mode of the substrate with respect to the catalyst plays an important role in understanding the mechanistic pathway.²⁰ A closer view of complex B shows that there is a favorable dispersion interaction between the methyl group of Me₂NCHO and the methyl group of the coordinated ligand $(L^2)^{2-}$ at a distance of 3.83 Å. As a result of this interaction, the N-U-U-N torsion angle (138.61°) in **B** is significantly smaller than that (152.77°) in **A** where this interaction is not possible due to the presence of H₂O instead of Me₂NCHO. In addition, there is another similar kind of interaction between the hanging -CH₃ of the coordinated (L²)²⁻ and one of the two –CH₃ groups of the 3,5-DTBC (distance between the methyl groups being 3.94Å). It appears that the decrease in the N-U–U–N torsion angle in **B** is responsible for the additional dispersion interactions between the $-CH_3$ group of the 3,5-DTBC and that of $(L^2)^{2-}$ as well as the weakening of the hydrogen bond between the 3,5-DTBC –OH and the bridging alkoxide-O leading to the η^2 -syn type conformation of the 3,5-DTBC favorable for effective catalytic oxidation of it.

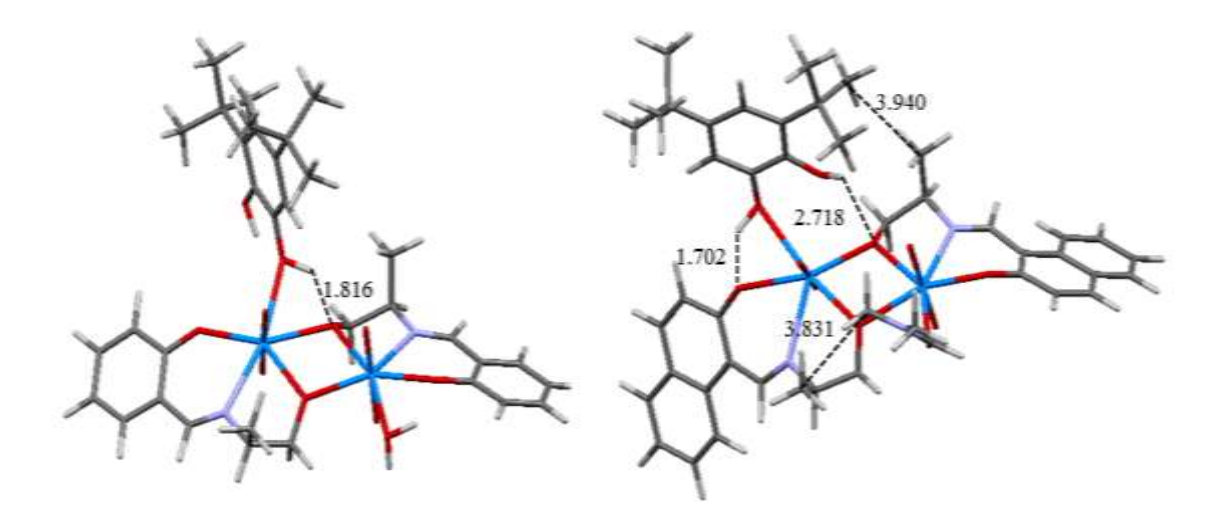


Figure 20: η^1 -anti and η^2 -syn conformations of the optimized structures **A** (left) and **B** (right).

The formation of η^2 -syn conformation only in complex **B** was further investigated by studying two different systems; i) by removing the tert-butyl groups of the catechol (optimized structure B1) and ii) by replacing Me₂NCHO with H₂O as the coordinating solvent (optimized structure **B2**) (Figure 21). In the first case, the hydrogen bonds in the new optimized complex (B1) that is formed between the catalyst and the substrate (as discussed earlier) has a little change in their bond length with no other major alterations as compared to the optimized structure B. But in the second case, we observe that in the new optimized complex **B2**, the conformation of the substrate i.e. 3,5–DTBC is η^1 –anti with respect to the catalyst. This anti conformation in B2 is similar to the substratecatalyst conformation in the optimized structure A. Due to the absence of the Me₂NCHO molecule as the coordinated solvent in **B2**, two of the –OH hydrogens are involved in H-bond with the phenolate oxygen and -trans oxo atom of the same metal center. The distance between methyl groups of 3,5-DTBC and hanging methyl groups of ligand moiety is increased by 0.5Å as compared to the optimized structure **B** and is at a distance of 4.36Å as similar to structure **A**. This

result clearly infers that the weak dispersion interaction between the methyl group of coordinated solvent moiety (Me₂NCHO in this case) and methyl of coordinated ligand plays the primary role in the formation of the *syn* substrate—catalyst conformation in the optimized structure **B** (Figure 21). The dispersion interaction between the *tert*—butyl groups of 3,5—DTBC and the hanging –CH₃ moiety of the complex is also helpful in the formation of the favorable η^2 -*syn* type conformation, which is the pre-requisite for the catalysis of 3,5—DTBC to 3,5—DTBQ. The experimental results also show that the catalysis activity does not take place when 3,5—DTBC is replaced by pure catechol and thus support the computational results.

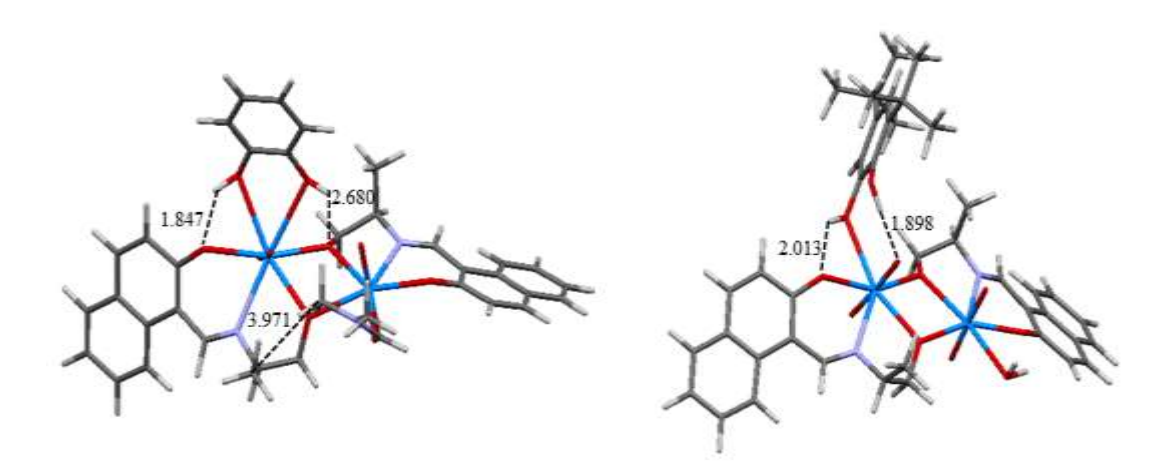


Figure 21: (Left) **B1**(η^2 -syn) complex in presence of modified 3,5-DTBC and (Right) **B2** (η^1 -anti) complex in presence of water as solvent.

Figure 22 shows the energy diagram of different transition states involved in the catalytic conversion of 3,5–DTBC to 3,5–DTBQ in presence of complex **3** as catalyst. The formation of **B** occurs *via* two transition states (TS1 and TS2) where *tert*-butyl groups between 3,5–DTBC and the uranyl catalyst move to distance below 4Å leading to favorable dispersion interaction. Further there is a loss of proton from –OH group of 3,5–DTBC which is closer to the catalyst leading to the formation of three transition states (TS3, TS4 and TS5) where the hydrogen bond of other –OH group of 3,5-DTBC shifts from axial oxo group of uranyl moiety to phenoxy oxygen of ligand. The loss of second proton from 3,5–DTBC

occurs via the formation of a radical in its triplet state as shown in TS6. The formation of the radical intermediate is also confirmed by the observation of an EPR signal at g = 1.99. The relative energy for the formation of singlet state is higher ($\Delta E = 31.3 \text{ eV}$) than TS6 state ($\Delta E = 29.9 \text{ eV}$) and has no imaginary frequency that further suggests that catalytic reaction proceeds through the formation of triplet transition state. The spin density plot for TS6 complex shows that atomic spin density is localized on the aromatic rings of 3,5-DTBC and methylene groups of one of the ligands of uranium complex as shown in Figure 23.

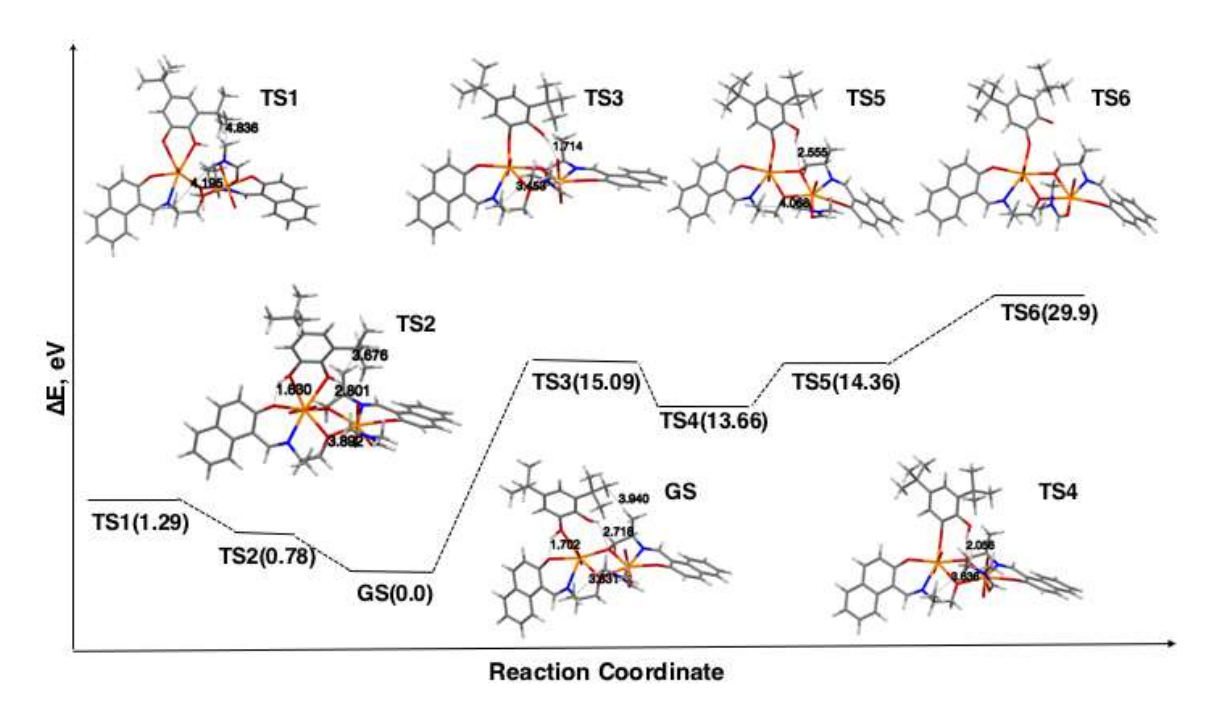


Figure 22: Relative energy diagram for different transition states involved in the catalytic oxidation of 3,5-DTBC to quinone *via* **B** as catalyst.

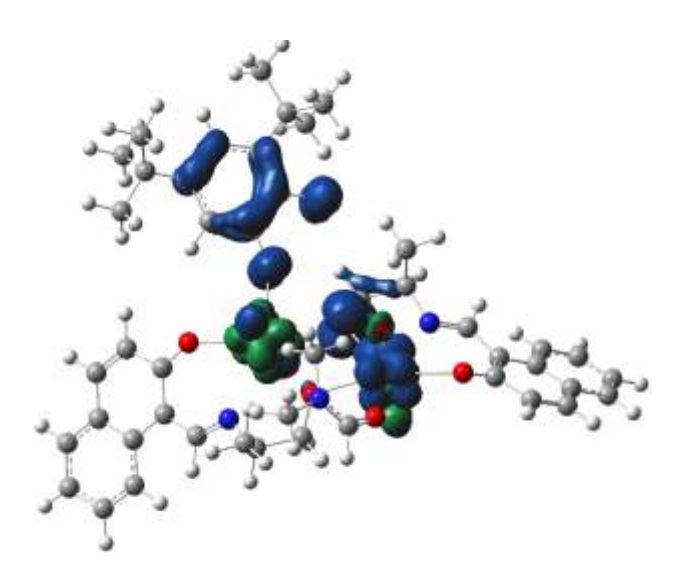


Figure 23: Spin density plot for B

5.4. Conclusions

Herein, we report the syntheses and characterization of two pairs of enantiomers of molecular formulas $[(UO_2)_2(R/S-L^1)_2(H_2O)_2]\cdot 2CH_3CN$ (1·2MeCN and 2.2MeCN) and $[(UO_2)_2(R/S-L^2)_2(Me_2NCHO)_2]$ (3 and 4). X-ray crystallographic analysis of each of the four complexes shows an edge-shared pentagonalbipyramidal structure. Complexes 1·MeCN and 2·MeCN form one-dimensional linear supramolecular structures via classical hydrogen bonds in their corresponding crystal lattices. The IR and NMR spectroscopic data compliment the molecular structures of all the complexes. The electronic spectra of $[(UO_2)_2(R/S-L^1)_2(H_2O)_2]\cdot 2MeCN$ (1·2MeCN and 2·2MeCN) reveal three major transitions. Whereas the spectral profiles of $[(UO_2)_2(R/S-L^2)_2(Me_2NCHO)_2]$ (3) and 4), display four major transitions. In both pair of enantiomers, the highest energy band is attributed to a ligand centered transition and the preceding lower energy transitions are assigned to ligand to metal charge transfer transitions. Investigation of the catecholase activity of all four complexes brings forward some very interesting facts. Complexes 3 and 4 show efficient catecholase activity with TOF 3686 and 3774 h⁻¹, respectively in Me₂NCHO solution. On the other hand, under the same experimental conditions complexes 1 and 2 are completely inert towards catecholase activity. Low temperature EPR analysis of the substrate-catalyst mixture (1:100) confirms that the catalytic reaction follows a radical pathway for oxidation of 3,5-DTBC to 3,5-DTBQ. Computational elucidation reveals that the catecholase like activities of these complexes depend on the type of coordinated solvent molecule present in them. The catecholase activity is favored when the conformation of the substrate is η^2 -syn over η^1 -anti in its adduct with the catalyst. In the cases of in 3 and 4, the dispersion interactions between the methyl groups of the coordinated Me₂NCHO with that of 3,5-DTBC as well as the methyl group of the coordinated ligands $(R/S-L^2)^{2-}$ play a key role in the η^2 -syn binding mode of the substrate to the catalyst. In contrast, in absence of such interactions the n^{1} -anti binding mode of the substrate to the catalyst is preferred for H₂O coordinated complexes 1 and 2 and hence they become inactive towards catechol oxidation. To the best of our knowledge, till date there is no report of uranyl(VI) complexes to mimic catecholase activity. The turnover number (TOF) and the rate constants (V_{max}) obtained for the catalytic cycles are quite notable as well as comparable or better than the already reported transition metal catalysts.

5.5. References

- (a) S. Itoh, S. Fukuzumi, *Acc. Chem. Res.* 2007, 40, 592. (b) M. Rolff, J. Schottenheim, H. Decker, F. Tuczek, *Chem. Soc. Rev.* 2011, 40, 4077.
 (c) S. Burton, *Catal. Today* 1994, 22, 459. (d) C. Gerdemann, C. Eicken, B. Krebs, *Acc. Chem. Res.* 2002, 35, 183. (e) C. Eicken, B. Krebs, J. C. Sacchettini, *Curr. Opin. Struct. Biol.* 1999, 9, 677.
- (a) S. K. Dey, A. Mukherjee, *Coord. Chem. Rev.* 2016, 310, 80. (b) L. I. Simándi, T. M. Simándi, Z. May, G. Besenyei, *Coord. Chem. Rev.* 2003, 245, 85.
- (a) K. Selmeczi, M. Réglier, M. Giorgi, G. Speier, *Coord. Chem. Rev.* 2003, 245, 191. (b) R. Silavia, A. Divsalara, A. A. Saboury, *J. Biomol. Struc. Dynamics.* 2012, 30, 752. (c) I. A. Koval, C. Gamez, P. G. Belle, K. Reedijk, *Chem. Soc. Rev.* 2006, 35, 814.
- (a) S. K. Dey, A. Mukherjee, New J. Chem. 2014, 38, 4985. (b) A. Panja, N. C. Jana, A. Bauza´, S. Adak, T. M. Mwania, D. M. Eichhorn, A. Frontera, ChemistrySelect 2017, 2, 2094. (c) Y. Hitomi, A. Ando, H. Matsui, T. Ito, T. Tanaka, S. Ogo, T. Funabiki, Inorg. Chem. 2005, 44, 3473. (d) M. U. Triller, D. Pursche, W.-Y. Hsieh, V. L. Pecoraro, A. Rompel, B. Krebs, Inorg. Chem. 2003, 42, 6274. (e) M. Ruf, B. C. Noll, M. D. Groner, G. T. Yee, C. G. Pierpont, Inorg. Chem. 1997, 36, 4860.
- (a) D. Bansal, R. Gupta, *Dalton Trans.* 2017, 46, 4617. (b) S. Mandal, J. Mukherjee, F. Lloret, R. Mukherjee, *Inorg. Chem.* 2012, 51, 13148. (c)
 A. Hazari, L. K. Das, R. M. Kadam, A. Bauzá, A. Frontera, A. Ghosh, *Dalton Trans.* 2015, 44, 3862. (d) A. Jana, N. Aliaga-Alcalde, E. Ruiz, S. Mohanta, *Inorg. Chem.* 2013, 52, 7732.
- (a) S. Dasgupta, J. Adhikary, S. Giri, A. Bauza, A. Frontera, D. Das, *Dalton Trans.*, 2017, 46, 5888.
 (b) N. Nanjundan, R. Narayanasamy, S. Geib, K. Velmurugan, R. Nandhakumar, M. D. Balakumaran, P. T. Kalaichelvan, *Polyhedron* 2016, 110, 203.
 (c) M. Das, R. Nasani, M. Saha, S. M. Mobin, S. Mukhopadhyay, *Dalton Trans.* 2015, 44, 2299.
 (d) A. Guha, T. Chattopadhyay, N. D. Paul, M. Mukherjee, S. Goswami, T. K. Mondal, E. Zangrando, D. Das, *Inorg. Chem.* 2012, 51, 8750.

- 7. (a) R. G. Denning, *Struct. Bonding* **1992**, *79*, 215. (*b*) R. G. Denning, *J. Phys. Chem. A*, **2007**, *111*, 4125.
- (a) H. D. Burrows, T. J. Kemp, Chem. Soc. Rev. 1974, 3, 139. (b) Z. R. Ismagilov, S. V. Lazareva, Cat. Rev. Sci. Eng. 2013, 55, 135. (c) K. –X. Wang, J. –S. Chen, Acc. Chem. Res. 2011, 44, 531. (d) D. P. Halter, F. W. Heinemann, J. Bachmann, K. Meyer, Nature 2016, 530, 317. (e) S. Ghosh, A. K. Srivastava, R. Govu, U. Pal, S. Pal, Inorg. Chem. 2019, 58, 14410. (f) S. Ghosh, A. K. Srivastava, S. Pal, New J. Chem. 2019, 43, 970.
- (a) J. A. Bertrand, J. A. Kelley, J. L. Breece, *Inorg. Chim. Acta* 1970, 4, 247.
 (b) A. Syamal, D. Kumar, *J. Less-Common Met.* 1980, 71, 113.
 (c) V. Barba, R. Santillan, N. Farfán, *J. Braz. Chem. Soc.* 2005, 16, 449.
- 10. APEX3: *Program for Data Collection on Area Detectors*, Bruker AXS Inc., Madison, Wisconsin, USA, **2016**.
- 11. G. M. Sheldrick, Acta Crystallogr. Sect. A 2008, 64, 112.
- 12. L. J. Farrugia, J. Appl. Crystallogr. 2012, 45, 849.
- F. Macrae, I. J. Bruno, J. A. Chisholm, P. R. Edgington, P. M. Cabe, E. Pidcock, L. Rodriguez-Monge, R. Taylor, J. Van de Streek, P. A. Wood *J. Appl. Crystallogr.* 2008, 41, 466.
- E. Monzani, L. Quinti, A. Perotti, L. Casella, M. Gullotti, L. Randaccio,
 S. Geremia, G. Nardin, P. Faleschini, G. Tabbi, *Inorg. Chem.* 1998, 37,
 553.
- (a) D. Feller, J. Comp. Chem. 1996, 17, 1571. (b) Gaussian 09, Revision E.01, M. J. Frisch, G. W. Trucks, H. B. Schlegel, G. E. Scuseria, M. A. Robb, J. R. Cheeseman, G. Scalmani, V. Barone, B. Mennucci, G. A. Petersson, H. Nakatsuji, M. Caricato, X. Li, H. P. Hratchian, A. F. Izmaylov, J. Bloino, G. Zheng, J. L. Sonnenberg, M. Hada, M. Ehara, K. Toyota, R. Fukuda, J. Hasegawa, M. Ishida, T. Nakajima, Y. Honda, O. Kitao, H. Nakai, T. Vreven, J. A. Montgomery, Jr., J. E. Peralta, F. Ogliaro, M. Bearpark, J. J. Heyd, E. Brothers, K. N. Kudin, V. N. Staroverov, R. Kobayashi, J. Normand, K. Raghavachari,

- A. Rendell, J. C. Burant, S. S. Iyengar, J. Tomasi, M. Cossi, N. Rega, J. M. Millam, M. Klene, J. E. Knox, J. B. Cross, V. Bakken, C. Adamo, J. Jaramillo, R. Gomperts, R. E. Stratmann, O. Yazyev, A. J. Austin, R. Cammi, C. Pomelli, J. W. Ochterski, R. L. Martin, K. Morokuma, V. G. Zakrzewski, G. A. Voth, P. Salvador, J. J. Dannenberg, S. Dapprich, A. D. Daniels, Ö. Farkas, J. B. Foresman, J. V. Ortiz, J. Cioslowski, D. J. Fox, *Gaussian, Inc.*, *Wallingford CT*, **2009**.
- (a) B. Masci, P. Thuéry, *Polyhedron* **2005**, 24, 229. (d) K. Lyczko, L. Steczek, *J. Struct. Chem.* **2017**, 58, 102. (b) C. J. Burns, A. P. Sattelberger, *Inorg. Chem.* **1988**, 27, 3692.
- (a) S. Ghosh, S. K. Kurapati, A. Ghosh, A. K. Srivastava, S. Pal, *ChemistrySelect* **2018**, *3*,4865. (b) A. Sarkar, S. Pal, *Polyhedron* **2006**, 25, 1689; (c) A. Sarkar, S. Pal, *Polyhedron* **2007**, 26, 1205. (d) K. Nagaraju, R. Raveendran, S. N. Pal, S. Pal, *Polyhedron* **2012**, *33*, 52.
- (a) A. K. Sah, C. P. Rao, P. K. Saarenketo, E. K. Wegelius, E. Kolehmainen, K. Rissanen, Eur. J. Inorg. Chem. 2001, 2773. (b) C. C. Gatto, E. S. Lang, A. Kupfer, A. Hagenbach, U. Abram, Z. Anorg. Allg. Chem. 2004, 630, 1286. (c) P. L. Arnold, A. J. Blake, C. Wilson, J. B. Love, Inorg. Chem. 2004, 43, 8206. (d) M. S. Bharara, K. Strawbridge, J. Z. Vilsek, T. H. Bray, A. E. V. Gorden, Inorg. Chem. 2007, 46, 8309. (e) M. Azam, S. I. Al-Resayes, G. Velmurugan, P. Venuvanalingam, J. Wagler, E. Kroke, Dalton Trans. 2015, 44, 568. (f) C. Camp, L. Chatelain, V. Mougél, J. Pécaut, M. Mazzanti, Inorg. Chem. 2015, 54, 5774. (g) Y. Zhang, D. J. Fanna, N. D. Shepherd, I. Karatchevtseva, K. Lu, L. Kong, J. R. Price, RSC Adv. 2016, 6, 75045.
- 19. Z. Asadi, M. Asadi, A. Zeinali, M. Ranjkeshshorkaei, K. Fejfarova, V. Eigner, M. Dusek, A. Dehnokhalaji, *J. Chem. Sci.* **2014**, *126*, 1673.
- (a) J. Adhikary, I. Majumdar, P. Kundu, H. Kornweitz, H. Kara, D. Das, ChemistrySelect 2018, 3, 1445. (b) J. Ackermann, F. Meyer, E. Kaifer, H. Pritzkow, Chem. Eur. J. 2002, 8, 247. (c) S. Torelli, C. Belle, S. Hamman, J. Pierre, Inorg. Chem. 2002, 41, 3983. (d) A. Granata, E. Monzani, L. Casella, J. Biol. Inorg. Chem. 2004, 9, 903. (e) A. Szorcsik,

F. Matyuska, A. Bnyei, N. V. Nagy, R. K. Szil gyie, T. Gajda, *Dalton Trans.* **2016**, *45*, 14998.

Appendix

Tables for atomic coordinates (x 10^4) and equivalent isotropic displacement parameters (Å 2 x 10^3). U(eq) is defined as the one third of the trace of the orthogonalized U^{ij} tensor.

Table A.1. $[(UO_2)_2(\mu\text{-OAc})_2(L^1)_2]$ (1) (Chapter 1)

Atom	x	y	Z	U(eq)
U(1)	336(1)	3095(1)	4517(1)	29(1)
O(1)	749(13)	2906(11)	3537(6)	55(4)
O(2)	-1090(11)	2551(10)	4384(7)	45(3)
O(3)	1766(11)	3676(9)	4655(6)	41(3)
O(4)	-179(11)	3905(10)	5431(6)	42(3)
O(5)	497(14)	5342(9)	5885(7)	57(4)
N(1)	399(12)	1630(11)	5328(7)	34(3)
N(2)	1800(14)	738(11)	4758(8)	45(4)
N(3)	1687(13)	1436(11)	4297(7)	36(3)
C(1)	-367(18)	1649(14)	5816(11)	49(5)
C(2)	-362(19)	909(15)	6280(10)	53(5)
C(3)	435(19)	73(15)	6234(10)	52(5)
C(4)	1153(17)	2(13)	5733(9)	41(4)
C(5)	1130(17)	800(12)	5276(8)	39(4)
C(6)	2321(16)	1257(14)	3808(10)	43(4)
C(7)	2375(18)	1887(14)	3259(9)	44(4)
C(8)	1613(17)	2742(15)	3157(8)	44(4)
C(9)	1780(20)	3365(18)	2619(9)	62(6)
C(10)	2700(30)	3125(19)	2208(13)	80(9)
C(11)	3440(30)	2300(20)	2316(11)	78(9)
C(12)	3284(19)	1699(17)	2815(10)	55(5)
C(13)	430(14)	4370(12)	5851(8)	34(4)
C(14)	1170(20)	3749(16)	6308(10)	55(5)

Table A.2. $[(UO_2)_2(\mu\text{-OAc})_2(L^2)_2]$ (2·4MeOH) (Chapter 1)

Atom	х	у	Z	U(eq)
 U(1)	3712(1)	730(1)	3069(1)	21(1)
O(1)	1411(15)	-700(10)	1827(8)	34(3)
O(2)	2126(17)	1390(14)	3705(10)	36(3)
O(3)	5334(15)	97(13)	2424(11)	37(3)
O(4)	5820(18)	1678(12)	4784(10)	42(3)
O(5)	6884(18)	756(13)	5953(10)	46(4)
N(1)	5214(17)	2964(12)	3005(11)	21(3)
N(2)	4310(20)	2355(13)	1033(11)	34(4)
N(3)	3376(17)	1184(12)	1074(10)	21(3)
C(1)	6010(30)	3871(16)	3964(15)	41(5)
C(2)	6670(30)	5097(17)	3942(16)	36(4)
C(3)	6600(30)	5371(19)	2945(18)	55(7)
C(4)	5910(30)	4421(18)	1938(15)	36(5)
C(5)	5150(20)	3228(14)	2010(13)	20(4)
C(6)	2700(20)	420(16)	99(12)	24(4)
C(7)	1640(20)	-852(15)	-123(12)	20(3)
C(8)	1120(30)	-1602(18)	-1251(14)	34(4)
C(9)	100(20)	-2782(17)	-1570(14)	33(4)
C(10)	-480(30)	-3333(19)	-689(16)	39(5)
C(11)	-60(20)	-2650(15)	421(14)	23(4)
C(12)	980(20)	-1430(16)	731(12)	23(4)
C(13)	-350(30)	-3550(20)	-2846(18)	68(8)
C(14)	6960(20)	1650(15)	5528(13)	21(3)
C(15)	8620(30)	2810(20)	5970(20)	77(8)
O(6)	4353(18)	3060(12)	-994(9)	50(4)
C(16)	5910(40)	3060(30)	-1390(30)	87(9)
O(7)	1726(17)	1546(15)	-2617(10)	59(4)
C(17)	1900(40)	970(20)	-3694(16)	71(8)

Table A.3. $[(UO_2)_2(\mu\text{-OAc})_2(L^3)_2]$ (3) (Chapter 1)

Atom	X	у	Z	U(eq)
U(1)	2110(1)	7850(1)	4567(1)	32(1)
O(1)	2673(7)	6598(4)	6239(4)	40(1)
O(2)	4515(7)	8166(5)	4265(4)	43(1)
O(3)	-311(6)	7581(4)	4842(4)	35(1)
O(4)	1349(8)	9683(5)	3281(5)	54(1)
O(5)	-1164(7)	10839(4)	4114(4)	40(1)
O(6)	1310(7)	2169(5)	9144(5)	50(1)
N(1)	3102(7)	7496(5)	2385(5)	35(1)
N(2)	2908(7)	5484(5)	3145(5)	35(1)
N(3)	2671(7)	5649(5)	4307(5)	32(1)
C(1)	3544(9)	8382(7)	1419(6)	38(2)
C(2)	4008(9)	8219(7)	241(6)	42(2)
C(3)	3980(10)	7099(7)	53(7)	44(2)
C(4)	3582(9)	6185(7)	1023(6)	40(2)
C(5)	3221(8)	6396(6)	2197(6)	33(2)
C(6)	2515(8)	4674(6)	5122(6)	31(1)
C(7)	2203(8)	4571(6)	6406(6)	32(1)
C(8)	2236(9)	5522(7)	6928(7)	38(2)
C(9)	1931(10)	5294(7)	8195(6)	41(2)
C(10)	1622(9)	4190(7)	8901(6)	42(2)
C(11)	1614(9)	3253(7)	8375(6)	39(2)
C(12)	1892(9)	3446(6)	7143(6)	38(2)
C(13)	176(13)	10629(7)	3229(7)	52(2)
C(14)	350(20)	11527(10)	2056(9)	114(5)
C(15)	1532(11)	1183(7)	8616(8)	54(2)

Table A.4. $[(UO_2)_2(\mu\text{-OH})_2(L^1)_2]$ (1·H₂O·2Me₂NCHO) (Chapter 3)

Atom	X	у	Z	U(eq)
U(1)	7397(1)	3945(1)	6567(1)	27(1)
U(2)	7683(1)	1898(1)	8388(1)	28(1)
Cl(1)	6677(6)	729(2)	5277(2)	93(1)
Cl(2)	7558(5)	5269(2)	9553(2)	72(1)
O(1)	7154(10)	5435(4)	6603(3)	49(2)
O(2)	4843(7)	3907(4)	6542(3)	44(1)
O(3)	9907(8)	4009(4)	6491(3)	42(1)
O(4)	7558(8)	3541(3)	7837(2)	34(1)
O(5)	7616(8)	2315(3)	7092(3)	36(1)
O(6)	7717(12)	403(4)	8393(3)	64(2)
O(7)	5231(9)	1898(4)	8435(3)	50(2)
O(8)	10210(8)	1898(4)	8427(3)	49(1)
N(1)	7480(8)	5107(4)	5220(3)	31(1)
N(2)	7348(9)	4719(4)	4628(3)	38(2)
N(3)	7235(9)	3248(4)	5450(3)	36(1)
N(4)	7037(11)	2296(5)	5592(4)	45(2)
N(5)	7680(9)	816(4)	9756(3)	32(1)
N(6)	7803(10)	1252(4)	10318(3)	38(2)
N(7)	7724(9)	2700(4)	9446(3)	32(1)
N(8)	7665(10)	3656(4)	9278(3)	39(2)
C(1)	7576(11)	6304(5)	6275(4)	36(2)
C(2)	7691(13)	6971(6)	6676(5)	49(2)
C(3)	8086(16)	7888(7)	6333(6)	65(3)
C(4)	8415(16)	8194(7)	5581(6)	66(3)
C(5)	8289(13)	7563(6)	5168(5)	55(2)
C(6)	7898(11)	6610(5)	5497(4)	36(2)
C(7)	7766(10)	6013(5)	5006(4)	37(2)
C(8)	7201(10)	3791(5)	4753(4)	33(2)
C(9)	7013(13)	3395(7)	4146(5)	50(2)
C(10)	6834(14)	2457(7)	4294(5)	58(2)
C(11)	6854(14)	1951(6)	5043(5)	53(2)
C(12)	7476(13)	-479(5)	8768(4)	41(2)
C(13)	7411(11)	-738(5)	9544(4)	34(2)
C(14)	7198(12)	-1694(5)	9932(5)	47(2)

C(15)	7028(15)	-2362(6)	9560(5)	59(3)
C(16)	7067(16)	-2100(6)	8793(6)	62(3)
C(17)	7293(16)	-1169(6)	8397(5)	60(3)
C(18)	7468(12)	-98(5)	9999(4)	39(2)
C(19)	7802(11)	2190(5)	10157(4)	34(2)
C(20)	7861(13)	2615(6)	10747(4)	47(2)
C(21)	7788(14)	3570(6)	10570(4)	48(2)
C(22)	7700(13)	4051(5)	9813(4)	42(2)
O(9)	7728(10)	507(4)	11837(3)	60(2)
N(9)	7795(12)	-807(5)	12821(4)	52(2)
C(23)	7441(12)	-333(6)	12131(4)	44(2)
C(24)	7346(14)	-1808(6)	13106(5)	57(2)
C(25)	8830(30)	-379(10)	13305(7)	121(6)
O(10)	5742(13)	3696(6)	12126(6)	102(3)
N(10)	7401(11)	5037(5)	11965(4)	51(2)
C(26)	5828(16)	4571(8)	11971(7)	70(3)
C(27)	9149(16)	4531(8)	12168(7)	77(3)
C(28)	7386(17)	6057(7)	11777(7)	78(3)
O(11)	6870(30)	1854(10)	12751(7)	231(9)

Table A.5. $[(UO_2)_2(\mu\text{-OH})_2(L^2)_2]$ (2·1.5H₂O) (Chapter 3)

Atom	X	y	z	U(eq)
U(1)	6592(1)	1783(1)	257(1)	32(1)
Cl(1)	10026(3)	777(3)	3700(3)	125(2)
O(1)	5120(5)	1573(4)	-864(4)	44(2)
O(2)	6239(5)	2718(4)	763(5)	44(2)
O(3)	6927(5)	804(4)	-205(5)	43(2)
O(4)	6843(4)	2679(4)	-864(4)	38(1)
O(5)	1419(6)	1772(6)	-1218(7)	76(2)
N(1)	5568(5)	883(5)	964(5)	35(2)
N(2)	6041(6)	396(6)	1812(6)	50(2)
N(3)	7465(5)	953(5)	1885(5)	38(2)
N(4)	8389(6)	1029(6)	2312(6)	51(2)

O(7)	0	3030(20)	-2500	129(13)
O(6)	5000	780(6)	-2500	44(2)
C(12)	1137(12)	1429(12)	-575(15)	117(6)
C(11)	8833(7)	581(7)	3115(8)	58(3)
C(10)	8393(8)	-11(7)	3518(7)	58(3)
C(9)	7460(8)	-78(7)	3099(7)	50(3)
C(8)	6984(7)	446(6)	2243(6)	42(2)
C(7)	4665(7)	867(6)	677(6)	39(2)
C(6)	3998(7)	1292(6)	-170(7)	42(2)
C(5)	3051(7)	1328(7)	-271(8)	51(3)
C(4)	2360(7)	1702(7)	-1065(8)	50(3)
C(3)	2591(8)	2033(7)	-1803(8)	55(3)
C(2)	3499(8)	2007(6)	-1703(8)	51(3)
C(1)	4224(6)	1647(6)	-903(6)	38(2)

Table A.6. $[(UO_2)_2(\mu-L)_2]$ (1) (Chapter 4)

Atom	X	у	Z	U(eq)
U(1)	4258(1)	6571(1)	4410(1)	30(1)
O(1)	6453(6)	5982(6)	5140(2)	37(1)
O(2)	1825(7)	6105(7)	3847(2)	51(1)
O(3)	5502(7)	5361(7)	4008(2)	50(1)
O(4)	3092(6)	7960(6)	4800(2)	43(1)
O(5)	-2274(8)	3082(8)	3210(3)	74(2)
N(1)	6867(7)	8745(7)	4512(2)	42(1)
N(2)	3857(7)	9235(7)	3775(2)	41(1)
C(1)	8126(10)	6807(11)	5205(3)	57(2)
C(2)	8422(9)	7778(11)	4729(3)	48(2)
C(3)	6972(10)	9791(11)	4052(3)	55(2)
C(4)	5272(10)	10592(11)	3848(4)	61(2)
C(5)	2544(9)	9631(9)	3441(3)	41(2)
C(6)	923(8)	8587(9)	3295(2)	36(2)
C(7)	-370(9)	9340(9)	2930(2)	38(2)
C(8)	-1931(9)	8489(10)	2744(3)	40(2)

C(9)	-2122(9)	6761(10)	2917(3)	41(2)
C(10)	-874(9)	5905(9)	3284(3)	36(2)
C(11)	658(8)	6856(9)	3490(2)	34(2)
C(12)	-3331(11)	9382(12)	2366(3)	64(2)
C(13)	-1145(10)	4040(10)	3424(3)	49(2)

Table A.7. $[(UO_2)_2(R-L^1)_2(H_2O)_2]\cdot 2MeCN$ (1·2MeCN) (Chapter 5)

Atom	X	y	Z	U(eq)
U(1)	-1944(1)	5219(1)	5413(1)	35(1)
U(2)	1990(1)	4684(1)	4814(1)	36(1)
O(1)	-4132(8)	5761(4)	5700(4)	43(2)
O(2)	469(8)	5658(4)	5221(5)	50(2)
O(3)	4108(9)	4105(4)	4476(5)	47(2)
O(4)	-363(8)	4245(4)	5102(5)	46(2)
O(5)	-1604(8)	5029(4)	6289(4)	49(2)
O(6)	-2422(9)	5387(5)	4543(5)	53(2)
O(7)	2574(9)	4487(4)	5662(4)	49(2)
O(8)	1492(8)	4879(5)	3973(5)	58(2)
O(9)	-3691(8)	4149(5)	5396(5)	41(2)
O(10)	3746(8)	5733(5)	4781(5)	43(2)
N(1)	-1578(9)	6599(5)	5752(6)	46(3)
N(2)	1500(9)	3300(5)	4501(5)	39(2)
C(1)	-4520(13)	6149(6)	6269(6)	41(3)
C(2)	-5799(15)	5974(8)	6596(7)	58(4)
C(3)	-6247(18)	6396(11)	7147(9)	84(5)
C(4)	-5446(16)	7007(11)	7367(8)	76(5)
C(5)	-4202(15)	7192(8)	7040(7)	57(4)
C(6)	-3680(12)	6758(7)	6490(6)	39(3)
C(7)	-2319(13)	6993(7)	6163(7)	46(3)
C(8)	-202(16)	6923(7)	5474(10)	74(5)
C(9)	931(16)	6335(8)	5590(11)	88(6)
C(10)	-430(20)	7158(10)	4745(12)	135(10)
C(11)	4418(12)	3721(6)	3905(6)	39(3)
C(12)	5636(14)	3914(8)	3524(8)	58(4)

C(13)	5999(18)	3511(9)	2955(9)	73(5)
C(14)	5168(17)	2881(9)	2766(8)	65(4)
C(15)	3966(15)	2701(7)	3148(7)	51(3)
C(16)	3541(11)	3122(6)	3710(6)	38(3)
C(17)	2218(12)	2903(6)	4077(6)	41(3)
C(18)	108(13)	2980(6)	4785(7)	46(3)
C(19)	-337(13)	3495(6)	5364(7)	48(3)
C(20)	-1057(15)	2927(10)	4229(9)	81(5)
N(3)	-4426(18)	3883(8)	6825(8)	88(5)
C(21)	-4110(20)	4178(12)	7302(10)	80(5)
C(22)	-3770(30)	4612(18)	7915(12)	179(14)
N(4)	4350(20)	6138(9)	3382(8)	101(6)
C(23)	4070(20)	5856(10)	2900(10)	79(5)
C(24)	3690(30)	5519(18)	2261(11)	161(12)

Table A.8. $[(UO_2)_2(S-L^1)_2(H_2O)_2]\cdot 2MeCN$ (2·2MeCN) (Chapter 5)

Atom	X	у	Z	U(eq)
U(1)	3057(1)	10218(1)	-412(1)	29(1)
U(2)	6990(1)	9684(1)	189(1)	31(1)
O(1)	873(4)	10758(2)	-698(2)	37(1)
O(2)	5470(4)	10659(2)	-214(2)	47(1)
O(3)	9122(4)	9113(2)	521(2)	41(1)
O(4)	4636(4)	9244(2)	-97(2)	40(1)
O(5)	2585(4)	10391(2)	455(2)	43(1)
O(6)	3402(3)	10031(2)	-1285(2)	42(1)
O(7)	6497(3)	9886(2)	1046(2)	48(1)
O(8)	7562(4)	9484(2)	-656(2)	42(1)
O(9)	1313(4)	9151(2)	-396(2)	37(1)
O(10)	8733(4)	10736(2)	221(2)	39(1)
N(1)	3424(4)	11594(3)	-740(3)	40(1)
N(2)	6506(4)	8301(2)	506(2)	31(1)
C(1)	494(5)	11146(3)	-1262(3)	35(1)
C(2)	-792(7)	10968(4)	-1606(3)	56(2)
C(3)	-1227(8)	11391(5)	-2152(4)	76(2)

C(4)	-442(7)	12006(5)	-2372(4)	69(2)
C(5)	824(7)	12184(4)	-2042(3)	54(2)
C(6)	1318(6)	11755(3)	-1489(3)	35(1)
C(7)	2690(6)	11985(3)	-1156(3)	41(2)
C(8)	4808(7)	11922(3)	-483(5)	67(2)
C(9)	5932(7)	11324(4)	-579(5)	84(3)
C(10)	4563(11)	12163(5)	242(6)	149(6)
C(11)	9419(5)	8729(3)	1092(3)	35(1)
C(12)	10640(6)	8908(4)	1481(4)	53(2)
C(13)	11002(8)	8491(4)	2040(4)	68(2)
C(14)	10179(8)	7883(5)	2242(3)	60(2)
C(15)	8960(7)	7692(4)	1856(3)	46(2)
C(16)	8547(5)	8125(3)	1293(3)	33(1)
C(17)	7210(5)	7903(3)	928(3)	33(1)
C(18)	5104(6)	7972(3)	223(3)	41(1)
C(19)	4651(6)	8494(3)	-354(3)	44(2)
C(20)	3959(6)	7921(5)	771(4)	75(2)
N(3)	574(8)	8875(4)	-1825(4)	83(2)
C(21)	887(9)	9168(5)	-2302(4)	71(2)
C(22)	1257(11)	9574(8)	-2924(5)	170(7)
N(4)	9373(9)	11133(4)	1620(4)	98(3)
C(23)	9075(9)	10851(5)	2106(4)	73(2)
C(24)	8697(12)	10495(7)	2739(5)	142(5)

Table A.9. $[(UO_2)_2(R-L^2)_2(Me_2NCHO)_2]$ (3) (Chapter 5)

Atom	X	у	Z	U(eq)
U(1)	8837(1)	3868(1)	2905(1)	28(1)
U(2)	6004(1)	2316(1)	2138(1)	27(1)
O(1)	10573(3)	4418(5)	3527(3)	42(1)
O(2)	7708(3)	2067(5)	3145(2)	32(1)
O(3)	4272(3)	1718(5)	1530(3)	41(1)
O(4)	7099(3)	4222(4)	1938(3)	34(1)
O(5)	9108(3)	2838(4)	2062(3)	38(1)
O(6)	8612(3)	4892(5)	3773(3)	44(1)

O(7)	6308(3)	1242(5)	1325(3)	40(1)
O(8)	5669(3)	3347(4)	2947(3)	38(1)
O(9)	8984(3)	6192(5)	2218(3)	50(1)
O(10)	5911(3)	-22(5)	2865(3)	46(1)
N(1)	9744(3)	1882(5)	4006(3)	32(1)
N(2)	5060(3)	4153(5)	956(3)	32(1)
N(3)	9563(5)	8419(6)	2016(4)	55(2)
N(4)	5301(4)	-2280(6)	2973(4)	47(2)
C(1)	11442(4)	3639(7)	3677(4)	36(2)
C(2)	12318(4)	4320(8)	3531(5)	48(2)
C(3)	13219(5)	3582(8)	3663(5)	53(2)
C(4)	13348(4)	2101(9)	3979(4)	39(2)
C(5)	14295(5)	1347(9)	4121(5)	49(2)
C(6)	14421(5)	-51(10)	4443(5)	60(2)
C(7)	13589(5)	-739(9)	4599(5)	62(2)
C(8)	12656(5)	-52(8)	4453(5)	53(2)
C(9)	12497(4)	1425(7)	4151(4)	36(2)
C(10)	11531(4)	2207(9)	4009(4)	36(2)
C(11)	10715(4)	1543(7)	4262(4)	38(2)
C(12)	9054(4)	980(7)	4364(4)	40(2)
C(13)	7985(4)	1702(6)	4072(3)	35(1)
C(14)	8997(5)	-570(7)	4031(5)	60(2)
C(15)	3410(4)	2487(8)	1381(4)	33(1)
C(16)	2551(5)	1852(7)	1570(5)	45(2)
C(17)	1651(5)	2582(8)	1434(5)	49(2)
C(18)	1498(4)	4048(8)	1086(4)	37(2)
C(19)	560(5)	4787(9)	949(5)	49(2)
C(20)	415(5)	6176(9)	596(5)	55(2)
C(21)	1230(5)	6838(9)	403(5)	60(2)
C(22)	2160(5)	6133(8)	538(5)	52(2)
C(23)	2336(4)	4701(7)	874(4)	34(2)
C(24)	3297(4)	3913(9)	1013(4)	35(1)
C(25)	4101(4)	4531(7)	713(4)	32(1)
C(26)	5753(4)	4934(7)	564(4)	36(2)
C(27)	6701(5)	5423(7)	1343(4)	46(2)
C(28)	6028(6)	3977(8)	-88(5)	64(2)
C(29)	9690(5)	7113(8)	2343(4)	46(2)

C(30)	8533(7)	8917(13)	1470(6)	95(3)
C(31)	10444(8)	9422(9)	2137(7)	98(3)
C(32)	5185(5)	-907(7)	2699(4)	42(2)
C(33)	6292(6)	-2852(11)	3518(6)	80(3)
C(34)	4395(7)	-3234(8)	2808(6)	84(3)

Table A.10. $[(UO_2)_2(S-L^2)_2(Me_2NCHO)_2]$ (4) (Chapter 5)

Atom	X	у	Z	U(eq)
U(1)	1163(1)	6132(1)	7095(1)	28(1)
U(2)	3995(1)	7684(1)	7863(1)	27(1)
O(1)	-572(4)	5573(7)	6475(4)	43(2)
O(2)	2291(4)	7940(7)	6857(4)	33(1)
O(3)	5729(4)	8280(7)	8473(4)	42(2)
O(4)	2897(4)	5771(6)	8060(4)	34(2)
O(5)	890(5)	7174(7)	7943(4)	43(2)
O(6)	1377(5)	5114(7)	6222(4)	44(2)
O(7)	3685(5)	8774(7)	8678(4)	45(2)
O(8)	4324(5)	6653(6)	7046(4)	38(2)
O(9)	1023(5)	3803(8)	7789(5)	51(2)
O(10)	4082(5)	10020(7)	7134(5)	47(2)
N(1)	253(5)	8111(8)	5988(4)	34(2)
N(2)	4936(5)	5853(8)	9042(5)	34(2)
N(3)	436(8)	1571(9)	7985(6)	58(3)
N(4)	4693(6)	12276(9)	7025(6)	49(2)
C(1)	-1431(6)	6367(11)	6318(6)	39(2)
C(2)	-2317(6)	5682(11)	6468(7)	49(3)
C(3)	-3219(7)	6423(12)	6340(7)	52(3)
C(4)	-3347(6)	7884(13)	6019(6)	39(2)
C(5)	-4291(7)	8675(13)	5886(7)	51(3)
C(6)	-4421(7)	10048(14)	5554(8)	61(3)
C(7)	-3592(7)	10742(13)	5396(7)	60(3)
C(8)	-2652(7)	10057(11)	5547(7)	48(3)
C(9)	-2496(6)	8575(11)	5846(6)	36(2)
C(10)	-1529(6)	7794(13)	5995(5)	36(2)

C(11)	-710(6)	8460(11)	5724(6)	37(2)
C(12)	946(6)	9031(11)	5633(6)	40(2)
C(13)	2014(6)	8296(10)	5930(5)	38(2)
C(14)	1008(8)	10583(11)	5968(8)	59(3)
C(15)	6574(5)	7535(11)	8621(5)	35(2)
C(16)	7453(6)	8152(11)	8439(7)	48(2)
C(17)	8354(6)	7416(12)	8574(7)	48(3)
C(18)	8498(6)	5957(13)	8916(5)	38(2)
C(19)	9438(7)	5221(13)	9057(7)	51(3)
C(20)	9588(7)	3835(13)	9402(7)	56(3)
C(21)	8777(7)	3164(13)	9599(8)	64(3)
C(22)	7850(7)	3873(13)	9465(8)	58(3)
C(23)	7661(6)	5295(10)	9120(6)	34(2)
C(24)	6701(6)	6089(14)	8976(5)	38(2)
C(25)	5891(6)	5467(9)	9287(6)	33(2)
C(26)	4247(6)	5070(10)	9440(6)	39(2)
C(27)	3298(6)	4587(10)	8654(6)	44(2)
C(28)	3965(9)	6021(13)	10092(7)	68(3)
C(29)	299(7)	2885(12)	7651(6)	46(2)
C(30)	1476(11)	1070(20)	8516(9)	100(5)
C(31)	-453(11)	586(14)	7855(11)	101(5)
C(32)	4816(7)	10904(11)	7304(6)	43(2)
C(33)	3707(9)	12838(16)	6477(8)	82(4)
C(34)	5605(10)	13223(13)	7179(9)	91(4)

List of Publications

Thesis Work:

1. Di- μ -acetato Diuranyl(VI) Complexes with N-(2-pyridyl)-N'-(5-R-salicylidene)hydrazines: Syntheses, Structures, Properties and Extraction Studies

Sabari Ghosh, Sathish Kumar Kurapati, Arpita Ghosh, Ankit Kumar Srivastava, Samudranil Pal*

ChemistrySelect **2018**, *3*, 1–9.

2. Dihydroxo-bridged diuranyl(VI) complexes with 2-((2-(6-chloropyridazin-3- yl)hydrazono)methyl)-4-R- phenols: Structural insight and visible light driven photocatalytic activities

Sabari Ghosh, Ankit Kumar Srivastava and Samudranil Pal*

New J. Chem. **2019**, 43, 970–978.

3. A Diuranyl(VI) Complex and Its Application in Electrocatalytic and Photocatalytic Hydrogen Evolution from Neutral Aqueous Medium **Sabari Ghosh**, Ankit Kumar Srivastava, Radha Govu, Ujjwal Pal* and Samudranil Pal* *Inorg. Chem.* **2019**, *58*, 14410–14419.

 Chiral Diuranyl(VI) Complexes and Their Catecholase Activities: Experimental and Computational Insight
 Sabari Ghosh, Manju Sharma* and Samudranil Pal*
 To be communicated.

Other Works:

- 1. Complexes of *cis*-dioxomolybdenum(VI) with a chiral tetradentate tripodal-like ligand system: Syntheses, structures and catalytic activities **Sabari Ghosh**, Sathish Kumar Kurapati, Samudranil Pal* *Polyhedron* **2017**, *125*, 26 33.
- 2. Ternary pentagonal-bipyramidal oxovanadium(V) complexes containing five- and six- membered chelate rings: Syntheses, structures and properties

Ankit Kumar Srivastava, **Sabari Ghosh**, Subhendu Jana, Samudranil Pal* *Inorganica Chimica Acta* **2018**, *483*, 329–336.

3. A one-dimensional polymeric mixed valent Mn(II)Mn(III) complex with a macrocyclic compartmental ligand: structure, properties and catecholase like activity

Ankit Kumar Srivastava, **Sabari Ghosh**, Samudranil Pal* Polyhedron **2019**, *172*, 112–119.

4. Coordination mode variation of oximate in complexes of VO(OMe)²⁺ and VO²⁺ with biacetylmonoxime salicyloylhydrazone: structural confirmation, properties and photocatalytic applications
Ankit Kumar Srivastava, **Sabari Ghosh**, Samudranil Pal* *Under Revision*

Diuranyl(VI) Complexes with Some Tri- and Tetradentate Ligands and Their Applications

by Sabari Ghosh

Submission date: 26-Nov-2019 10:43AM (UTC+0530)

Submission ID: 1221946391

File name: thesis_sabari_for_plagiarism.pdf (4.49M)

Word count: 28205

Character count: 133647

Diuranyl(VI) Complexes with Some Tri- and Tetradentate Ligands and Their Applications

ORIGINALITY REPORT

61%

13%

60%

13%

SIMILARITY INDEX

INTERNET SOURCES

PUBLICATIONS

STUDENT PAPERS

PRIMARY SOURCES

Sabari Ghosh, Ankit Kumar Srivastava, Radha Govu, Ujjwal Pal, Samudranil Pal. "A Diuranyl(VI) Complex and Its Application in Electrocatalytic and Photocatalytic Hydrogen Evolution from Neutral Aqueous Medium", Inorganic Chemistry, 2019

20%

Publication

Sabari Ghosh, Ankit Kumar Srivastava,
Samudranil Pal. "Dihydroxo-bridged diuranyl(VI)
complexes with 2-((2-(6-chloropyridazin-3yl)hydrazono)methyl)-4-R-phenols: Structural
insight and visible light driven photocatalytic
activities", New Journal of Chemistry, 2018
Publication

17%

Sabari Ghosh, Sathish Kumar Kurapati, Arpita Ghosh, Ankit Kumar Srivastava, Samudranil Pal. "Di- -acetato Diuranyl(VI) Complexes with - (2-pyridyl)- -(5-R-salicylidene)hydrazines: Syntheses, Structures, Properties and Extraction Studies ", ChemistrySelect, 2018

16%

- Sabari Ghosh, Ankit Kumar Srivastava, 2% 4 Samudranil Pal. " Dihydroxo-bridged diuranyl() complexes with 2-((2-(6-chloropyridazin-3yl)hydrazono)methyl)-4-R-phenols: structural insights and visible light driven photocatalytic activities ", New Journal of Chemistry, 2019 Publication baadalsg.inflibnet.ac.in 1% 5 Internet Source Sabari Ghosh, Sathish Kumar Kurapati, Samudranil Pal. "Complexes of cisdioxomolybdenum(VI) with a chiral tetradentate tripodal-like ligand system: Syntheses, structures and catalytic activities", Polyhedron, 2017 Publication M. Fleck. "Syntheses, structures, and <1% electrochemistry of a dinuclear compound and a mononuclear-mononuclear cocrystalline compound of uranyl(VI)", Crystal Research and Technology, 11/2008 Publication <1%
 - Ankit Kumar Srivastava, Sabari Ghosh, Subhendu Jana, Samudranil Pal. "Ternary pentagonal-bipyramidal oxovanadium(V) complexes containing five- and six-membered

chelate rings: Syntheses, structures and
properties", Inorganica Chimica Acta, 2018

Publication

9	Submitted to Indian Institute of Technology, Kharagpure Student Paper	<1%
10	Hazra, S "Synthesis, molecular and supramolecular structure, spectroscopy and electrochemistry of a dialkoxo-bridged diuranyl(VI) compound", Polyhedron, 20080407	<1%
11	Sathish Kumar Kurapati, Uppala Ugandhar, Swamy Maloth, Samudranil Pal. "Dioxomolybdenum(VI) complexes with 2-((2-(pyridin-2-yl)hydrazono)methyl)phenol and its derivatives", Polyhedron, 2012 Publication	<1%
12	Submitted to University of KwaZulu-Natal Student Paper	<1%
13	www.science.gov Internet Source	<1%
14	Balavardhana Rao, A.R., and Samudranil Pal. "Regioselective cyclometallation with some platinum group metal ions", Journal of Organometallic Chemistry, 2014. Publication	<1%

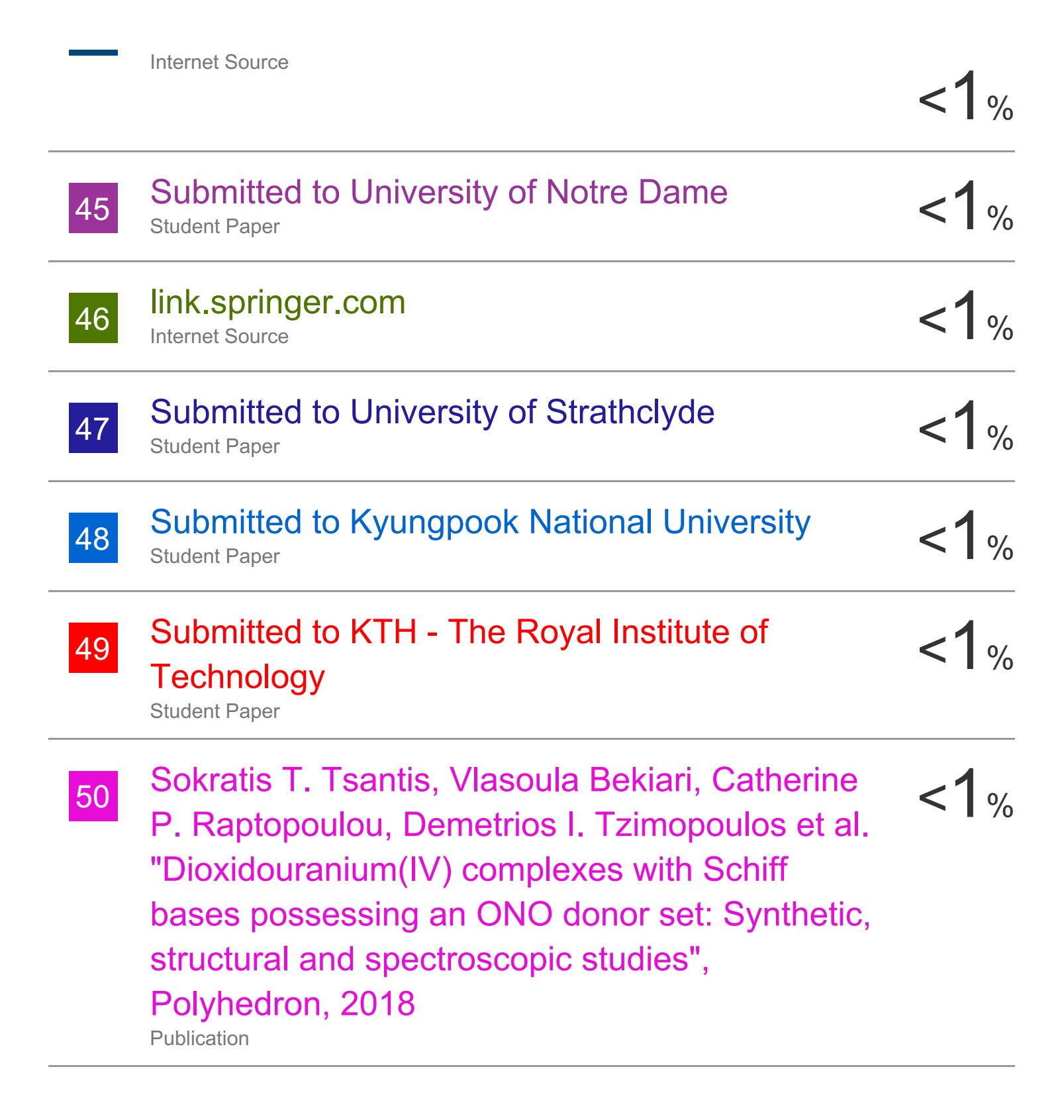
15	Submitted to Birla Institute of Technology Student Paper	<1%
16	Submitted to IIT Delhi Student Paper	<1%
17	Submitted to Queen Mary and Westfield College Student Paper	<1%
18	Submitted to University of Hong Kong Student Paper	<1%
19	tel.archives-ouvertes.fr Internet Source	<1%
20	Maloth, Swamy, Sathish Kumar Kurapati, and Samudranil Pal. "Synthesis, structure, and properties of a pentanuclear cobalt(III) coordination cluster", Journal of Coordination Chemistry, 2015. Publication	<1%
21	Kurapati, Sathish Kumar, and Samudranil Pal. "cis-{MoO2}2+ assisted Mannich-type addition of acetylacetonate methine to the azomethine of tridentate Schiff bases: racemic complexes with chiral transformed ligands", Dalton Transactions, 2014. Publication	<1%
22	edoc.ub.uni-muenchen.de Internet Source	<1%

23	Ankit Kumar Srivastava, Sabari Ghosh, Samudranil Pal. "A one-dimensional polymeric mixed-valent Mn(II)Mn(III) complex with a macrocyclic compartmental ligand: Structure, properties and catecholase like activity", Polyhedron, 2019 Publication	<1%
24	Rupesh Narayana Prabhu, G. Narendra Babu, Samudranil Pal. "Triphenylphosphinopalladium(II) complexes with ONO-donor ligands: syntheses, structures and catalytic applications in CCC cross-coupling reactions", Applied Organometallic Chemistry, 2017 Publication	<1%
25	Submitted to Indian School of Mines Student Paper	<1%
26	etheses.dur.ac.uk Internet Source	<1%
27	almutairi.ucsd.edu Internet Source	<1%
28	G Narendra Babu, Samudranil Pal. "N-(acyl)- \$\$\textit{N}^\prime \$\$ N ' - (ferrocenylidene)hydrazines and their nickel(II) complexes: Syntheses, structures and physical properties", Journal of Chemical Sciences, 2017 Publication	<1%

29	www.sciatl.com Internet Source	<1%
30	www.worldscientific.com Internet Source	<1%
31	G. Narendra Babu, A.R. Balavardhana Rao, Srinivas Keesara, Samudranil Pal. "Syntheses, structures and catalytic activities of two cyclopalladated complexes derived from N' -(2- naphthylidene)benzohydrazide", Journal of Organometallic Chemistry, 2017 Publication	<1%
32	Submitted to University of Durham Student Paper	<1%
33	studentsrepo.um.edu.my Internet Source	<1%
34	Sarkar, A "Decavanadates with [Et"3NH]^+ and [Me"2HN(CH"2)"2NHMe"2]^2^+: Variation in protonation state and self-assembly", Polyhedron, 20081125 Publication	<1%
35	G. Narendra Babu, Samudranil Pal. "Mono- and tetranuclear cyclopalladated complexes with N'- (9-anthracenylidene)benzothiohydrazide: Syntheses, structures and catalytic applications", Journal of Organometallic Chemistry, 2016	<1%

36	onlinelibrary.wiley.com Internet Source	<1%
37	pubs.rsc.org Internet Source	<1%
38	www.jove.com Internet Source	<1%
39	Carter W. Abney, Richard T. Mayes, Tomonori Saito, Sheng Dai. "Materials for the Recovery of Uranium from Seawater", Chemical Reviews, 2017 Publication	<1%
40	Submitted to University of Edinburgh Student Paper	<1%
41	Submitted to University of Basel Student Paper	<1%
42	Koppanathi Nagaraju, Raji Raveendran, Satyanarayan Pal, Samudranil Pal. "Synthesis and structures of ruthenium(III) complexes with 4-R-2-((2-(pyridin-2- yl)hydrazono)methyl)phenol", Polyhedron, 2012 Publication	<1%
43	scholarbank.nus.edu.sg Internet Source	<1%

www.mdpi.com



Exclude quotes On Exclude matches < 14 words

Exclude bibliography O